PV SYSTEM DESIGN AND YIELD SIMULATIONS FOR A FARM IN RYGGE MUNICIPALITY

SYSTEMDESIGN AV SOLCELLEANLEGG OG PRODUKSJONSSIMULERINGER FOR EN GÅRD I RYGGE KOMMUNE

ANDREAS MADLAND STØRDAL

Norwegian University of Life Sciences
Department of Mathematical Sciences and Technology
Master Thesis 30 credits 2013

Preface

This thesis was carried out in order to investigate the possibility of installing a roof photovoltaic (PV) system on a farm in Rygge. Thousands of farms exist in Norway today, and many of these have in common that they have high electricity consumption and large roof surfaces. These surfaces could be utilized for power production by installing a PV system, which would provide clean, locally produced electricity.

The thesis was a part of a project initiated by Multiconsult AS where the different possibilities for local energy production in the agricultural sector were considered. In addition to this thesis concerning PV systems, two other master theses have been written simultaneously, considering local wind- and biogass production, respectively.

I would like to thank my supervisor, Dr.Ing Espen Olsen, for his assistance during my work on this thesis. He has contributed through discussions, by assisting in the search for relevant information and with his general insight into the PV industry.

Furthermore, I would like to thank Dr.Ing Bjørn Thorud, co-supervisor and Head of Solar at Multiconsult, and Siv Helene Nordahl, consultant at the same company. Bjørn initiated this thesis, and provided with me answers to technical and economical questions regarding PV systems. He also gave me a great start to this project by inviting me to a two-day course in PV system design. Siv Helene helped me particularly in the work with the simulation software used in the thesis, and also answered technical questions regarding PV system design.

I would also like to thank Per Olaf Roer for letting me use his farm as a case study, and for providing me with all the information I needed regarding technical specifications on the farm.

Finally, I would like to thank my friends and colleagues at room TF209 for many good laughs and interesting discussions during this semester.

Ås, May 13th 2013

_____

Andreas Madland Størdal

Abstract

In this thesis, the possibility of installing a roof PV system on a farm in Rygge, Norway has been evaluated. The farm has electricity consumption equivalent to about eight Norwegian households, and several large, southward facing roof surfaces.

Meteorological data for the area has been assessed in order to determine the resource base for solar power production. The collection process has revealed that the amount of irradiation in this area is uncertain, and different sources provide different values with respect to the amount of irradiation in the area. In the main simulations, irradiation data from a weather station located approximately 30 kilometres from the farm was used. The data from this weather station suggest that the annual irradiation on the horizontal plane is approximately 880 kWh/m^2.

Different factors that affect the performance of a PV system have been evaluated, including module orientation, shading and efficiency losses. A shade analysis for the different roofs on the farm has been made. The analysis shows that there is limited shading on the farm roofs, and that shading losses mainly occur during winter when irradiance levels are low.

The simulation software PVsyst have used to design and simulate several PV systems for each of the three largest roofs on the farm. Different module- and inverter types were used in the simulations in order to find the best-performing system for each roof. All the best-performing systems included REC modules. Two systems included inverters from Eltek Valere, while one system included inverters from SMA.

The simulations show that systems with a combined peak power of 105.5 kWp could be installed on the three largest roofs on the farm. The simulated specific yield for the three roofs was 821 kWh/kWp year, and the combined production was 86 607 kWh/year. The production would cover 50% of the local consumption in 2012.

The amount of installed PV systems in Norway is limited, and several of the parameters used in the simulations are therefore subject to uncertainties. Additional simulations were performed in order to investigate the sensitivity in system performance to a change in three key parameters: Irradiation data, soiling losses and module U-value. The sensitivity analysis shows that a change of source for the irradiation data could affect the simulated system performance by 15%. A change in soiling loss settings, mainly determined by snow cover on the modules, could also have significant impact on the simulated system yield. The impact of change in the module U-value on the simulation results was limited.

The simulated production is not very well correlated with the local consumption. The larger fraction of the production will occur during spring and summer, while a large part of the local consumption takes place during fall and winter. The construction of a roof PV system will therefore lead to an export situation during parts of the summer months, where some of the electricity will be supplied to the grid. The farmer would then become a part of the surplus customer arrangement.

An economical evaluation of the different systems shows that the Net Present Value (NPV) of all the simulated systems is negative. The lowest real levelized cost of electricity (LCOE) has been estimated to 1.47 NOK/kWh. There are large uncertainties in the economical evaluation of the systems due to the immature market for such systems in Norway, and the previously mentioned uncertainties with respect to system performance.

Sammendrag

I denne oppgaven har muligheten for å installere et PV-system på en gård i Rygge blitt undersøkt. Gården har et elektrisitetsforbruk som tilsvarer ca. 8 norske husstander, og har flere store, sørvendte tak.

Værdata har blitt samlet inn for området for å kunne vurdere ressursgrunnlaget for produksjon av solstrøm. Innsamlingsprosessen har avslørt at mengden solinnstråling i dette området er usikker, og ulike kilder gir ulik informasjon med hensyn til årlig mengde solinnstråling. I simuleringer utført i oppgaven er det brukt innstrålingsdata fra en værstasjon 30 kilometer fra gården. Data fra denne værstasjonen indikerer at årlig innstråling på horisontalplanet er ca. 880 kWh/m^2.

Ulike faktorer som påvirker et PV-systems ytelse har blitt vurdert, inkludert modulorientering, skygging og effektivitetstap. En skyggeanalyse for stedet har blitt gjennomført, og denne viser at skyggetap i hovedsak oppstår i vintermånedene når innstrålingsnivåene er lave.

Simuleringsprogrammet PVsyst er blitt brukt til å designe og simulere ulike systemer for hvert av de tre største takene på gården. Ulike moduler og vekselrettere har blitt brukt i simuleringene for å kunne finne et optimalt system for hvert tak. Alle de tre systemene som hadde best ytelse i simuleringene inneholdt moduler fra REC. To av systemene innehold vekselrettere fra Eltek Valere, mens et system innehold vekselrettere fra SMA.

Simuleringene viser at systemer med en samlet effect på 105.5 kWp kan installeres på de tre største takene på gården. Den spesifikke produksjonen for systemene vil være 821 kWh/kWp, noe som gir en samlet årlig produksjon på 86 607 kWh. Dette tilsvarer 50% av gårdens samlede forbruk i 2012.

Det er et begrenset antall PV-systemer installert i Norge i dag, og mange av parameterne som er brukt i simuleringene er derfor usikre. Oppfølgingssimuleringer ble derfor gjennomført for å vurdere konsekvensen av en endring i tre nøkkelparametere: Innstrålingsdata, tildekkingstap og modulens U-verdi. En sensitivitetsanalyse viser at bruk av en annen kilde for innstrålingsdata kan endre systemets årlige simulerte produksjon med 15%. En endring i innstillingene for tildekkingstap, som i hovedsak skyldes snø på modulene, kan også ha signifikant innvirkning på simuleringsresultatene. En endring i modulenes U-verdi hadde en begrenset innvirkning på simuleringsresultatene.

Den simulerte årlige produksjonen er dårlig korrelert med det lokale forbruket på gården. Den største delen av produksjonen foregår i vår- og sommermånedene, mens den største delen av forbruket finner sted i høst- og vintermånedene. En eventuell bygging av et PV-system vil derfor føre til at gården havner i en eksportsituasjon i deler av sommermånedene, hvor produsert elektrisitet vil leveres til strømnettet. I et slikt tilfelle vil gården bli en del av plusskundeordningen.

En økonomisk vurdering av anleggene viser at netto nåverdi(NNV) er negativ for alle de simulerte systemene. Den laveste beregnede elektrisitetskostnaden er 1.47 NOK/kWh. Det er store usikkerheter knyttet til den økonomiske vurderingen av anleggene på grunn av det umodne markedet for slike systemer i Norge, samt de tidligere nevnte usikkerhetene knyttet til produksjonen fra systemet.

Contents

List of figures

List of tables

List of symbols

Symbol	Explanation	Unit
A	Area	m^2 or mm^2
b_0	Module incidence constant	-
C_t	Cash flow in year t	NOK
E_g	Energy band gap	J or eV
F_{IAM}	Array incidence factor	-
G_{ex}	Extraterrestrial irradiance	W/m^2
G_{inc}	Inclined plane irradiance	W/m^2
G_{NOCT}	NOCT irradiance	W/m^2
H_G	Global irradiation	$Wh/m^2/day$
H_B	Direct beam irradiation	$Wh/m^2/day$
H_D	Diffuse irradiation	$Wh/m^2/day$
H_p	Plane irradiation	$Wh/m^2/day$
H_R	Reflected irradiation	$Wh/m^2/day$
h	The Planck constant	Js
h_s	Solar elevation	o
I	Electric current	A
I_{cable}	Cable current	A
I_D	Diode current	A
I_{gen}	Generated current	A
I_L	Load current	A
I_{MPP}	Current at MPP	A
I_{RP}	Leakage current	A
I_{sc}	Short-circuit current	A
I_t	Income in year t	NOK
i	Incidence angle	o
i	Discount rate	%
l	Length	m
n_{min}	Minimum amount of modules in a string	-
n_{max}	Maximum amount of modules in a string	-
Ot	Cash outflow in year t	NOK
P	Power	W
P_{cell}	Cell power	W
P_t	Present value of cashflow in year t	NOK
P_{cable}	Ohmic cable loss	W
R	Transposition factor	-
R_{cable}	Cable resistance	Ω

Symbol	Explanation	Unit
R_L	Load resistance	Ω
R_{RP}	Leakage resistance	Ω
R_S	Series resistance	Ω
S_0	The solar constant	W/m^2
S_{ex}	The instantaneous solar constant	W/m^2
T_A	Ambient temperature	^oC
T_{STC}	Temperature at STC	^oC
T_z	Cell temperature	^oC
U	Thermal loss factor	W/m^2 K
Uc	Constant thermal loss factor	W/m^2 K
Uv	Vind dependent thermal loss factor	$W/(m^2$ K(m/s))
V	Voltage	V
V_{OC}	Open-circuit voltage	V
V_L	Load voltage	V
$V_{max, inverter}$	Maximum inverter voltage	V
$V_{min, inverter}$	Minimum inverter voltage	V
V_{MPP}	Voltage at MPP	V
V_z	Cell voltage	V
v	Wind speed	m/s
Y_f	Yearly system yield	kWh
Y_r	Reference yield	kWh
α	Absorption coefficient	-
β	Tilt angle	o
$β_{opt}$	Optimum tilt angle	o
γ	Azimuth angle	o
γv	Voltage temperature coefficient	$V/^oC$
δ	Declination angle	o
η	Efficiency	%
$η_{cell}$	Cell efficiency	%
$η_M$	Module efficiency	%
θ	Zenith angle	o
ν	Frequency	Hz
ρ	Albedo factor	-
$ρ_{cable}$	Specific resistance of cable material	Ω mm^2/m
φ	Latitude	o
$ω_s$	Hour angle	o

Abbreviations

Symbol	Explanation
AC	Alternating current
AM	Air Mass
AO	Annual system operation cost
BoS	Balance of System
CIS	Copper Indium Selenide
DC	Direct current
EMF	Electromotive force
ETA	Ethyl vinyl acetate
IEC	International electrotechnical commision
IRR	Internal Rate of Return
kWh	Kilowatt hour
kWp	Kilowatt peak
LCOE	Levelized cost of electricity
MET	Norwegian Meteorological Institute
Mono-Si	Monocrystalline silicon
MPP	Maxium power point
MPPT	Maximum power point tracker
NOCT	Nominal Operating Cell Temperature
NPV	Net Present Value
NVE	Norwegian Water Resource and Energy Directorate
Poly-Si	Polycrystalline silicon
PF	Packing factor
PR	Performance Ratio
PV	Photovoltaic
RV	Residual value
ST	True Solar Time
SDR	System Degradation Rate
STC	Standard Test Conditions
TSO	Transmission System Operator
UMB	Norwegian University of Life Sciences
Wp	Watt peak

1. Introduction

1.1 Motivation

In recent years a massive increase in the installation of photovoltaic (PV) systems have been observed. Driven by generous subsidy schemes, the number of both residential and commercial PV systems has been steadily increasing. As a consequence, the costs of installing such a system have been reduced significantly.

In Norway however, only a limited amount of PV systems exist as of today. Most of these are not grid-connected, and are used to produce limited amounts of electricity to off-grid cabins and lighthouses.

Through the EU renewable energy directive, Norway is committed to increase their renewable energy share to 67.5% by 2020. A joint green-certificate with Sweden has been introduced with the goal of introducing 26.4 TWh of renewable energy in these two countries by 2020[1].

Farms often have large, southward facing roofs with limited surrounding items that could cause shading. The local electricity consumption on farms is usually high due to an extensive demand for heating and cooling during different seasons. A roof PV system on such farms could contribute to an increase in the renewable energy share and provide local, clean production of electricity.

1.2 Objectives and Limitations

The objective of this thesis is to evaluate the possibility of installing a PV system on a farm in Rygge. Included in this objective is the following:

- To collect information about the solar resource at the site and evaluate the reliability of these data.
- To evaluate the suitability of the different roofs considering an installation of a PV system.
- To suggest possible system designs, and determine the potential for PV power production on the farm.
- To estimate the potential production from the systems using the simulation software PVsyst, and determine if the farm in certain periods will become an exporter of electricity.
- To evaluate the economical consequences of installing a PV system on the farm.

This thesis is mainly written as a feasibility study, and will therefore not go into a great level of detail in matters such as mechanical dimensioning of the mounting systems, earthing of the PV systems, or rating of electrical components like wires and fuses.

1.3 The Farm

The farm considered in this thesis is located in Rygge municipal in Østfold, Norway. The farm produces chickens, vegetables, potatoes and grain.

The chicken production is located in the largest building on the farm. The chickens are dependent on a certain temperature and air quality in the building, and the building is therefore ventilated through 15 ventilators located on the roof. The vegetables produced on the farm are stored for distribution, and the farm therefore has a large storage building for vegetables. The storage building is cooled through an electrical cooling system.

A new storage building is also being planned, and will most likely be erected during the summer of 2013.

Figure 1: Panorama of the farm.

1.4 Outline

Chapter 1 gives an introduction to the thesis and the motivation behind it, as well as the objectives and limitations and a brief description of the farm considered in this thesis.

Chapter 2 provides an overview of the different components included in a grid-connected PV system, with a main focus on the solar modules and their characteristics, and the inverter and different inverter configurations. Chapter 3 describes the theory behind system design of photovoltaic systems, with a main focus on tilted roofs.

Chapter 4 describes the methodology used in this thesis, and the reasoning behind the choices made. The simulation software PVsyst is also introduced in this chapter.

Chapter 5 presents the results from the simulations, a comparison of the simulated electricity production and the local consumption and the results of the economical evaluation. These results are further discussed at the end of each subchapter.

Chapter 6 presents the main conclusions in the thesis based on the given objectives, and chapter 7 include suggestions for further work. Chapter 8 shows the references cited.

2. Components in Grid-connected PV Systems

A grid-connected photovoltaic (PV) system is dependent on several components in order to function. In addition to the solar modules, which convert solar radiation to DC current, a photovoltaic system consists of several Balance of System (BoS) components which ensures safe and efficient operation of the system.

A schematic of the most important components is shown in figure 2.

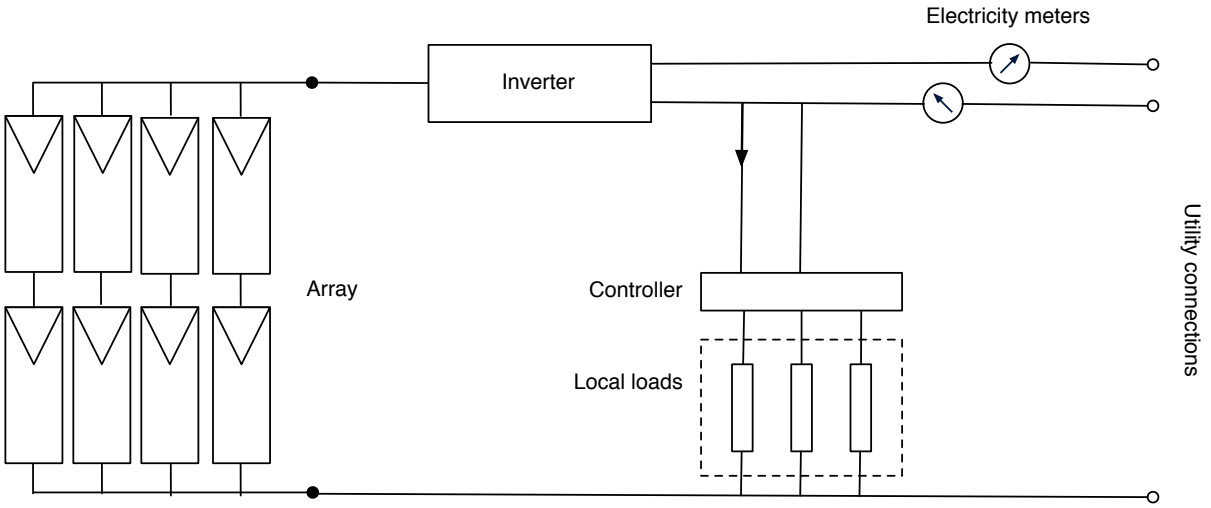

Figure 2: Schematic of a grid-connected PV system.

2.1 Solar Cells and Modules

The solar cell is the fundamental component of the PV system as it converts sunlight to DC current. As the operating voltage of a single solar cell is relatively low, several cells can be connected in series in order to a solar module. This chapter describes the basic concepts of solar cells and modules.

2.1.1 The Solar Cell

Solar cells are made of semiconducting materials which under the right circumstances can produce electricity from electromagnetic radiation. As of today, silicon is the most common semiconductor used for manufacturing solar cells.

Semiconducting materials are neither good conductors nor good insulators. Their electrical properties can be understood through use of the band gap model. This model is illustrated in figure 3.

In the band gap model, an electron can either be fixed in the valence band, or free to conduct in the conduction band. The electrons in a semiconductor are fixed in the valence band. However, if an electron absorbs an amount of energy equal to the difference between the conduction band and the valence band, the electron can be lifted from the valence band to the conduction band, and thus participate in conduction processes[2].

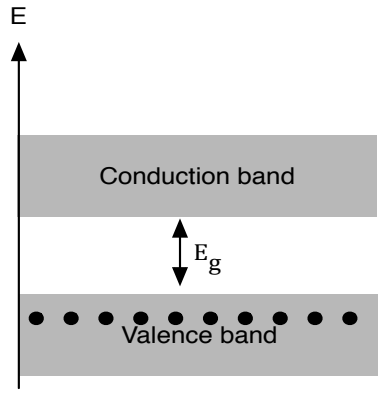

Figure 3: Semiconductor band structure.

In a solar cell, the energy necessary to lift an electron into the conduction band is provided by energy from solar radiation. When a light quanta, also known as a photon, is absorbed by an electron, the electron is lifted into the conduction band if the following criteria is met:

$$h\nu \geq E_g \tag{2.1}$$

Where h is the Planck constant, ν is the frequency of the radiation and E_g is the band gap.

Semiconducting materials can be doped in order to alter the electrical properties of the material. This is done by adding either a trivalent or a pentavalent substance to the semiconducting material. If a trivalent substance, like Aluminum or Gallium is added, a p-type material is formed. Adding a pentavalent substance, like Phosphorus, gives a n-type material.

In order to produce a current that can be used an external circuit, an electric field must be present to provide an electromotive force (EMF). This electric field is created when a p-type and an n-type material is connected to form a pn junction. The excess positive charge carriers in the p-type material and the excess negative charge carriers in the n-type material will diffuse to the other side of the junction, and leave behind space charges which create an electric field between the two materials[3].

An illustration of a crystalline solar cell is shown in figure 4. In this figure, it is shown how the connection of a n-doped and p-doped semiconductor leads to a formation of an electric field, and how charge carriers are lifted into the conduction band and mitigates to each side of the field.

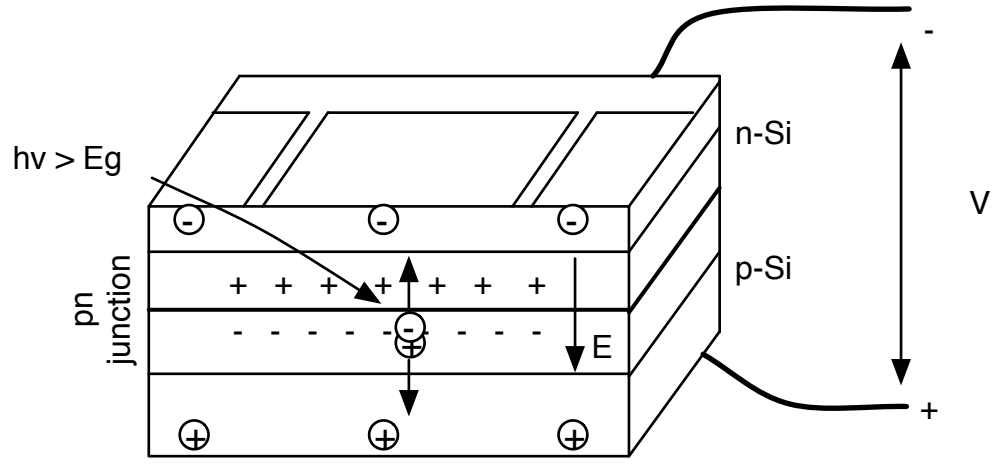

Figure 4: Illustration of a crystalline solar cell.

From an electrical perspective, the solar cell can be represented using the single-diode model. This model is shown in figure 5. I_{gen} represents the charge carriers generated as photons hits the solar cell and is a function of the global irradiation and the cell area. I_D is the diode current that flows through the pn junction. The series resistance R_s represents the voltage drop between the point at which the current is generated and the load, while the parallel resistance R_p represents leakage currents in the system.

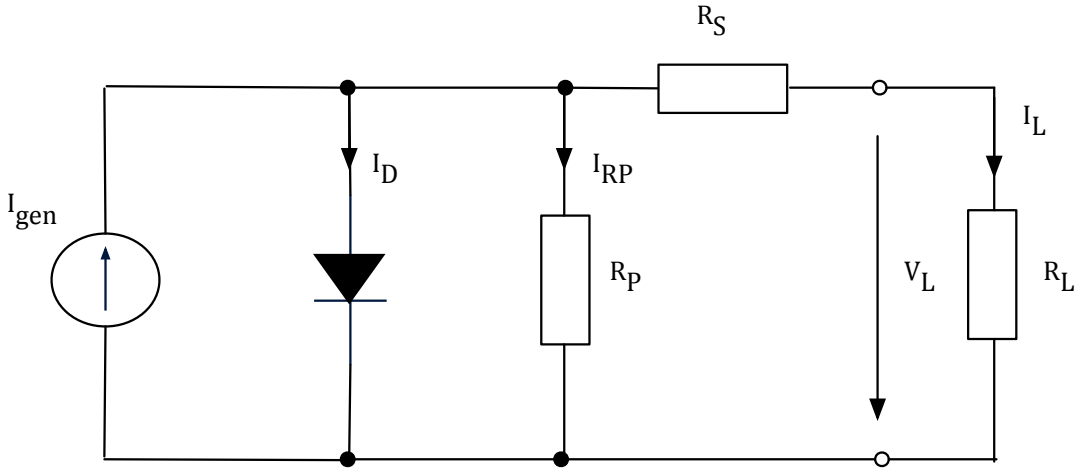

Figure 5: The single diode model for a solar cell.

If the resistance in the load circuit is zero, the charge carriers generated by the sunlight will flow through the external circuit in order to recombine on the other side of the pn junction. This is called *the short-circuit current*, I_{SC}, of the solar cell.

If the load circuit is open, all the charge carriers generated will accumulate in the two regions of the junction, and hence reduce the electric field over the junction. A forward diode current is created which is equal to the current generated by the photons, thus $I_{gen} = I_D$ at this condition. The voltage on the two terminals of the solar cell is then called the open-circuit voltage, V_{OC}[4].

The power P_{cell} generated by the solar cell is given by the equation:

$$P_{cell} = I_L \cdot V_L \tag{2.2}$$

where I_L is the current in the external circuit in amperes[A] and V_L the voltage over the external circuit in Volts[V].

The maximum power point (MPP) of the cell is given when the following criteria is met:

$$dP_{cell} = I_L\, dV_L + V_L\, dI_L = 0 \tag{2.3}$$

The power output at the MPP is then:

$$P_{MPP} = I_{MPP} \cdot V_{MPP} \tag{2.4}$$

The characteristic curve of a solar cell is shown in figure 6.

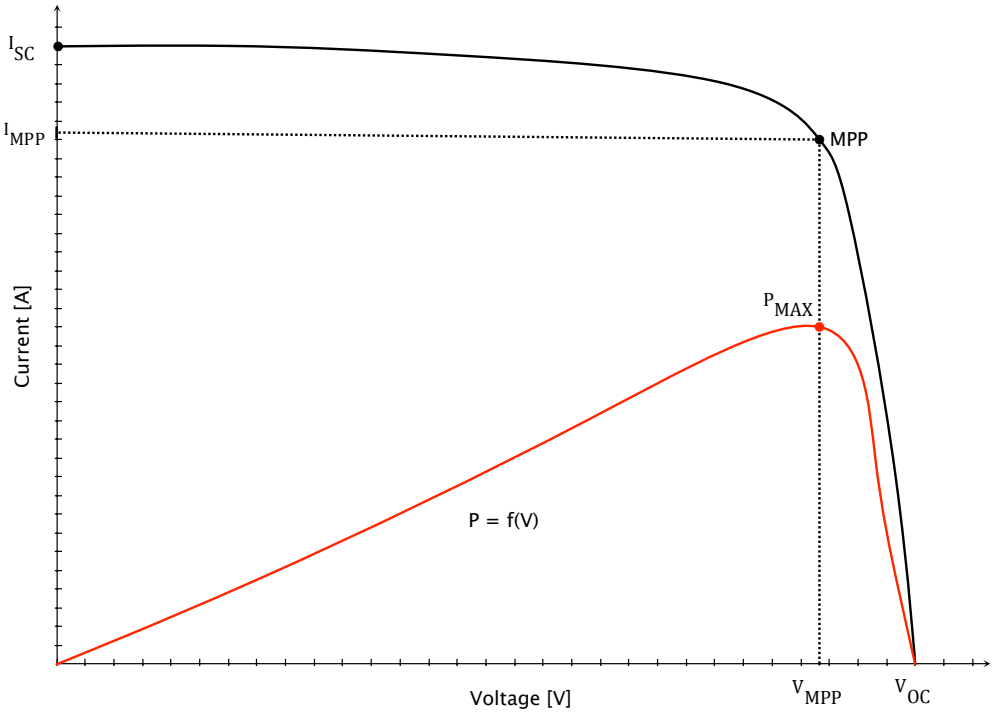

Figure 6: The characteristic curve of a solar cell.

2.1.2 Solar Modules

Several solar cells can be interconnected to form a solar module. A solar cell typically has an operating voltage in the range 0.5-0.6 V. Hence a module with 30 cells connected in series will have an operating voltage in the range 15 – 18 V[5].

The cells in a module are encapsulated in order to protect them against the surrounding environment. The most common encapsulant is ethyl vinyl acetate (EVA), as this material is transparent, stable at elevated temperatures and has low thermal resistance. In addition, the front of the module is usually covered by highly transparent glass and the back by Tedlar, which is a polymer that protects the cells from water and water vapour[6][p.127].

Solar modules can then be connected in series to form a string of modules, and the strings can again be connected in parallel and form an array of modules. This is shown in figure 7.

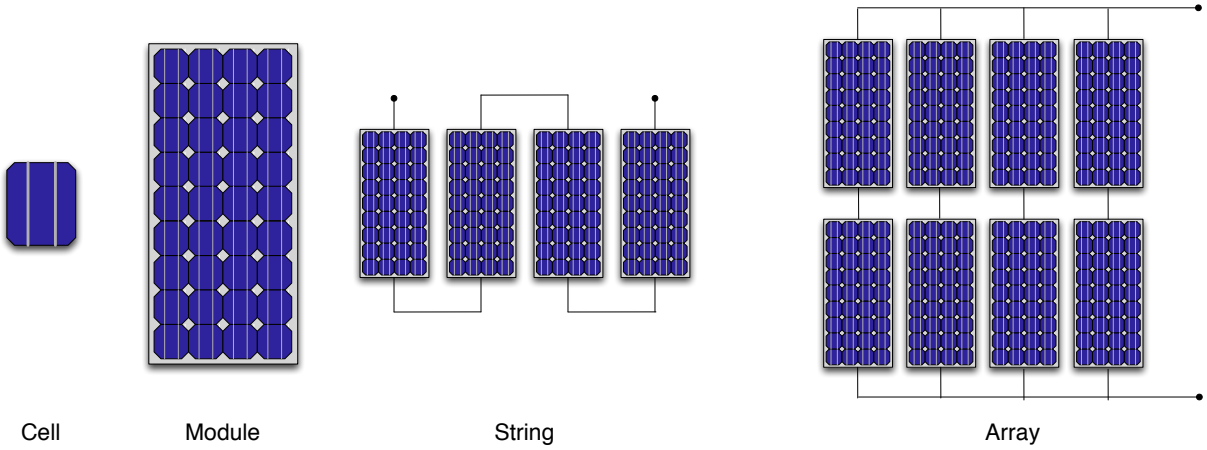

Figure 7: A solar cell, a module, a string and an array.

The characteristic curve of a solar module changes with temperature and irradiance level.
The amount of current generated in a solar module is proportional to the amount of sunlight it receives. The short-circuit current I_{SC} is therefore reduced when a module receives less

irradiance. This is illustrated in figure 8, which shows the characteristic curve of a solar module under different radiation levels for a constant cell temperature.

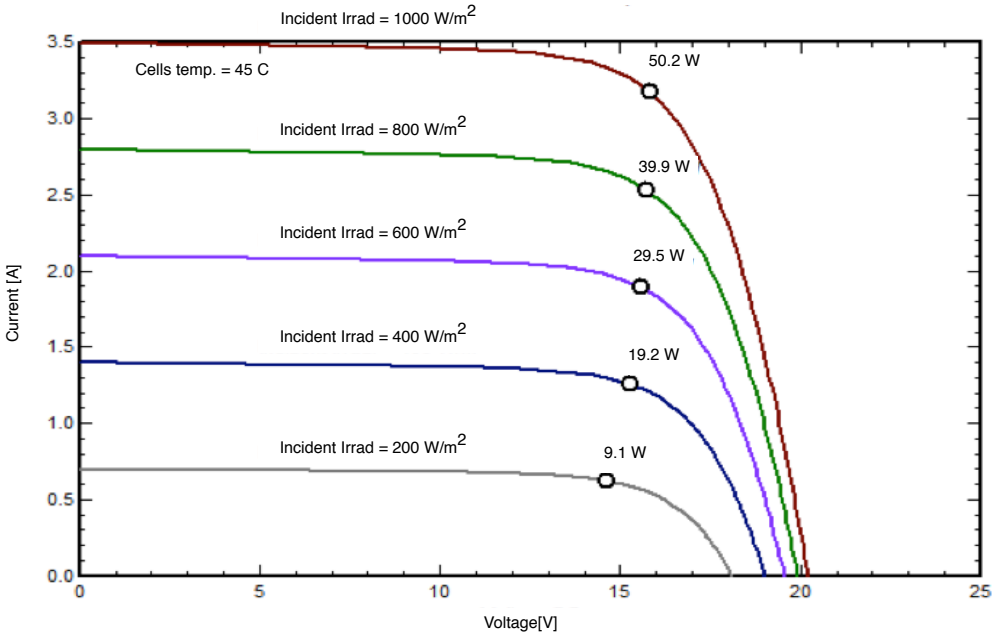

Figure 8: Characteristic curves for a solar module under different irradiance conditions. From PVsyst[7].

The operating temperature also affects the characteristic curve of a solar module. An increase in operating temperature reduces the open-circuit voltage and the power output of the module. Figure 9 shows characteristic curves for a module under different operating temperatures and constant radiation level. As the voltage increases with reduced operating temperature, the output power of the module will also increase, which can clearly be observed in the figure.

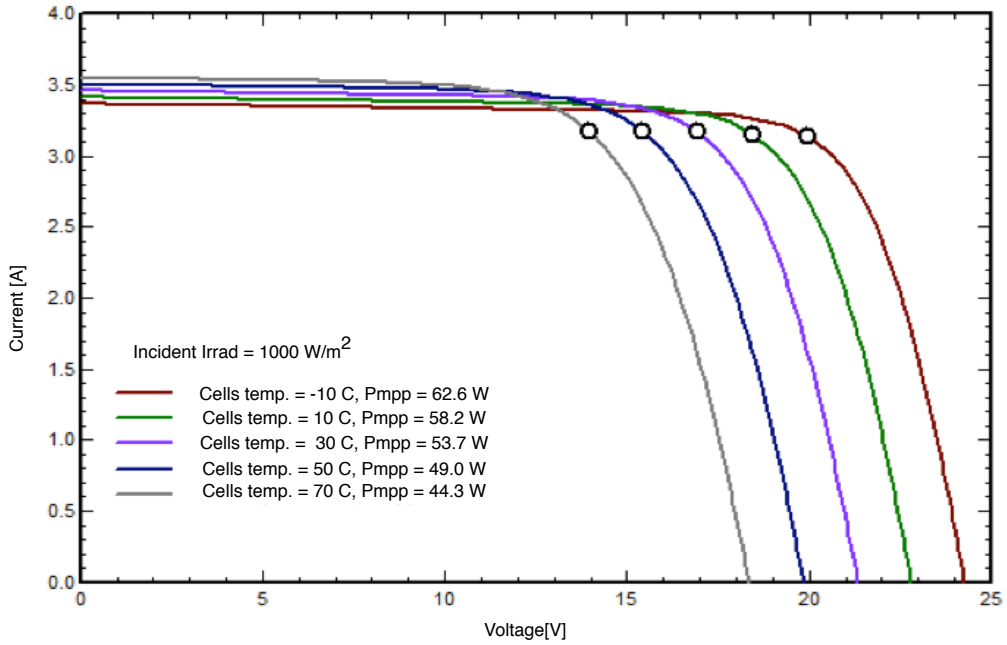

Figure 9:Characteristic curves for a solar module for different operating temperatures. From PVsyst[7].

2.1.3 Module Efficiency

The module efficiency loss is the most significant of the losses when solar irradiance is converted to electricity. Depending on the type of module, 10 – 25% of the irradiation that hits the module will be converted.

The efficiency of a solar cell is given by

$$\eta_{cell} = \frac{P}{G \cdot A_z} \tag{2.5}$$

where P is the power output of the cell in Watts[W], G is the irradiance on the cell[W/m^2] and A_z is the cell area[m^2].

The module efficiency is

$$n_M = \eta_{cell} \cdot PF \tag{2.6}$$

where PF is the packing factor of the module. The packing factor is the ratio of the solar cell area to the total module area.

The solar module efficiency is limited by physical laws that will not be discussed in detail here. It is however important to mark that the solar module efficiency is defined at standard test conditions (STC). The definition of STC is[8][p.49]:

- Cell temperature of 25°C
- Irradiance 1000 W/m^2
- Air mass (AM) 1.5

The module efficiency is not a constant size and will change when the operation conditions deviates from STC.

2.1.3 Solar Cell Technologies

There are several different sola cell technologies available on the market, although the basic concept remains more or less the same. The different technologies vary in efficiency and cost and have different material properties. An overview of the most common technologies including their efficiency, cost and market share is shown in table 1. It should be noted that the price of solar modules is fluctuating, and will also depend on the manufacturer and the volume in question.

Table 1:Different types of solar cells [4], [9] and [10].

Type	Efficiency[%]	Cost [$/Wp]*	Market share(%)
Monocrystalline Silicon	17-20	1.05	30
Polycrystalline Silicon	15-18	1.05	40
Amorphous Silicon	5-10	0.55	5
CIGS/CIS	11-13	0.98	5
CdTE	9-11	0.72	10

2.2 Inverters

The inverter transforms DC current generated in the PV array into AC current. The most important tasks for the inverter in a grid-connected PV system is[11]:

- To produce an AC current that matches the frequency of the grid.
- MPP-tracking in order to maximize production from the array.

In addition the inverter should provide safe and reliable operation over the lifetime of the facility, typically 20-25 years. This includes avoiding stand-alone operation as this could pose a threat to people maintaining the grid.

The inverter should have a high efficiency for a broadest possible range of outputs from the PV array[6]. A typical efficiency curve for an inverter is shown in figure 10.

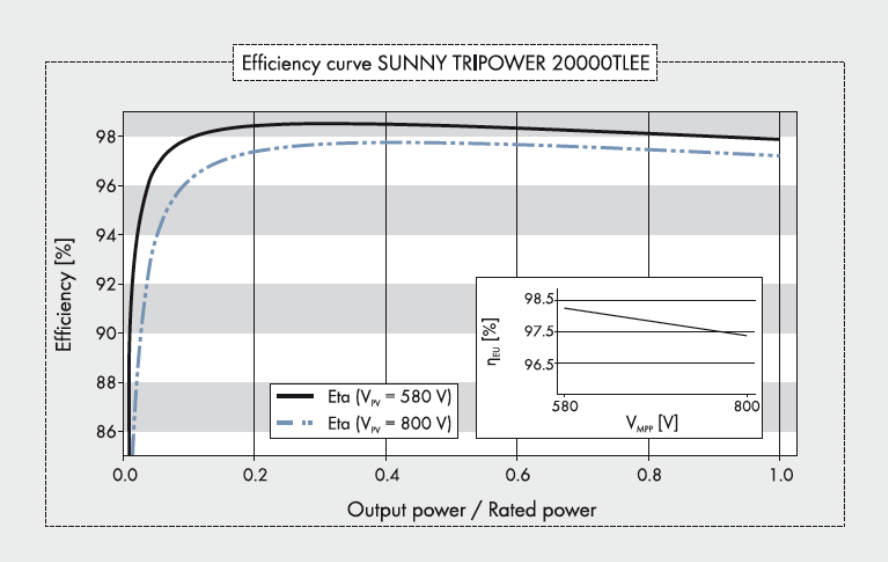

Figure 10: Efficiency curves for an SMA inverter for different voltage levels[11].

Inverters can be divided into different groups and types related to their technical specifications. They can also have different configurations depending on their size, and whether they are connected to the grid or not. For a grid-connected system, there are three main configurations:

- Central inverter configuration
- String inverter configuration
- Module inverter configuration

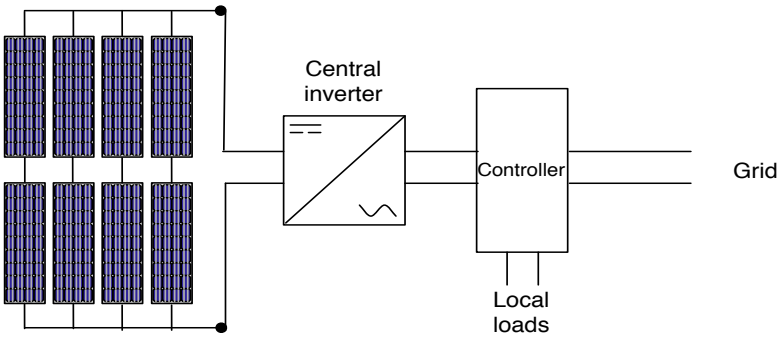

Figure 11: Central inverter configuration.

The central inverter configuration is shown in figure 11. In this configuration, all the strings in the array are connected to one inverter. Central inverters are cost efficient as only one inverter is used in the entire system. These inverters also have a high efficiency for a broad range of array outputs. However, this configuration requires a significant amount of DC cabling that increases array losses. It is also sensitive to partial shading, as shade on one module will affect the performance of the entire array. Furthermore, inverter failure will cause the production from the entire array to be lost for the entire inverter downtime.

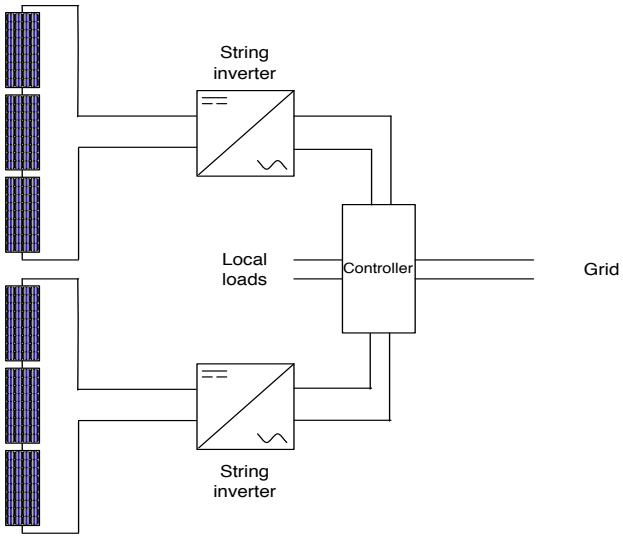

Figure 12: String inverter configuration.

The string inverter configuration is shown in figure 12. In this configuration, one or several strings are connected to one inverter. Use of a string inverter configuration reduces DC cabling and shading losses, on the cost of a lower DC/AC-conversion efficiency. A failure in a string inverter will only cause the production from the connected string to be lost, while the rest of the system remains operative. Some string inverters also have several MPPT inputs, which is an advantage if there are differences in the performance of the connected strings.

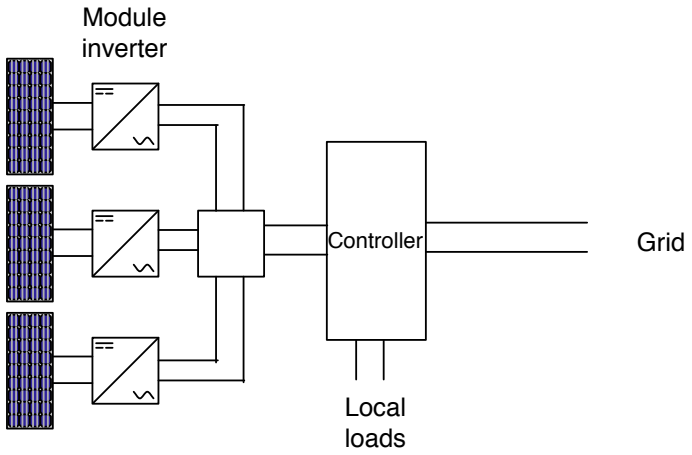

Figure 13: Module inverter configuration.

The module inverter configuration shown in figure 13 has practically no DC cabling, and partial shading losses are only generated from partial shading on a single module. Module inverters are usually mounted directly on the back of each module. However, this inverter configuration has the lowest DC/AC-conversion efficiency, and is therefore most suitable in PV systems with high sensitivity to partial shading. Module inverters are also exposed to the weather conditions at the installation site, and will usually have a shorter lifetime than the modules[6][p.264-265].

2.3 DC and AC Cables

DC cables are used to connect the modules together, and to connect an array or a string of modules to the inverter. As the operating voltage in the DC-part of the system is relatively low, a non-negligible ohmic loss is generated in the cables. Furthermore, the voltage drop in the cables could affect the operation of the inverter.

DC cables are expensive. The cable route of the system should hence be designed in order to minimize the use of DC cables. Losses in the cables can be limited by increasing the cross-sectional area of the cable, although this measure will increase the cable cost.

The DC cables are exposed to the local climate and should be insulated and protected. Cables are typically rated for different temperatures, sunlight and water resistance, and special cables have been designed for use in PV systems[8][p.147-148].

Depending on the distance from the inverter to the grid injection point, there could also be significant losses in the AC cables. AC cables will often be more shielded from the climate than the DC cables, and in the cases of short distance between the inverter and the injection point, AC losses are sometimes considered negligible. Nevertheless, attention should be paid to the length, cross-sectional area and quality of the AC cables as well.

2.4 Mounting Systems

A mounting system for the PV modules is required to ensure safe operation of the system at all times. There are a large amount of different solutions available for mounting of PV modules, depending on whether the system is building integrated (BIPV), building applied (BAPV) or ground mounted.

A PV mounting system should meet several criteria. The system must be able to support the weight of the modules, and additional loads from weather such as wind and snow. Furthermore, the mounting system should be designed to provide ventilation of the modules, as power output is reduced when the operating temperature of the modules are increased[8][p.85-98].

For BIPV and BAPV systems, the weight of the mounting system itself is an important factor. It is preferable that the mounting system does not penetrate the membrane of the roof, as penetration will increase the risk of water leaking into the building[6][p.166-174].

On pitched roofs there will in most cases be used a mounting system with the same tilt angle as the original roof angle. Brackets or bolts are used to mount the modules to cross beams slightly above the roof surface to allow for air to circulate between the roof and the modules. An illustration of a mounting system for a tilted roof is shown in figure 14.

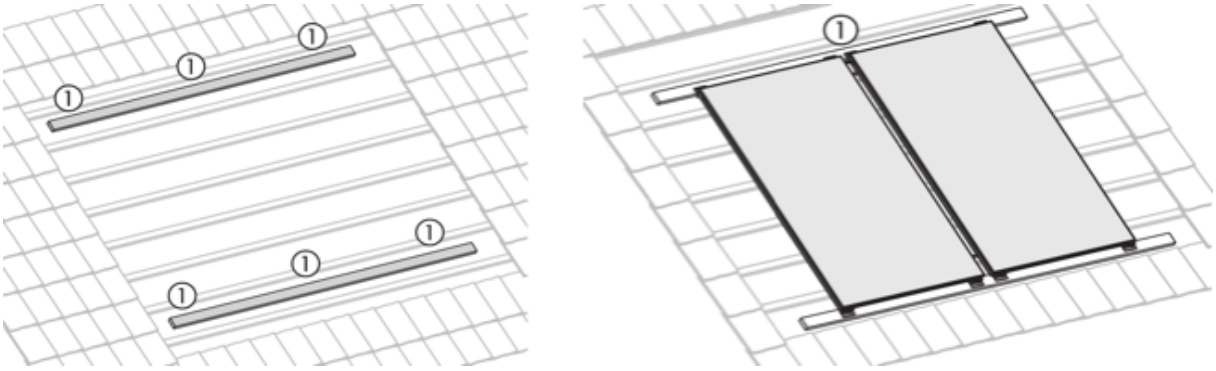

Figure 14: Illustration of a PV mounting system for tiled roofs[12].

2.5 Other BoS Components

Other balance of system (BoS) components are used in a grid-connected PV-system to maximize the lifetime of the system and ensure optimal operation. In addition to the components described earlier, BoS components will typically include those described in this chapter.

2.5.1 Protection and Disconnect Switches

Several components are installed in order to protect the system from being damaged by lightning, large currents or reverse currents.

Disconnection switches are usually installed on both the DC and the AC side of the inverter, and must often meet specific requirements set by the government or the grid operator. The disconnection switches allow the power in a circuit to be shut down. On the AC-side of the inverter, a utility external disconnect switch is also installed in grid-connected systems in order to avoid stand-alone operation of the PV system when the grid is down[8].

Fuses and circuit breakers are also widely used to protect the system against over-currents. DC currents are more difficult to break, as they do not pass through a zero voltage point. DC current circuit breakers are thus more complicated and expensive than AC current breakers.

Lightning protection may also be required in some cases, both on the DC side to protect the system against strikes on the array, and on the AC side to protect it against strikes in the grid.

2.5.2 System Monitoring and Metering

A PV system also needs a system to monitor important system parameters like voltage, frequency, time, temperature and energy production. This system is usually an integrated part of the inverter.

A grid-connected system will also need a metering system which registers the amount of energy produced, and whether the energy is consumed at the site or is fed into the electric grid.

There are two different ways for a utility company to measure the amount of electricity delivered to the grid by the PV system: Net metering and gross metering.

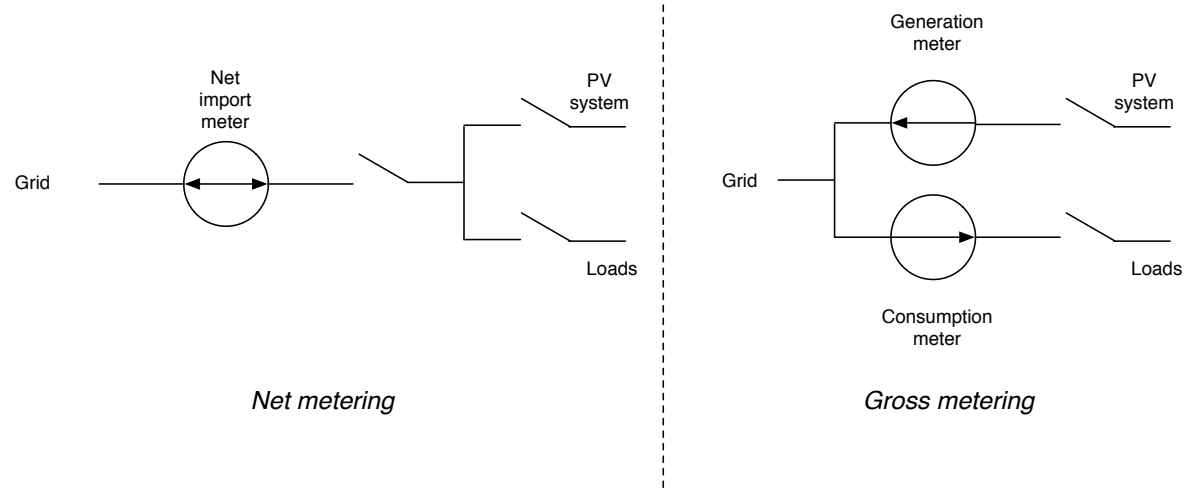

Figure 15: Schematic of the net metering system and the gross metering system.

When using net metering the utility measures the net difference between the amount of electricity exported and imported for the site. If the exported and imported amount are equal, the customer does not pay anything to the utility company. If the customer is a net exporter in the given period it will get paid for the net excess generation. In the opposite case the customer will pay for the net consumption of electricity. From a technical point of view this can be achieved by letting the meter run backwards in periods of export. The net-metering system is illustrated to the left in figure 15.

When the gross metering method is used the production and consumption is measured separately, and the import meter and export meter run separately. This system, which is illustrated to the right in figure 15, allows for differentiated pricing of electricity depending on time of day, spot price or other factors, and is the system currently being used in Norway[8].

3. Theory: Design and Optimization of Grid-connected PV systems

In this chapter, the most important factors to consider when designing a grid-connected PV power system are described.

Chapter 3.1 describes, in brief, how a site assessment can be conducted when considering installation of a PV-system.

Chapter 3.2 provides a theoretical background to the solar resource and how the resource is evaluated for a potential PV system site.

In chapters 3.3 to 3.5, the influence of module orientation, shading and system design on the performance of a PV system is explained, while chapter 3.6 presents the most common system losses and different parameters that are used in the evaluation of a PV system´s performance.

In chapter 3.7, an introduction to the regulatory regime in Norway and methods for evaluating the economics of a PV system are presented.

3.1 Site Assessment

A site assessment is usually conducted in the initial phase of a PV system development project. The purpose of such an assessment is to get an overview over key factors that will influence the performance of the system. After the initial assessment, a detailed design of the system can be made considering the factors described in this chapter.

For a roof PV system, the following information is usually collected during an initial site assessment[8]:

- Possible locations of the PV array
- Roof specifications, including orientation and tilt angle
- Shading items, like trees, vegetation, buildings and roof components
- Available area for PV installation
- Possible mounting system
- Possible location of BoS components

If available, an assessment of the local electricity consumption should be made in order to compare possible production and consumption for the site. This relationship could be of great importance in cases where there is a different economical value to a kWh delivered to the grid compared to a kWh consumed at the production site.

3.2 Solar Radiation and Meteorology

The amount of electricity produced by a photovoltaic system will depend on the amount of irradiation that the PV modules receive. An assessment of the solar radiation and the meteorology on the planned installation site is therefore of great importance when optimizing a photovoltaic system.

At the edge of the earth´s atmosphere, the solar irradiance has approximately the same value at a plane that is perpendicular to the direction of the sun. The average irradiation value is[6]:

$$S_0 = 1367 \pm 2\ W/m^2$$

S_0 is also known as the solar constant.

However, at the earth´s surface the irradiance will vary significantly, mainly due to atmospheric effects, latitude, season of the year and the time of day[3].

3.2.1 Season of the Year and the Time of Day

The earth uses 365 days to orbit the sun and 24 hours to rotate around its own axis. At a given location, the solar irradiance will therefore arrive from different directions at different times of the day and year.

The motion of the Earth around the sun is tilted by 23.45° to the equator. In the Northern hemisphere, the Earth will be tilted away from the sun in the period from autumnal equinox to vernal equinox, and tilted towards the sun from vernal equinox to autumnal equinox. The declination angle, δ, is 23.45° at summer solstice, $-23.45°$ at winter solstice, and 0° at the two equinoxes[5]. The variation in declination angle through the year is illustrated in figure 16.

The sun´s change in path during the day is described using the hour angle, ω_s, which is the angle between the meridian of the site and the meridian of the Sun. This angle is by definition 0° at solar noon. The hour angle can be calculated using equation 3.1. Note that the hour angle is negative in the morning and positive in the afternoon.

$$\omega_s = (ST - 12) \cdot 15° \tag{3.1}$$

where ST is the local time in hours.

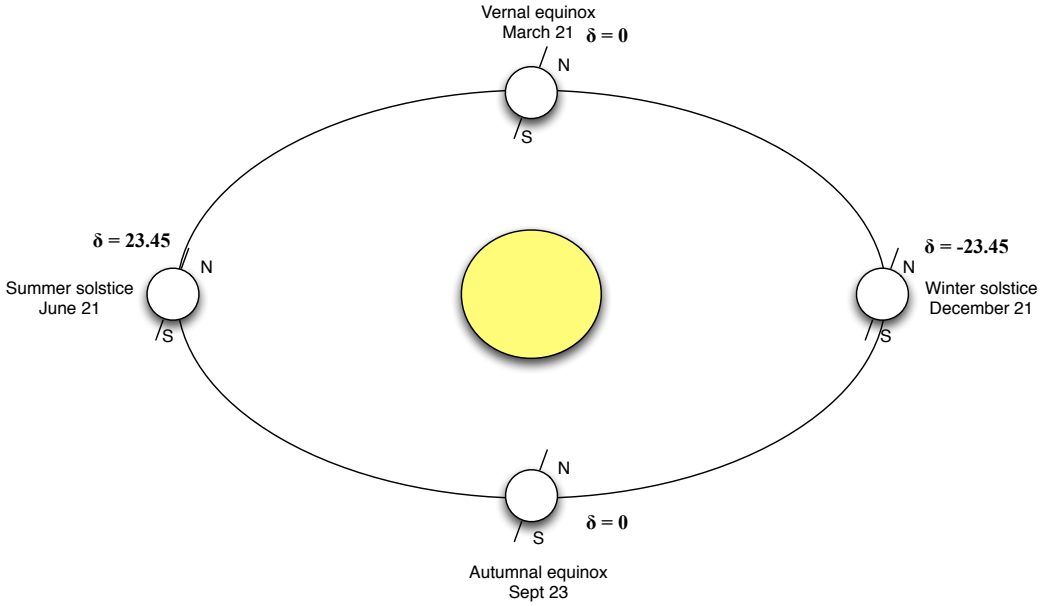

Figure 16: The Earth´s declination angle for different times of the year.

3.2.2 Latitude and solar elevation angle

The latitude φ of a site determines the highest elevation angle of the sun through the year and for each day. The highest elevation is not constant through the year, and in the Northern Hemisphere the elevation will be highest at solar noon on summer solstice.

The elevation of the sun is denoted h_s. The following relation is given between h_s, φ, δ and ω_s [3][p.96]:

$$\sin h_s = \sin\varphi \sin\delta + \cos\varphi \cos\delta \cos\omega_s \tag{3.2}$$

Equation 3.2 shows that the solar altitude varies depending on three factors: The time of year, which is expressed through the declination angle, δ, the site location, through the latitude, φ, and the time of day represented in the hour angle, ω_s.

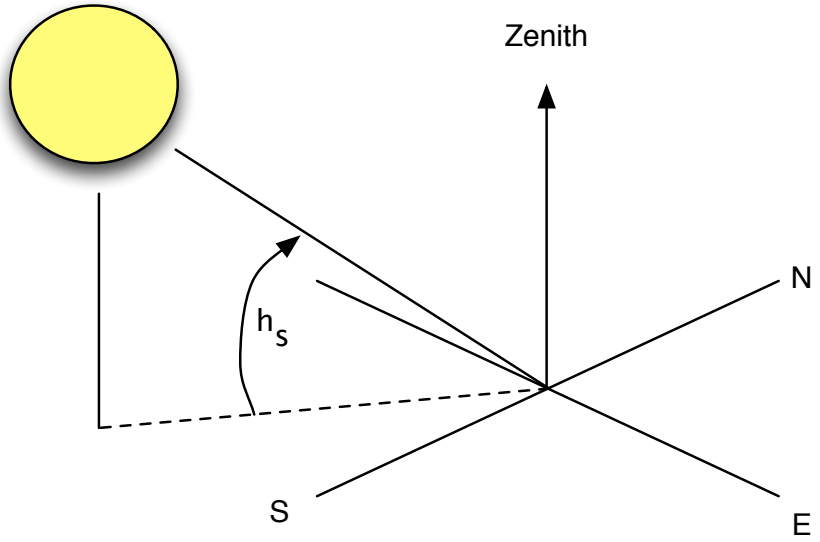

Figure 17: Illustration of the elevation angle h.

When the latitude, hour angle and declination angle of a given site is known, the extraterrestrial irradiance for the location at any given time can be calculated using the equation[6][p.31]:

$$G_{ex} = S_{ex} \cdot \sin h_s \tag{3.3}$$

Where G_{ex} is the extraterrestrial irradiance on a horizontal plane [W/m^2] and S_{ex} is the instantaneous solar constant varying between 1322 and 1414 W/m^2 depending on the time of year.

3.2.3 Atmospheric Effects

Different atmospheric effects like scattering, absorption and reflection influence the magnitude of the power received at the Earth´s surface, and also change the characteristics of the irradiance. The properties of the irradiation on ground level can thus be very different from the extraterrestrial irradiation.

As solar radiation passes through the atmosphere, components like CO_2, O_3 and water vapour (H_2O) will absorb some of the radiation, while some radiation is scattered back to space or towards the earth.

The atmospheric effects on the solar radiation will depend on the composition of the atmosphere and the length of the path that the radiation has to travel through the atmosphere. The path length is often described using the air mass (AM) concept, which is illustrated in figure 18 [3][p.98].

$$AM = \frac{1}{\cos\theta} \tag{3.4}$$

where θ is the angle between zenith and the sun. AM0 refers to zero atmosphere irradiance, which is the extraterrestrial irradiance at the edge of the atmosphere.

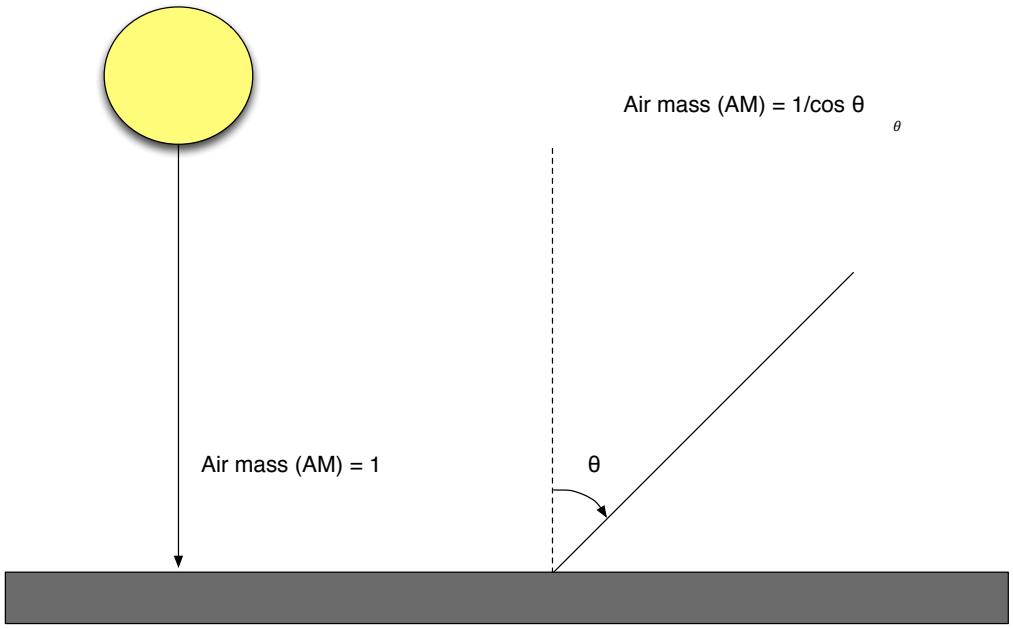

Figure 18: Illustration of the Air Mass (AM) concept.

Figure 19 shows how the irradiance spectrum changes due to atmospheric effects at AM1.5, compared to the extraterrestrial irradiance. As shown in equation 2.1, the current generated by the sun is dependent on the wavelength, and thus the frequency, of the irradiance. The performance of a solar module will thus change through the day as the irradiance spectrum changes.

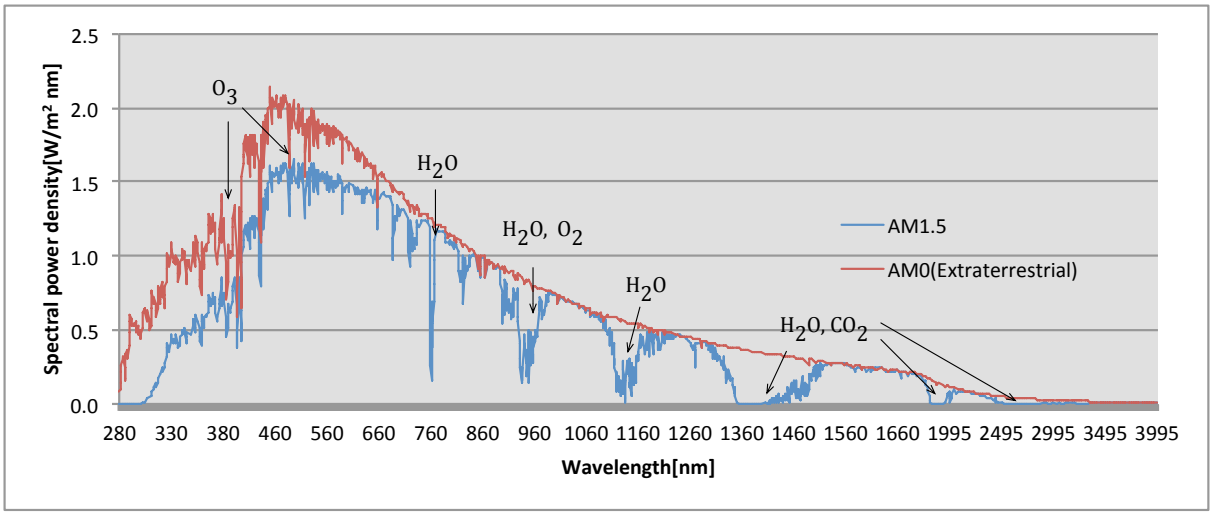

Figure 19: Irradiance spectrum for extraterrestrial irradiance and irraance at AM1.5[13].

When the irradiance passes through the atmosphere, two of the atmosphere´s main components, CO_2 and H_2O absorbed practically all the irradiance at certain frequencies. O_3 absorbs radiation in the ultraviolet (UV) part of the spectrum. Rayleigh scattering, which is caused by small particles in the atmosphere, also affects the irradiance spectrum[4][p.110].

The total amount of irradiation received at a given site at the Earth´s surface is given by the equation:

$$H_G = H_B + H_D + H_R \tag{3.5}$$

Where H_G is the total amount of irradiation, often referred to as global irradiation, expressed in the unit Wh/m²/day, MJ/m²/day or kWh/m²/year. H_B is the direct beam component of the global irradiation which passes through the atmosphere without being absorbed or scattered. H_D is the diffuse component which is first absorbed and later reemitted from the surroundings. H_R is radiation that is reflected from the surroundings. This three-component model is illustrated in figure 20.

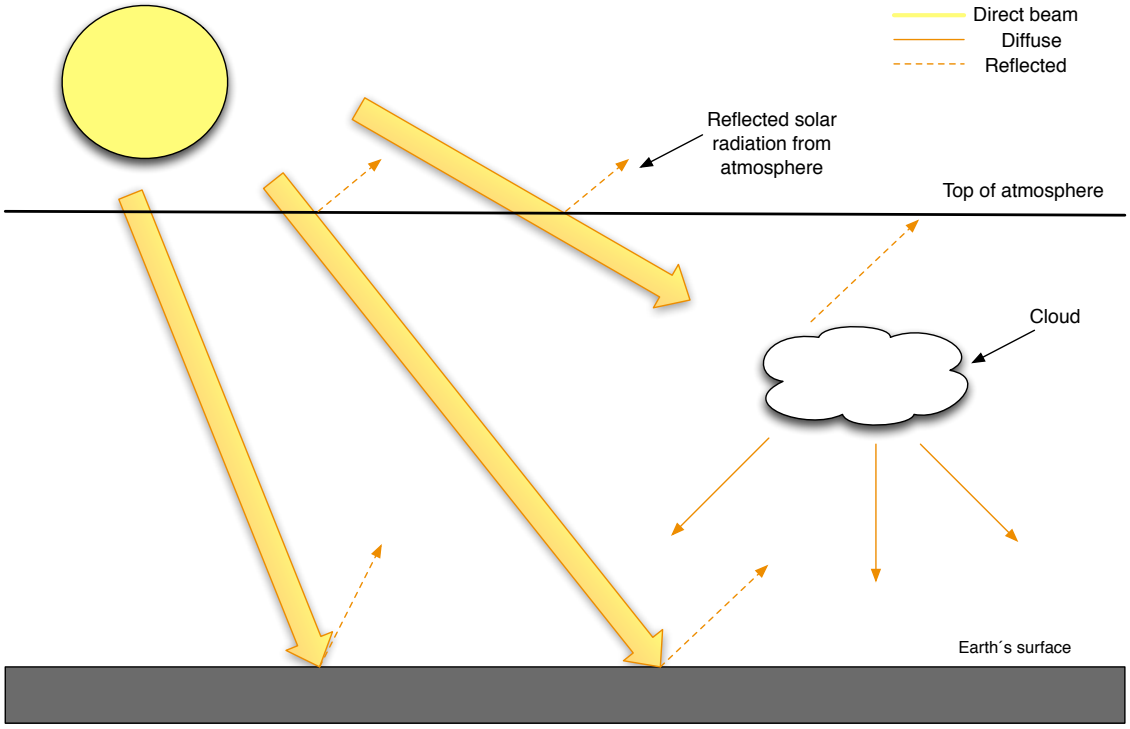

Figure 20:Different components of solar radiation.

H_R is a function of the total amount of solar radiation hitting the surface as well as the albedo, ρ, of the surroundings. It is calculated using the equation

$$H_R = \rho \cdot (H_B + H_D) \tag{3.6}$$

The albedo is a reflection factor indicating how much of the irradiation that is reflected of a surface. An albedo value of 1 indicates that all the radiation that hits the surface is reflected, while a value of 0 indicates that all the radiation is absorbed.

A table of representative albedo values for different surroundings is shown in table 2.

Table 2: Albedo values for different surfaces[6].

Surface	Albedo
Asphalt	0.1 - 0.15
Green forest	0.1 - 0.2
Wet ground	0.1 - 0.2
Dry ground	0.15 - 0.3
Glass-covered ground	0.2 - 0.3
Concrete	0.2 - 0.35
Desert sand	0.3 - 0.4
Old snow	0.5 - 0.75
Newly fallen snow	0.75 - 0.9

3.2.4 Collection and Assessment of Meteorological Data

Collection of accurate meteorological data is one of the important tasks when designing a PV system, as the system yield will be highly influenced by the amount of irradiation received by the modules. Meteorological data can be divided into two categories: Data collected from weather stations, and data collected from databases based on interpolation between different sources or satellite data.

The format of the data will also vary between the different sources. Weather station data could typically be hourly, daily or monthly time series. An example of an hourly time series is shown in figure 21.

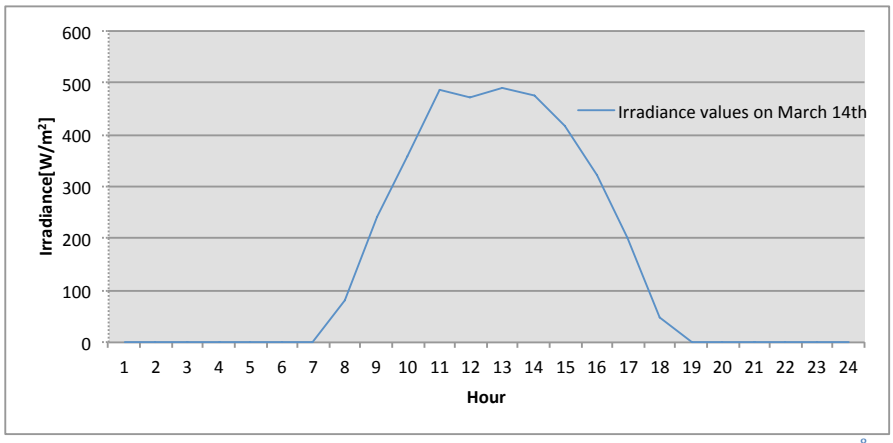

Figure 21: Irradiance values registered on March 14th at a weather station in Ås.

In many cases there are a limited number of weather stations near a site, and even fewer may hold reliable data sets for irradiation data. The use of databases in order to collect metrological data for a specific site is common, and a variety of different databases exist that allows for site-specific collection of weather data. Databases in most cases provide yearly, monthly, daily or in some cases hourly average irradiation values. An irradiation map from the PVGIS database is shown in figure 22.

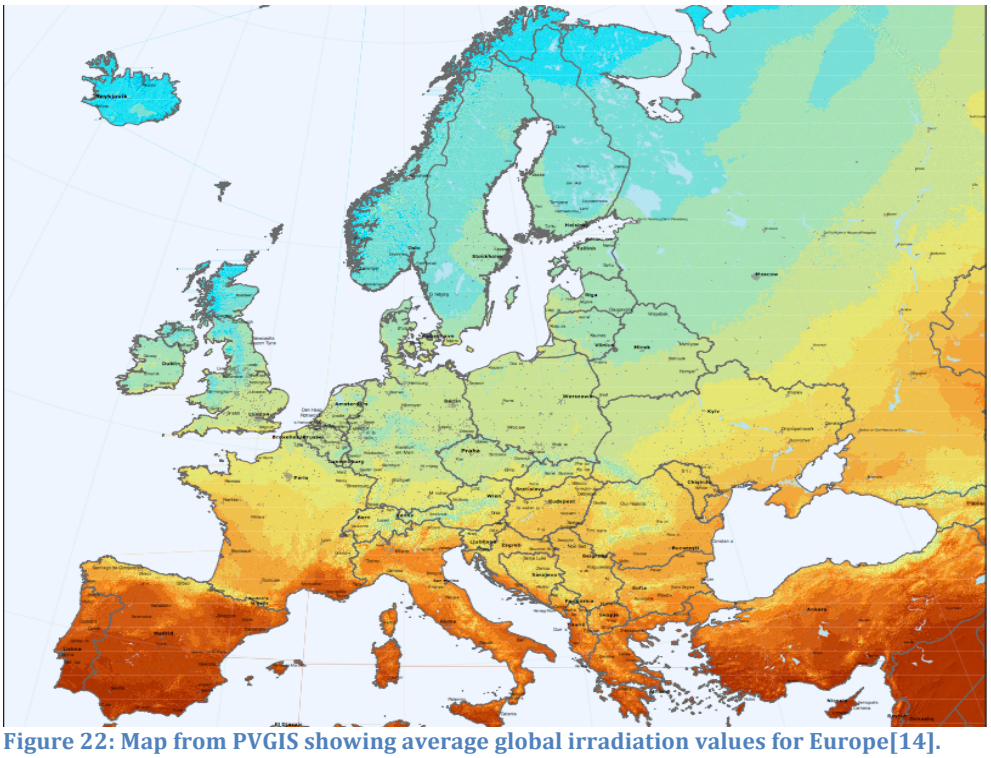

Figure 22: Map from PVGIS showing average global irradiation values for Europe[14].

The amount of irradiation on a site is not the only meteorological parameter affecting the system performance. The ambient temperature will, as shown in chapter 2.1, affect the module voltage level and therefore the operation of the entire system. Wind speeds also affect operating temperatures due to the increased cooling effect from high winds. Finally, snow cover could affect the performance of the array in two ways; positively, by increasing the surrounding albedo and thus the amount of reflected irradiance, and negatively, by covering the modules and thus reducing the amount of irradiance received. The meteorological data of a potential PV system site should therefore be carefully assessed at an early stage of the planning process.

3.3 Module Orientation

The irradiation on a solar module will be a function of two angles: The tilt angle, β, of the module, and the azimuth angle, γ. The tilt angle is the angle between the module and the horizontal plane. There are different mathematical definitions of the azimuth angle. In this thesis the azimuth angle is defined as the angle between south and the orientation of the module. Note that the azimuth angle by this definition is negative in the eastern direction.

An illustration of the two concepts is shown in figure 23. The two angles should be chosen so that the solar modules receive the largest possible amount of irradiation.

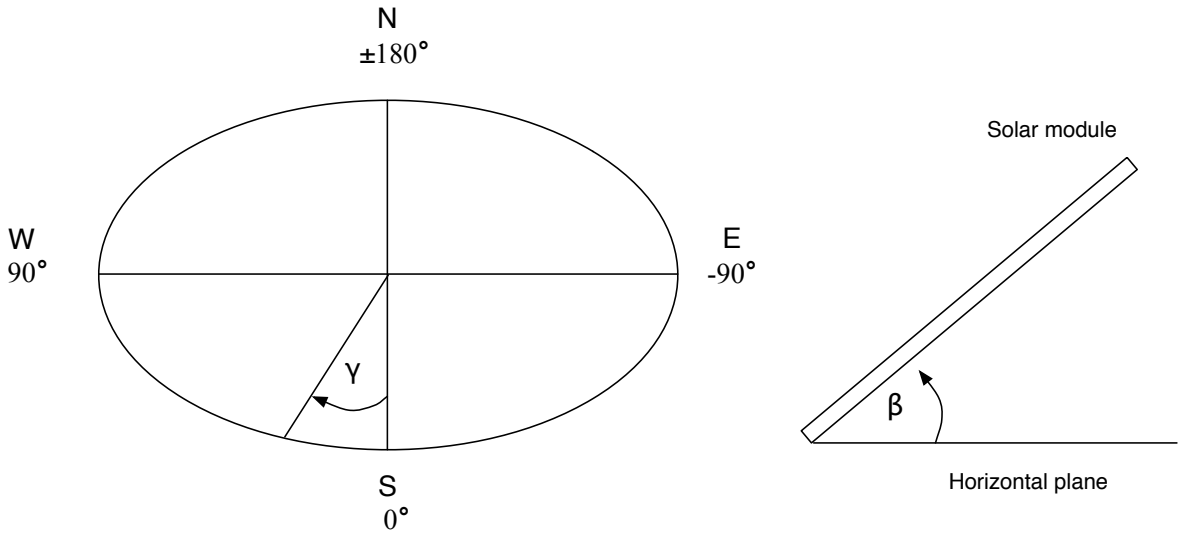

Figure 23: The azimuth angle and tilt angle.

3.3.1 Optimum Tilt Angle for a PV System

There are several different approaches suggested for the determination of the optimum tilt angle of a solar module. A general rule of thumb is that the tilt angle should be equal to the latitude of the site location[6][p.42]:

$$\beta_{opt} = \varphi \tag{3.7}$$

At latitudes far north this approach will significantly reduce the amount of diffuse radiation that the module receives, and a smaller tilt angle could therefore be desirable. Nevertheless, a large tilt angle will increase production during the winter as the sun path is lower and a larger fraction of the direct irradiation will hit the module.

At northern latitudes, snow cower could also affect the optimum tilt angle of a module. As shown in table 2, snow has a high albedo value, which increases the amount of reflected diffuse radiation. Nevertheless, snow cover on the modules can cause irradiation losses, and a module tilt angle of at least 60° is necessary in order for automatic snow shedding to occur[15].

A study performed at the University of Hannover by Beringer et.al showed that the tilt angle of the module is near irrelevant at mid-latitudes, with the differences in production being less than 6% over the year for fixed angles between 0 and 70 degrees[16]. Other site-specific studies have been made with different conclusions on the optimum tilt angle of the modules.

On horizontal surfaces, the tilt angle of the modules will also influence the distance between the rows, as shadowing effects between the modules should be avoided. An increase in the module tilt angle β will also increase the necessary distance between module rows in order to avoid reciprocal shading between rows.

3.3.2 Optimum Azimuth Angle

The solar modules should be oriented directly towards south, as the sun in the Northern Hemisphere is at its highest altitude when in south. This can also be deviated from equation 3.2, as the hour angle ω_s is zero when the sun is in south, which means that $\cos \omega_s = 1$.

However, a change in the azimuth angle of the modules by 20° or less will have a minimal impact on the energy produced by the system[6]. The optimum azimuth angle could also change in certain cases due to local meteorology conditions when PV systems are located close to mountains or in a valley[8].

3.3.3 Irradiation on a Plane as a Function of Tilt and Azimuth Angle

The total amount of irradiation that hits a plane is given by the equation

$$H_P = R\left(\beta, \gamma, \frac{D}{G}\right) \cdot H_G \tag{3.8}$$

where R is the transposition factor between the irradiation on the horizontal plane and the tilted plane, and $\frac{D}{G}$ is the ratio of diffuse to global irradiation[6][p.42]. When designing a PV system, a highest possible H_p is desirable.

Equation 3.8 shows that the transposition is not only dependent on the tilt and azimuth angle of the plane; the diffuse ratio also matters since the amount of diffuse irradiation is largest on the horizontal plane. Hence R is a site-specific parameter which is not only determined from the geometry of the modules.

3.4 Shading Effects on PV Systems

Shade on a PV array could greatly affect the performance of a PV system, as shade on one module connected in a string of several modules will affect the power output of the entire string. The power loss is a result of two effects: An energy loss as less irradiation hits the modules, and a loss due to an electrical mismatch effect between the modules connected in series.

As described in chapter 2, solar cells are in essence current generators. When several cells are connected in series, the series current is limited to the current in the weakest cell. Hence shading on one cell could severely reduce the performance of all the cells connected in series with the shaded cell, and shade on a module connected in a string of modules will reduce the output from all the modules in the string. The resulting change in power characteristics for partial shading of one cell connected in series with 35 other cells is shown in figure 24[6].

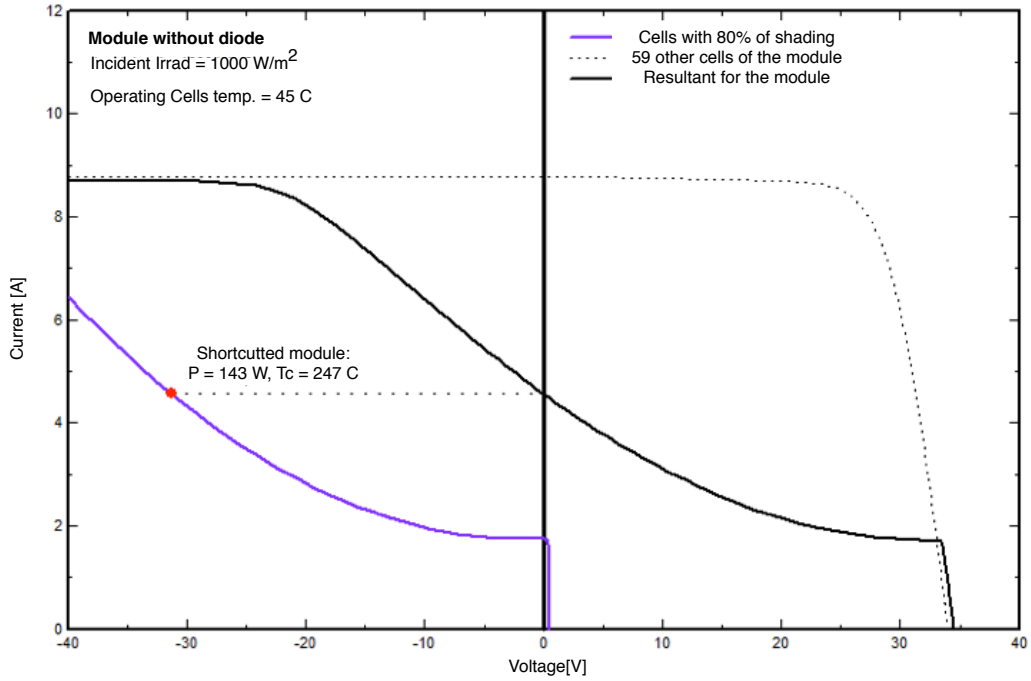

Figure 24: Electrical characteristic of a module with one shaded cell. From PVsyst [7].

Due to the change in characteristics, the cell becomes a load in the circuit and the power generated is dispatched as heat in the cell.

In addition to causing a significant reduction in the power output of a string, partial shading could also lead to hot-spot formation in the shaded module. Hot-spot formation, or hot-spot heating, occurs as a shaded cell starts to act like a load for the other cells, and heat is dispatched in this cell. A rise in the temperature in the shaded cell above a certain point could cause damage to the surrounding materials or the cell itself. This in turn will permanently damage the performance of the entire module. A schematic illustration of hot spot heating in a cell is shown in figure 25[5].

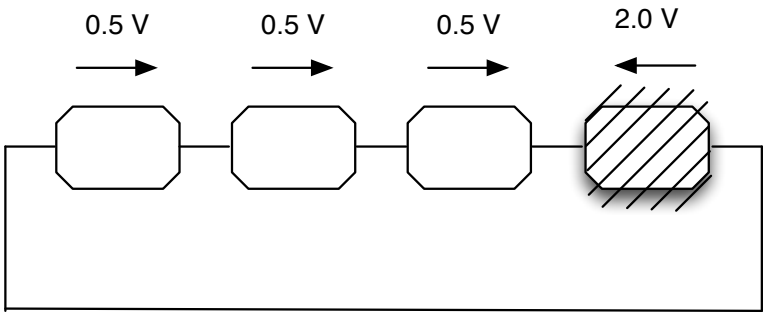

Figure 25: Hot-spot formation in a shaded solar cell in series with other non-shaded cells.

In order to avoid hot-spot heating in the solar cells, bypass diodes are connected over groups of cells. The bypass diode will protect the shaded cells from hot spot heating by providing a low resistance path for the current generated in the non-shaded cells. This concept is illustrated in figure 26[5].

As bypass diodes are expensive, it is common to connect one bypass diode over groups of solar cells. Studies have shown that one bypass diode per 18-20 cells is sufficient in order to avoid permanent damage from hot-spot heating[17].

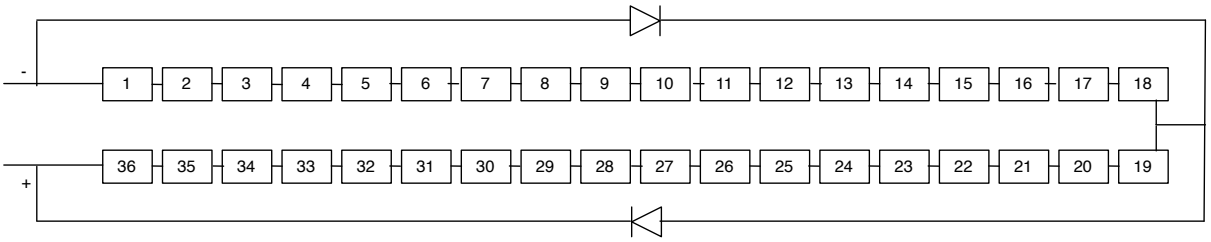

Figure 26:Schematic of a PV module with 36 cells connected in series and two bypass diodes.

Figure 27 shows the electrical characteristics of a solar module consisting of 60 cells with 3 bypass-diodes installed, one diode bypasses 20 cells. In the case of shading of one cell, the power from all the cells that are bypassed is lost. However, the module still has a power output of about 2/3 of the power production before the shading. Also, the temperature and power dissipation in the shaded cell has been significantly reduced compared to the values observed in the module characteristic in figure 24, where no bypass diodes are connected.

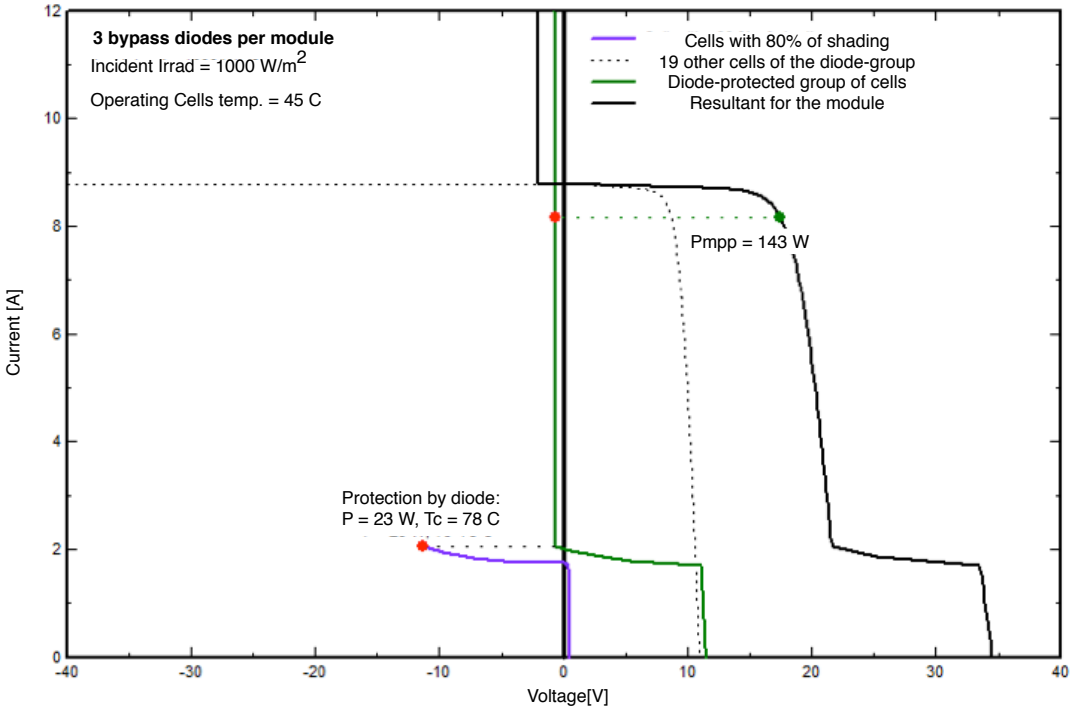

Figure 27:Electrical characteristic of a module with one shaded cell and three bypass diodes. From PVsyst.[7].

When designing a PV system, shading should be avoided to the extent possible. Nevertheless, some shading will in many cases be unavoidable. In such cases the design of the PV system should limit the shading to as few strings as possible in order to reduce the electrical mismatch effect between the modules[6][p.166].

3.5 System Design and Component Selection

The selection of modules and inverters for the PV system must take into account technical as well as economical factors. Equally important, the matching of array and inverter must ensure a highest possible production from the system.

3.5.1 Selection of Modules

Solar modules are available in practically all sizes, shapes and qualities. Numerous manufacturers exist from all over the world. Hence selecting modules for a PV system is

challenging and different alternatives should be analysed before choosing the module type for a PV system. Technical criteria that should be considered include[8][p.116-118]:

- Type: As described in chapter 2.1, the main types are monocrystalline silicon, polycrystalline silicon and thin film modules.
- Efficiency: The efficiency of a module can vary significantly also for modules based on the same technology.
- Module tolerance: Modules produced at the same factory with the same nameplate performance are usually not 100% equal. The manufacturer will therefore provide an uncertainty to the performance of the module, either given in Watts or as a percentage of the module performance at STC. This is referred to as the module tolerance. A low tolerance is preferred, as unequal modules connected in a string will reduce the system performance.
- Module components: The module should have a sufficient amount of bypass diodes in order to prevent hot-spot heating, a solid frame and a cover glass with high transparency.
- Mechanical strength: This is a particularly important factor when the PV system will be installed in an area with rough weather conditions or heavy snow loads.
- Weight: The weight of the module could be of great importance, especially for roof mounted PV systems.
- Standards: Several standards exist for module design and quality, e.g. IEC 61215, IEC 61646 and IEC 61730.
- Certifications: Several certification marks exist to ensure that a module adhere to a relevant set of standards.
- Warranties: A module typically has two different product warranties, one for the physical condition of the module and one for the minimum yield of the module, i.e. minimum 80 % of rated output after 20 years.

Furthermore, the availability and the cost of the module should be investigated and compared to the technical specifications of the module.

3.5.2 Selection of Inverter

The different possible inverter configurations for a PV system are described in chapter 2.2.

Several of the same criteria used in the selection of modules are also used for the selection of inverters, particularly with respect to efficiency, standard, certifications and ratings. Furthermore, it is important that the inverter has a high efficiency for a broad range of voltage and power levels. Also, price and availability are obvious criteria in the selection of inverters for the PV system.

3.5.3 Matching of Modules and Inverter

Irradiance level and operating temperature affects the characteristic curve of a module. All inverters have a maximum power point tracking system (MPPT). The main task of the MPPT is to locate the MPP of a module, string or array, and hence maximize the power produced.

The MPPT voltage range of an inverter is limited. When choosing an inverter it is desirable that the MPP of the array is within the MPPT range of the inverter for all operating temperatures and radiation levels. This is illustrated in figure 28.

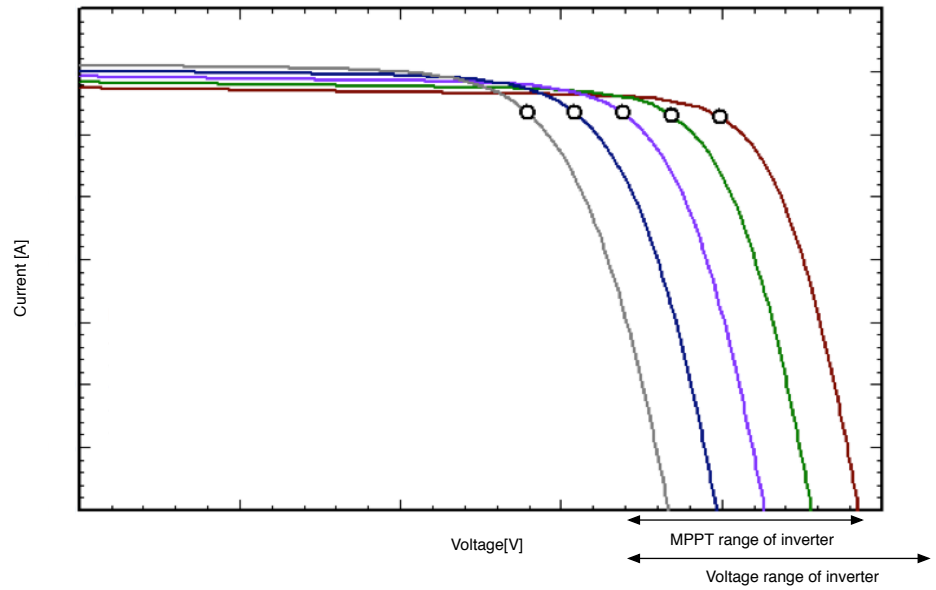

Figure 28: The MPPT and voltage range of an inverter. From PVsyst[7].

Although it is not always possible to keep the array voltage within the inverter MPPT range for all operating temperatures, it is an absolute requirement that the maximum voltage stays below the maximum inverter voltage and the maximum rated system voltage of the modules. The voltage range of an inverter will vary between different types, as will the maximum rated system voltage for the modules[8][p.130].

To ensure that the MPPT-range of the inverters covers the voltage range of the array, and that the maximum voltage of the system does not exceed the maximum inverter voltage, the different possible operating conditions should be evaluated. As shown in chapter 2, the module temperature determines the operating voltage of a module.

All modules have a defined nominal operating cell temperature (NOCT), which is defined as the cell temperature given an ambient temperature of $T_A = 20$ °C, irradiance G_{NOCT} = 800 W/m² and a wind speed of 1 meter per second. Assuming that the cell temperature is proportional to the amount of irradiance on the module G_{inc}, equation 3.9 can be used to estimate the operating temperature of the cell, T_{cell} [6][p.133].

$$T_{cell} = T_A + \left(NOCT - 20^{\circ}C\right) \cdot \frac{G_{inc}}{G_{NOCT}} \tag{3.9}$$

Equation 3.10 is used in order to calculate the change in operating voltage of a cell, and thus a module or string, as a result of a change in operating temperature[8][p.129].

$$V_{cell} = V_{STC} \pm [\gamma_V \cdot (T_{cell} - T_{STC})] \tag{3.10}$$

Where V_{STC} is the operating temperature of the module at STC, γ_V is the voltage temperature coefficient of the module in $[V/°C]$ and T_{STC} is the operating temperature at STC. The voltage increases when the temperature decreases, and the plus sign in the equation should therefore be applied when T_{cell} is below 25°C and vice versa.

Equation 3.9 will in many cases be inaccurate, as modules are not always well ventilated and wind speeds will deviate from the 1 m/s assumed in the equation[18]. In these cases the thermal balance of the modules could be used to estimate the module temperature. The thermal balance is given by[18]

$$U \cdot (T_{cell} - T_a) = \alpha \cdot G_{inc} \cdot (1 - \eta_M) \tag{3.11}$$

where U is the thermal loss factor[W/m^2 K], α is the absorption coefficient of the module, G_{inc} is the incident irradiance on the module[W/m^2] and η_M is the module efficiency.

Use of equation 3.11 requires detailed information about the module U-value, which can vary significantly depending on the mounting of the modules, wind speed and wind direction. For estimation of the voltage range of the array, the NOCT approach is therefore often used and a margin of error is added to ensure that the voltage levels fulfil the described requirements.

When the possible operating temperatures of the system and the associated voltage levels have been determined, the minimum and maximum amount of modules in a string can be determined.

The maximum amount of modules in a string is determined by the open-circuit voltage of the modules at the lowest possible operating temperature. The following two criteria must be fulfilled[8][p.131-134]:

$$n_{max} = \frac{V_{max,inverter}}{V_{OC,max,module}} \tag{3.12}$$

Where n_{max} is the maximum amount of modules in one string, $V_{max,inverter}$ is the maximum voltage of the inverter and $V_{OC,max,\,module}$ is the maximum open-circuit voltage of the module at the given site. As a voltage higher than the inverter maximum could cause severe damage to the inverter, it is also common to add a security margin.

The minimum amount of modules in a string is determined from the MPP-voltage of the modules at the highest possible operating temperature

$$n_{min} = \frac{V_{min,inverter}}{V_{MPP,min,module}} \tag{3.13}$$

where n_{min} is the minimum amount of modules in one string, $V_{min,,inverter}$ is the lower limit of the inverter, and $V_{MPP,min,module}$ is the minimum MPP voltage of the module.

Note that equation 3.12 is an absolute security requirement, and that connecting more modules in one string than this amount could lead to voltage levels in the array that could damage the inverter. Equation 3.13 is used as a requirement to ensure that the voltage does not become lower than the minimum voltage of the inverter at the highest operating temperatures. Such a situation would not cause any damage to the equipment; however, potential energy from the array would be lost. It is common to use a security margin of i.e. 10% for both calculations to account for extreme cases and cabling losses[8].

The array current should not exceed the maximum DC input current of the inverter. However, the array current does not vary to the same extent as the voltage levels, and most inverters will have DC inputs that are somewhat over-dimensioned with respect to current levels. Many inverters will react to a high current level by adjusting the voltage level along the characteristic curve of the array, and thus prevent too large currents to cause damage to the inverter[18]. Still,

it should always be checked that the short-circuit current of a string, I_{SC}, does not exceed the maximum inverter current[8][p.135].

Finally, the power rating of the array should match the power rating of the inverters. There are different opinions about whether the inverter should be oversized or undersized with respect to the array output power. An argument in favour of oversizing the inverter is that it ensures that all the power from the array is utilized, particularly on very sunny days. However, oversizing also increases the risk of the inverter shutting down at low irradiance levels, as the inverter has a minimum power threshold. If the array output power is below this threshold, the inverter will not operate. Also, an undersized inverter will lower the cost of the system[8][p.136-137].

3.6 System Losses and System Performance

System losses and performance ratio are important factors to evaluate when designing a PV system, as they provide an indication as to how well the system is designed. Several parameters are used to describe the performance of a PV system. These include[6][p.488-497]:

- **Total yield [kWh/year]** – The total amount of electricity produced by the system during one year.
- **Specific yield [kWh/kWp]** – The amount of electricity produced per installed kWp. This is sometimes called the load factor, and could be expressed in the percentage ratio of full load hours to the total amount of hours in one year.
- **Specific cost [NOK/kWp]** – The cost in NOK or any other currency per installed kWp. This number includes modules, BoS components and installation costs.
- **Performance ratio (PR) [%]** – The performance ratio represents the ratio of energy delivered by the system to the theoretical output of a system without array and system losses. Mathematically, this ratio can be expressed using equation 3.14.

$$PR = \frac{Y_F}{Y_R} \tag{3.14}$$

In equation 3.14, Y_F is the actual yield of the system for a year, while Y_R is the reference yield. Y_R is the electricity produced from the system if all the available irradiation was converted at the STC-efficiency of the module, and all other components in the system had an efficiency of 100%[6][p.489].

Although the efficiency of the modules accounts for a significant fraction of the overall energy losses in the PV system, there are also other losses in the system that affects the system performance. This chapter explains the most common system losses. Note that the system losses can be divided into two categories: Losses caused by a reduction in the amount of irradiation received by the modules, and efficiency losses occurring in the conversion process somewhere in the PV system.

3.6.1 Array Incidence Angle (IAM) Losses

As the incidence angle between a solar module and the incoming solar irradiation increases,an increased amount of the irradiation will be reflected of the surface of the module. This is in accordance with basic theory for the behaviour of light when moving between two media. The reflection of irradiance due to low incidence angle is illustrated in figure 29.

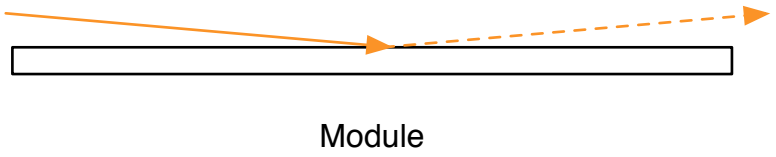

Figure 29: Reflection of irradiance due to low incidence angle.

To calculate the amount of irradiation being reflected by the module is however complicated, as it depends on material properties of the antireflective coatings as well as multi-reflexions in the covering glass. One approach that has been suggested is[18][Array losses]

$$F_{IAM} = 1 - b_0 \cdot \left(\frac{1}{\cos i} - 1\right) \tag{3.15}$$

where F_{IAM} is the module absorption factor, b_0 is a module specific constant and i is the incidence angle on the module. Note that when the incidence angle is zero, the absorption factor F_{IAM} is one and there are no array incidence losses. The b_0 value for a crystalline module has been measured to be approximately 0.05[18].

3.6.2 Soiling Losses

Soiling losses occurs as pollution, dust, bird droppings or snow accumulate on the modules and reduce the amount of irradiation absorbed by the module. There is a great amount of uncertainty related to these losses, as they will depend heavily on the local area and climate[18]. Soiling losses are in many cases highly seasonal, i.e. in areas with heavy snowfall or agricultural areas with seasonal fertilisation.

Research done in the south-western part of the US has shown that average yearly soiling losses could be as high as 15 %, although the average annual soiling losses would typically be between 2 and 5 % in this region[19]. Nevertheless, this shows that soiling losses could reduce the performance of a PV system significantly.

Soiling losses are less significant in areas with sufficient rainfall, and in cases where the module tilt angle β is large. Soiling losses have in many cases been observed to be minor on many PV installations in Europe[6][p.206]. On framed modules, moss and dust can accumulate around the frame edges and reduce the output of the modules. Hence frameless modules could be a good solution in cases where soiling is expected[18]. The use of a cleaning agent will in many cases reverse the power loss, and is recommended in areas where soiling losses are observed to be significant[6][p.205].

3.6.3 PV Losses due to Irradiance Level

The efficiency of a PV module is given for STC conditions, and will change when the system operates under conditions different from STC. Most PV modules will have reduced efficiency at low irradiance levels. Figure 30 shows the efficiency of a polycrystalline module for different irradiance levels.

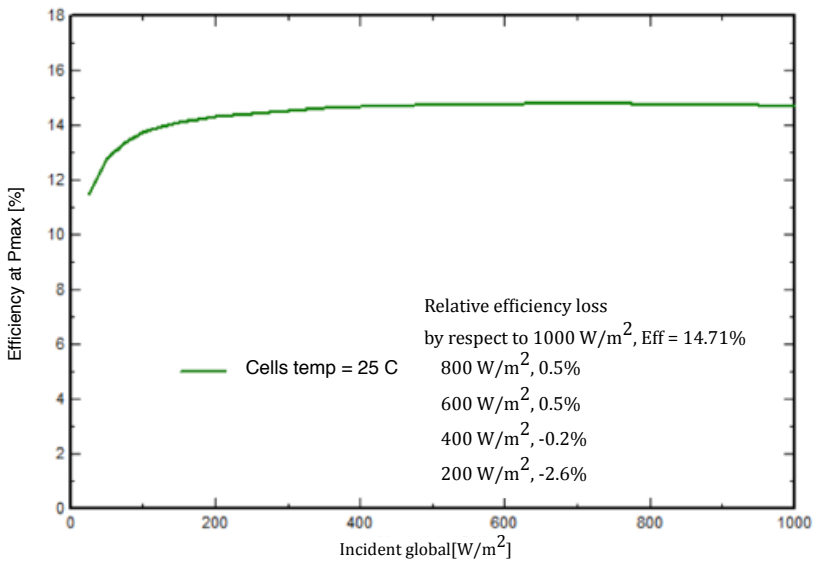

Figure 30: Efficiency of a crystalline module at different irradiance levels. From PVsyst[7].

The extent of the efficiency change in a module with respect to a change in irradiance level will depend on the type and the quality of the module. Thin film solar cells will usually experience a smaller drop in efficiency than other solar cells at low irradiance values[18].

3.6.4 PV Losses due to Temperature

As the temperature of the solar module changes, the conversion efficiency of the module will change accordingly. An increase in the module temperature will cause a drop in the module voltage and thereby reduced module efficiency. Figure 31 shows the efficiency of a polycrystalline module for different operating temperatures.

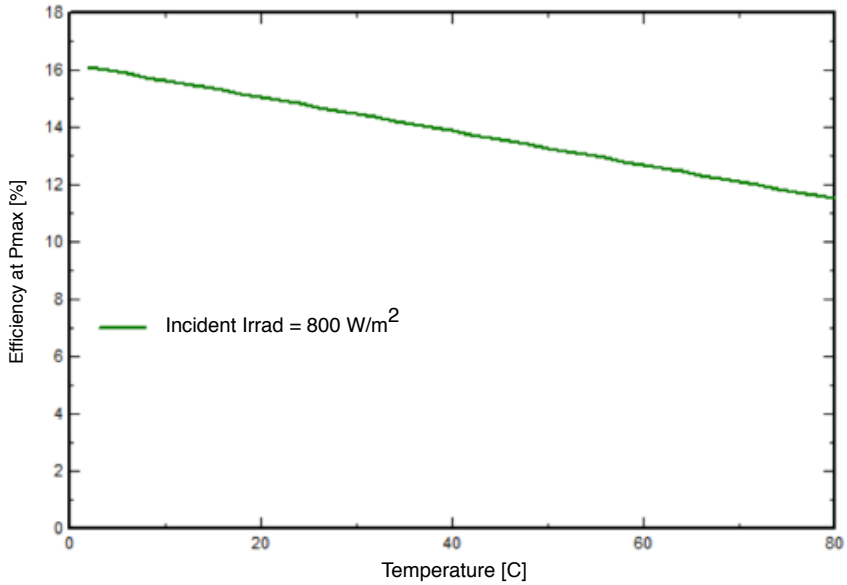

Figure 31: Efficiency of a crystalline module for different operating temperatures. From PVsyst[7].

As observed in figure 31, the efficiency of a solar module is reduced significantly at elevated operating temperatures. Hence careful attention should be paid to the mounting system of the modules, as a mounting system that ensures sufficient cooling of the modules will increase the performance of the system.

The operating temperature of the module is calculated by using the thermal energy balance of the module from equation 3.11. The thermal loss factor, U, must then be determined. The thermal loss factor is a function of natural convection, which depends mainly on the mounting of the module, and forced convection caused by the wind.

$$U = U_c + U_v \cdot v \tag{3.16}$$

In equation 3.16, U_c is a constant component depending on the mounting of the module, and U_v is a factor which is proportional to the wind velocity v.

The impact of a temperature increase on the module efficiency will, like the irradiance impact, vary depending on module type and quality.

3.6.5 Module Quality Losses

Depending on the module quality, some modules show reduced power output during the lifetime of the module. As standards have been introduced and many producers provide productions warranties for their modules, the risk for PV system developers has been reduced. If modules have only positive tolerances, the modules used will on average be better than expected, and these losses could actually turn out to be power gains.

There are several IEC standards made regarding the production and the quality of both crystalline and thin film modules. Choosing modules that are verified according to these standards will reduce the risk of module quality losses during the lifetime of the system.

When the modules have been in operation for a while, they will naturally degrade. Several studies have been made on the long-term degradation of solar modules. These studies have concluded that long term degradation in most cases is lower than 0.75% per year, and a reduction in ouput between 0.3% and 0.8% per year has been suggested as typical values[20].

3.6.6 Module Mismatch Losses

The current in a string of modules is limited to the lowest module current in the string. Hence connecting modules with different characteristics in one string will lead to mismatch losses in the PV system[18].

Module characteristics are not identical even for modules of the same type and rating, and are usually statistical distributions over a given interval. A module rated at 240 Wp at STC could in reality prove to be a 238 Wp or 243 Wp module, depending on the module tolerance.

As in the case of module quality losses, the introduction of standards and warranties has reduced the impact of module array mismatch losses. The IEC 61215 and the IEC 61646, concerning crystalline and thin film modules respectively, states that: *"The measured average power shall be equal to or higher than the nominal nameplate power rating at STC and no individual module power shall be more than 3% below nominal"[21]*.

3.6.7 Ohmic Cabling Losses

The ohmic loss in the DC cabling can be calculated using the standard equation for ohmic losses:

$$P_{cable} = I_{cable} \cdot R_{cable}^2 \tag{3.17}$$

The resistance of a DC cable is given by the following equation:

$$R_{cable} = \rho_{cable} \frac{l}{A} \tag{3.18}$$

In equation 3.17, R_{cable} is the resistance in Ohm, ρ_{cable} [$\Omega\frac{mm^2}{m}$] is the specific resistance of the cable material, l [m] is the cable length, and A [mm^2] is the cross section area of the cable.

Equation 3.18 shows the importance of using a cable material with a low specific resistance, like copper. Furthermore it is important to keep the DC cabling length at a minimum, and have a cross section area that is large enough in order to prevent high ohmic losses and voltage drops[6][p.196-197].

Ohmic losses are often estimated using a value relative to the array output of the PV system, i.e 1 % of the array output at STC, or calculated directly using equations 3.17 and 3.18.

3.6.8 Inverter Losses

As described in chapter 2.2, the inverter efficiency will vary depending on the array output. In addition, additional inverter losses can occur when the array power is outside the operation limits of the inverter. In these cases the array will have potential energy available that cannot be utilized by the inverter.

Inverter losses can to a large extent be avoided by sizing the inverter correctly, although some inverter losses will occur as the array operating characteristics vary.

3.7 Economical Evaluation of PV Systems

For an investor in a PV system, the objective will in most cases be to design and build a PV system that gives a reasonable profit. The regulatory regime of the area where the system is installed and available support schemes are of great importance in this regard.

This chapter present the most important laws and regulations that affects the installation of a PV system in Norway, available support schemes and methods used in economical evaluation of PV systems.

3.7.1 Laws and Regulations

The laws and regulations affecting a PV system can roughly be divided into two categories: Governmental laws regulating the production of electricity, and security and quality regulations set by the local grid-operator.

3.7.1.1 The Surplus Customer Amendment

In 2010, the Norwegian Water Resources and Energy Directorate (NVE) amended the Regulation no. 302 of March 11 1999 in order to facilitate the connection of *surplus customers* to the grid. A surplus customer in this regard means a customer that for a limited period of the year produces more electricity than it consumes. The yearly production should not exceed the yearly consumption, hence the customer should still be a net-consumer of electricity. Furthermore, the generator maximum power can not exceed 100 kVA.

The amendment states that the local grid-operator can buy excess electricity production from the customer at a price agreed to by the grid-operator and the surplus consumer. The surplus customer is not required to make a balancing agreement with Statnett, the national transmission system operator (TSO), which is usually required for grid-connected power producers.

A customer with a roof PV system could be an example of a surplus customer who in periods of high production and low consumption during the summer can supply electricity to the grid[22].

3.7.1.2 Grid-operator Requirements

The local grid-operator will have several requirements before connecting a PV system to the grid. Such requirements could be made with regards to[23]:

- Stable operation of the production source
- Voltage quality
- Component protection
- Phase compensation
- Upper limit for the amount of production fed into the grid
- Grounding

These requirements will vary depending on the local grid and national standards and regulations.

3.7.2 Support Schemes

Different support schemes have been used in order to support the development of renewable energy in different parts of the world. Some of these are[24]:

- Investment subsidies
- Feed-in tariffs
- Environmental taxes
- Electricity certificates

All the different schemes have advantages and disadvantages that will not be discussed in detail here. A "green" electricity certificate scheme has been the main support scheme in Norway since 2012.

3.7.2.1 Electricity Certificates

As of 01.01.2012 Norway is part of a common green certificate market with Sweden with the goal of increasing renewable energy production by 26,3 TWh before the end of 2020[25].

The green certificate system is a combined tax and subsidy system. Producers of new renewable energy receives one certificate per MWh produced from their facility which can be sold, hence providing an added value to the power production. Consumers are required by law to buy a certain amount of certificates depending on their total electricity consumption, and the price of the certificates is determined by supply/demand balance[26]. Figure 32 shows the price development in the common certificate market in 2012.

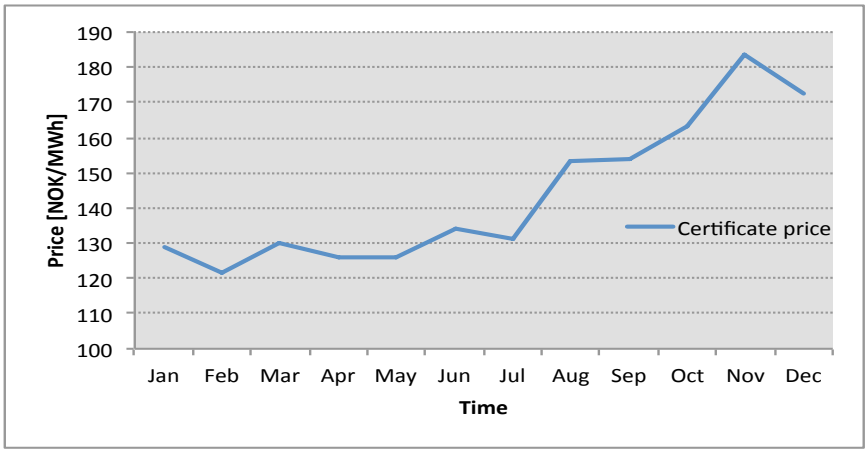

Figure 32: Price development for electricity certificates in 2012.

3.7.2.2 Other Support Schemes

Enova, a subsidiary of the Norwegian Ministry of Petroleum and Energy, gives investment support to energy efficiency measures in private households. However, support for roof PV systems is not included in this support scheme today, although solar thermal collectors receives investment support. Investment in a solar collector system receives support equal to 20 % of the total investment cost with a maximum support limit of 10 000 NOK[27].

Innovation Norway, a government organisation promoting innovation, has a support scheme for green buildings. However, this support scheme mainly targets new, innovative projects in the commercial sector[28].

3.7.3 The Net Present Value (NPV) Method

The most common way of evaluating a PV system is by using the net present value (NPV) method. Another alternative is the internal rate of return (IRR) method. The two methods will often lead to similar results. However, as NPV is considered more applicable only this method will be used here.

The first step of an NPV evaluation is to calculate the cash flow for each year of the project lifetime. The net cash flow for a certain year is simply given by the following equation:

$$C_t = I_t - O_t \tag{3.19}$$

Where C_t is the net cash flow of year t, I_t is the cash inflow of year t and O_t is the cash outflow of year t.

The cash flows are then discounted using a discount rate specific to the investment. The discount rate is set in accordance with the risk level of the project, and should reflect other investment options with a similar risk level. Each cash flow is discounted using the equation:

$$P_t = \frac{C_t}{(1+i)^t} \tag{3.20}$$

Where P_t is the present value of the cash flow C_t and i is the discount rate. The present value of the cash flows is summarized in order to calculate the NPV of the project.

$$NPV = \sum_{t=0}^{N} P_t = \sum_{t=0}^{N} \frac{C_t}{(1+i)^t} \tag{3.21}$$

If the NPV > 0, the project is considered profitable[29].

3.7.4 Levelized Cost of Electricity (LCOE)

The Levelized Cost of Electricity (LCOE) is used to evaluate the cost of producing electricity from a power producing facility. The levelized cost is calculated by adding up all system costs, like construction, maintenance and financial costs, and then divide it by the lifetime electricity production of the system[30].

$$LCOE = \frac{Lifecycle\ cost}{Lifetime\ energy\ production} \tag{3.22}$$

For a PV-system, this equation could be expressed more specifically as[30]

$$LCOE = \frac{Project\ cost + \sum_{n=1}^{N} \frac{AO}{(1+i)^n} - \frac{RV}{(1+i)^n}}{\sum_{n=1}^{N} \frac{Initial\ kWh \times (1-SDR)^n}{(1+i)^n}} \tag{3.23}$$

where AO is the annual system operation cost, i is the discount rate, RV is the residual value of the system, and N is the lifetime of the system. SDR is the system degradation rate, that is, an assumed reduction in system output for each year.

The method has clear resemblance with the NPV method, and the LCOE could also be considered as the necessary average value of electricity in order to get an NPV = 0[31].

4. Methodology: Design and simulation of PV systems

This chapter presents suggested PV systems for the farm, and the methodology used in order to find the most suitable systems for the farm. A flow chart illustrating the methodology used is shown in figure 33.

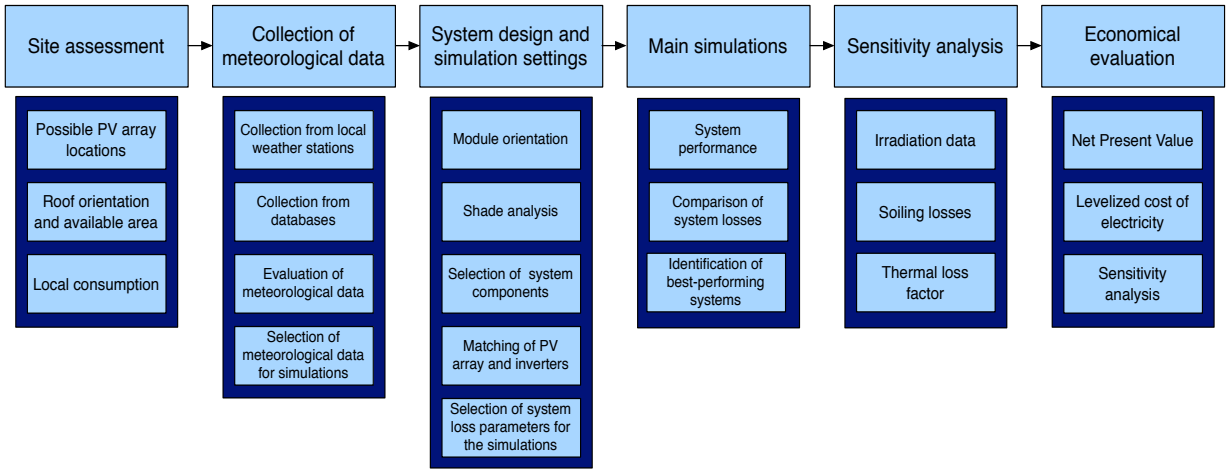

Figure 33: Flow chart of the methodology used in this thesis.

Chapter 4.1 provides a brief introduction to the PVsyst software, which is used in order to design and evaluate systems, and eventually determine the most suitable system for the farm.

Chapter 4.2 presents the results from two site assessments conducted at the farm on February 27th and April 4th 2013.

Chapter 4.3 presents how meteorological data for the simulations was collected and evaluated. The data used in the simulations is presented at the end of the chapter.

The chapters 4.4 to 4.7 present data and conditions used in the simulations, and the reasoning behind the choices made regarding the simulation settings. The first subchapter of these chapters explains how the data and simulation conditions are implemented in PVsyst.

As some of the selected parameters used in the simulations were considered highly uncertain, the best-performing systems in the main simulations were used in further simulations to investigate sensitivies to a change in simulation settings. The settings used in the sensitivity analysis is shown in chapter 4.8

Chapter 4.9 shows the methodology behind the economical evaluation of the different systems and explains the conditions used in the evaluation.

4.1 PVsyst

PVsyst is a simulation tool developed by Dr. André Mermoud of the University of Geneva. The software is considered to be one of the leading tools for simulation of PV systems, and takes into account the different factors described in chapter 3 in order to determine the performance of a PV system. The co-supervisor of the thesis also had prior knowledge of this software.

In March 2013, version 6 of the software was released and version 6.04 was used in the simulations presented here.

PVsyst 6.04 includes both mandatory and optional input sections. The mandatory input sections are:

- Orientation
- System
- Detailed losses

The optional input sections are:

- Horizon
- Near shadings
- Module layout
- Economical evaluation

Furthermore, a site must be specified and meteorological data for the site must be imported unless it is already available in the PVsyst meteorological database.

Both the "Horizon" and the "Near shadings" section is used in order to determine the shading effects on the PV system. However, the "Horizon" section is mainly used for far shadings at a distance larger than ten times the system length from the PV system site[18][Horizon]. As the surrounding area of the site consist of flat fields, only the "Near shadings" section was used in these simulations. The economical evaluation for the suggested PV systems was done separately and hence the "Economical evaluation" section was not used.

4.2 Site Assessment

A site assessment was conducted on February 27th 2013, and the elements described in chapter 3.1 were considered. A second site assessment was conducted on April 4th.

4.2.1 Possible Location of a PV Array

The farm has a total of four roof surfaces facing south. These are the southward-facing roofs on the chicken house, the grain storage building, the vegetable storage building and one side of the garage.

In addition, a new storage facility for vegetables will be constructed during the summer of 2013 which will also have get a southward-facing roof orientation.

An overview of the possible system locations with assigned numbers is given in table 3.

Table 3: Possible locations of a PV array.

Number	Location
1	Chicken house
2	Grain storage
3	Vegetable storage
4	Garage
5	New Vegetable Storage

Figure 34 shows a 3D-illustration of the farm, and figure 35 shows pictures of the different southward-facing roofs. Building 5 is also included in the 3D illustration.

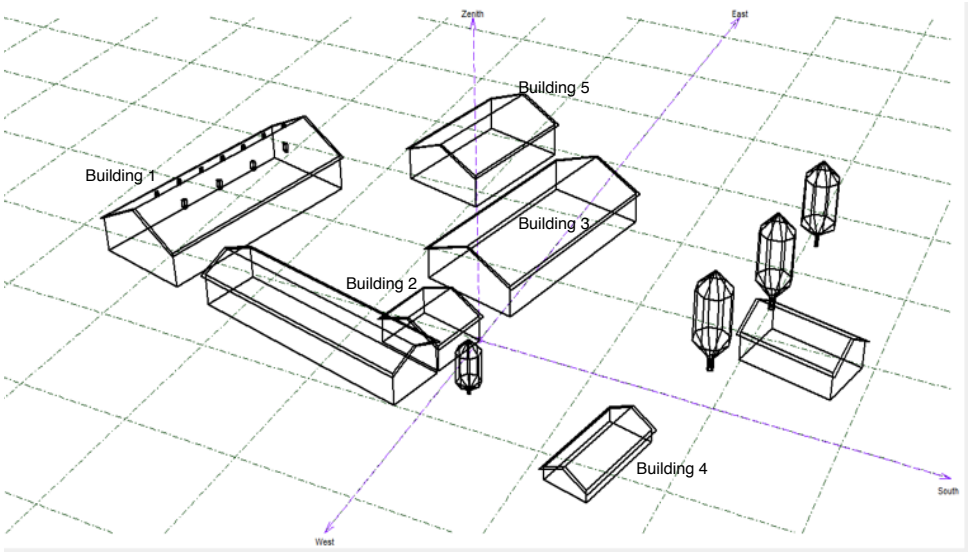

Figure 34: 3D illustration of the farm made in PVsyst.

Figure 35: Southward-facing roofs on the chicken house(upper left), the grain storage building(upper left), the garage(lower left) and the vegetable storage building.

4.2.2 Roof Specifications

The length, width, wall height and tilt angle of each roof were measured. When the tilt angle and the width of the building is known, the width of the southward roof can be calculated using the equation

$$w_{roof,south} = \frac{w_{building}}{2\cos\alpha} \tag{4.1}$$

where $w_{building}$ is the width of the building and α is the roof tilt angle. The approximate area of the southward-facing roof can then be calculated using

$$A_{roof,south} = w_{roof,south} \cdot l \tag{4.2}$$

where l is the length of the building.

The main roof specifications are presented in table 4. As building 5 was not yet constructed, the values given are based on information from the farm owner.

Table 4: Roof specifications

Building	Length[m]	Width[m]	Wall height[m]	Roof tilt angle	Roof width[m]	Southward-facing roof area[m^2]
1	40	18	6	27	10.1	404.0
2	11	12	3	22	6.5	71.2
3	36	18	5.3	22	9.7	349.4
4	16	7.5	1.5	27	4.2	67.3
5	24	16	5.3	22	8.6	207.1

4.2.3 Shading Items

Potential shading items were identified at and near the different buildings.

For Building 1, the ventilators were identified as potential shading elements in a case were solar modules is mounted at the upper part of the roof. These elements are shown in figure 36. The western end of building 1 is located 8 metres away from the northern end of building 2, which could cause shading on the roof of building 1 from building 2.

Figure 36: Shading items on building 1.

Building 2 is situated close to a relatively large tree which could cause a substantial amount of shading. A power distribution line and a utility pole are also located close to building 2.

Building 3 faces several large trees in the southern direction. Elevated terrain in the same direction increases the likeliness of shading effects from these trees on the modules. This is shown in the picture in figure 37.

Figure 37: Shading items south of building 3.

Building 4 has few near shading elements, except for a tree located 15 metres to the south. There are also some buildings located between 100 and 200 metres south, although the impact of these buildings seems negligible.

Building 5 will be located 8 metres north of building 3, hence building 3 is the most significant of the potential shading elements for building 5. The large trees south of building 3 could also cause shading on the roof of building 5.

4.2.4 Possible Mounting Systems

The roofs on buildings 1 and 4 have roof tiles while buildings 2 and 3 have metal roofs. The two roof types will most likely require different mounting solutions.

Building 3 is a steel frame building and the mechanical properties of this roof should be carefully evaluated when selecting a mounting system for this building. Building 5 will also be a steel frame building when constructed.

Roofs in the Rygge area should be able to hold a snow load of up to 300 kg/m^2, and a mounting should meet the same criteria[32].

4.2.5 Possible Location of BoS Components

Some initial thoughts were given to possible locations of the main BoS components, primarily the location of the inverter.

Building 1 has a service room which is currently used for monitoring conditions in the building, like temperature and CO_2 level. This room could be a suitable inverter location, although the relatively small size could become a limitation. The rest of the building is unsuitable for inverter location, as entering this part if prohibited for hygienic reasons for a large part of the year.

Building 2 is the connection point between the farm and the electricity grid, and has several suitable locations for one or more inverters.

Building 3 has several suitable locations for one or more inverters in the centre of the building. Installation of the inverter close to the roof could also be possible in order to limit the necessary amount of DC cabling.

Building 4 is relatively small. Hence the room for inverter installation is limited.

Building 5 is not yet constructed and possible inverter locations were therefore not suggested for this building.

4.2.6 Local Electricity Consumption

The local utility company provided an hourly overview of the site electricity consumption for 2011 and 2012. The load profile of the site is shown in figure 38. The consumption data shows that the consumption is particularly high during the fall. This is due to an extensive demand for cooling in the months following the harvesting of vegetables. As more and more vegetables are delivered to wholesalers and the ambient temperature decreases, the cooling demand also decreases. In June, all the vegetables have been delivered and the remaining electricity demand is due to the required ventilation in the chicken house.

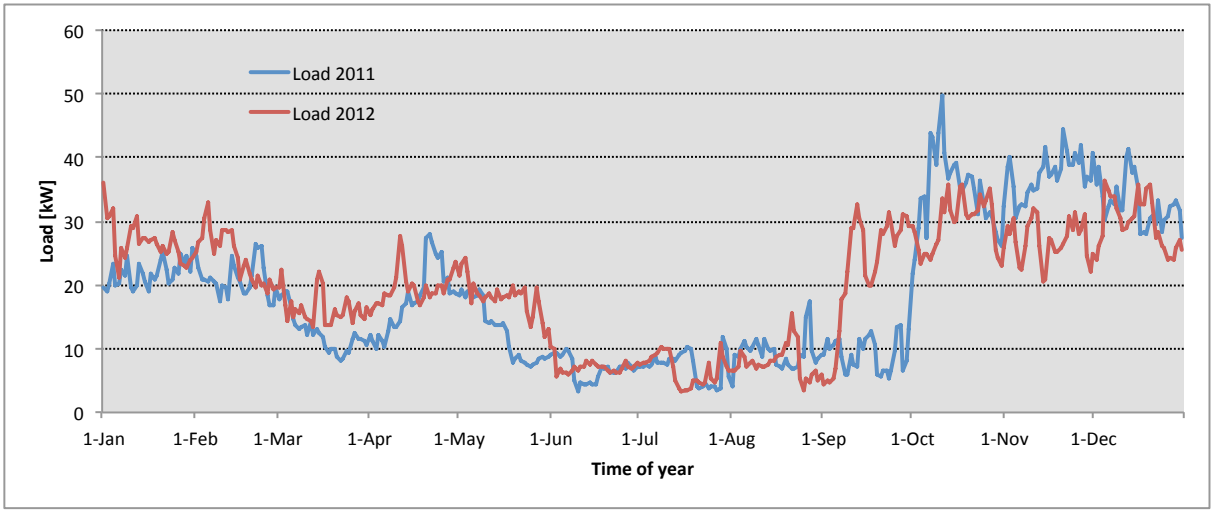

Figure 38: On-site electricity consumption in 2011 and 2012.

A load duration curve for the site was also made. In this curve the load data are arranged in descending order of magnitude. The load duration curve is shown in figure 38.

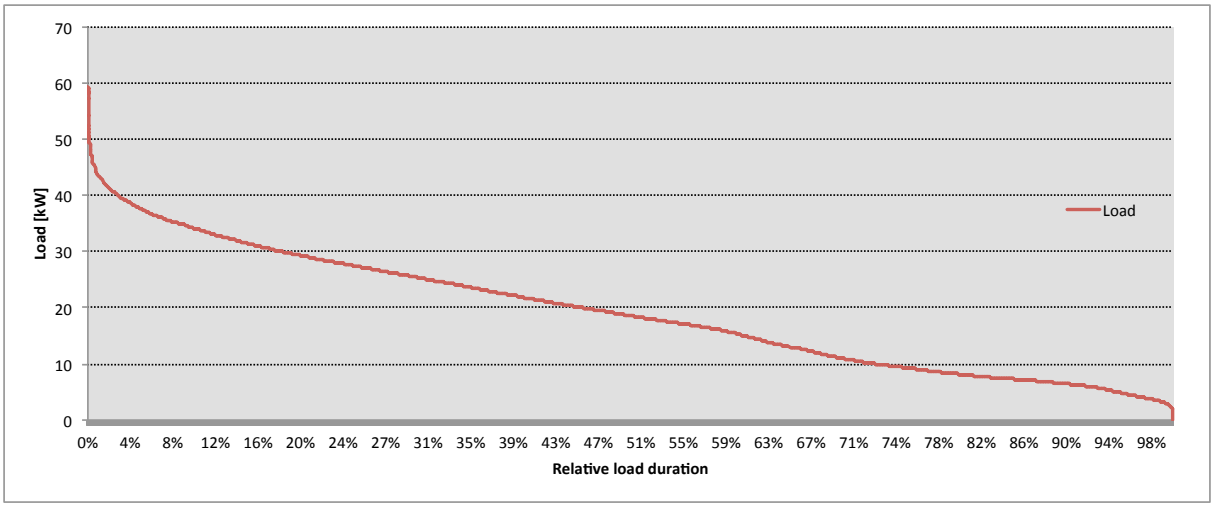

Figure 39: Relative load duration in 2011 and 2012.

The on-site electricity consumption for 2011 and 2012 is shown in figure 39.

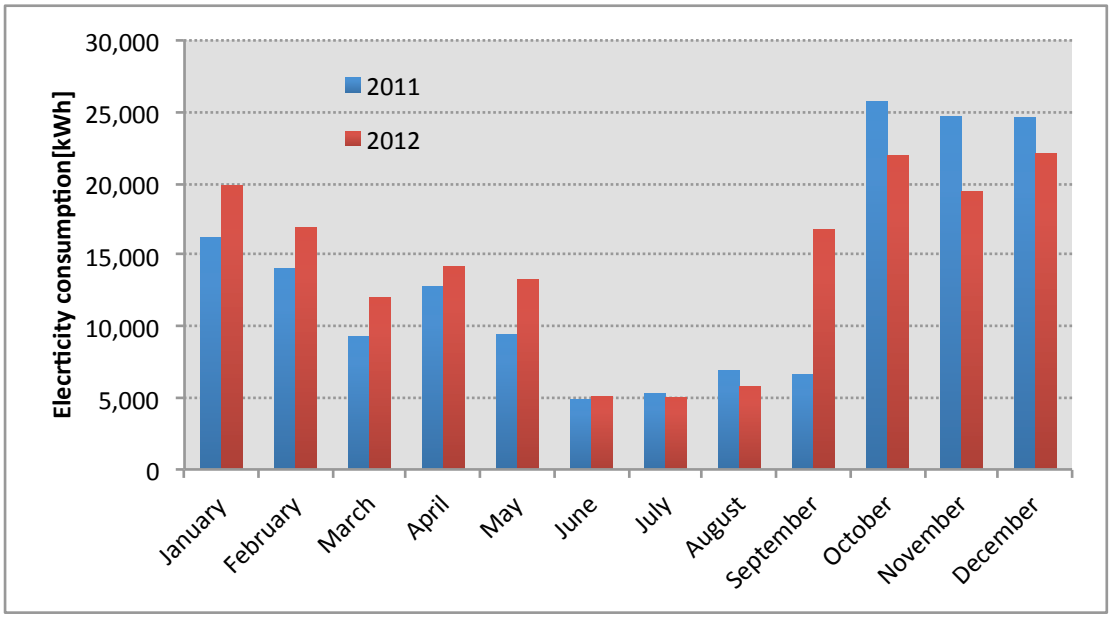

Figure 40: On-site electricity consumption in 2011 and 2012.

4.3 Meteorological Data

Different sources of meteorological data were assessed to get an overview of the potential for solar power production at the site.

The sources can be divided into two categories: Meteorological data from weather stations located close to the site, and data collected from different databases constructed from satellite data or by use of interpolation between weather stations. While there are a limited number of relevant weather stations, there are several providers of interpolated data concerning global and diffuse irradiation, temperature and wind speed.

4.3.1 Meteorological Data in PVsyst

In PVsyst, the latitude and longitude are used as input in order to calculate the solar paths for a given site. This is done using the theory and equations described in chapter 3.2. Figure 41 shows an example of solar paths calculated by PVsyst.

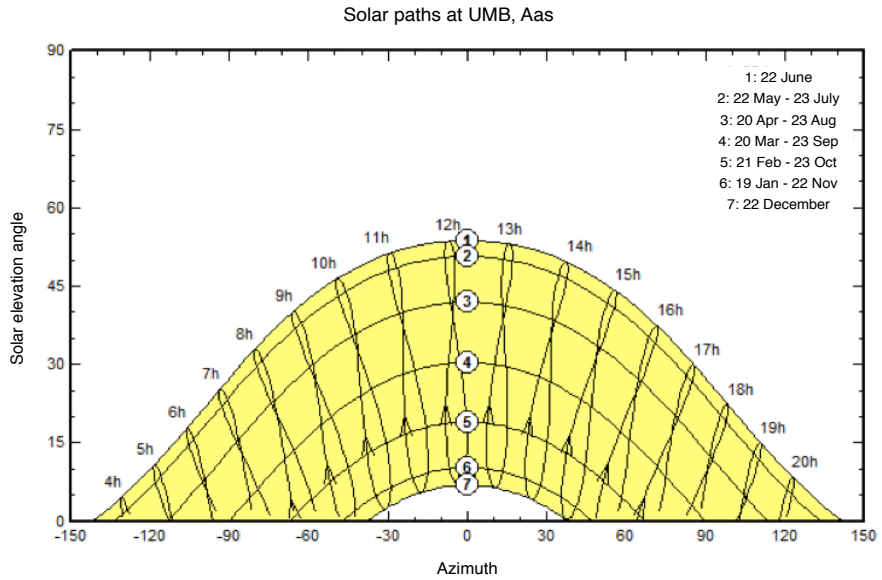

Figure 41: Solar paths for different times of the year generated in PVsyst.

PVsyst allows for import of meteorological data with different formats. However, in order to perform a simulation the program requires hourly values for the following parameters[18][Synthetic hourly data generation]:

- Global irradiance on the horizontal plane
- Diffuse irradiance on the horizontal plane
- Ambient temperature
- Wind velocity

PVsyst has built-in mechanisms for the generation of diffuse irradiance data and wind velocity data, hence global irradiance and ambient temperature are the data that must in any case be provided by the user. Nevertheless, the result of the simulations will be more accurate if all parameters for the site are available.

As the meteorological data collected for this site consists of monthly average irradiation values and monthly average temperatures, the "Synthetic hourly data generation" function was used to generate hourly values for the irradiance and temperature data.

Hourly irradiance values are constructed using a transposition mechanism that is closely linked to the solar geometry described in chapter 3.2, and the latitude and longitude of the site is therefore used as an input to calculate the solar path of each day. Daily values are then created using probability matrices based on data from different weather stations. Finally, hourly values are generated using a Gaussian model. An example of generated hourly irradiance values for one day is shown in figure 42.

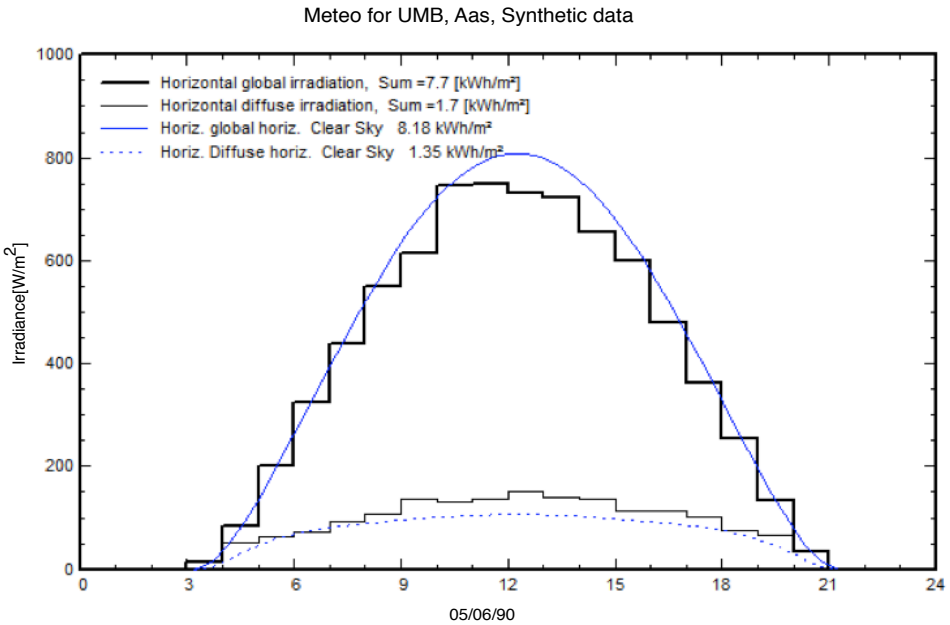

Figure 42: Example of synthetic hourly irradiation values generated in PVsyst.

As for the generation of hourly temperature values, the model used is less general and mainly based on Swiss meteorological data. Temperature will typically take a sinusoidal function with a phase shift of between two and three hours from the irradiance function. The generated temperature values are therefore slopes based on amplitude and phase shift values from Swiss regions, and monthly average temperatures supplied by the user are used as constraints in the generation.

Hourly values are not generated for the wind data, as a general model for such a transposition is unavailable and most likely non-existent. The monthly average values are therefore used. However, wind data are only used in order to estimate the wind component of the U-value for the module as shown in equation 3.16 and will hence only have a limited impact on the simulation results[18].

4.3.2 Meteorological Data from Local Weather Stations

Data from four weather stations were assessed. Table 5 displays information about the different stations and the available variables at each station.

Table 5: Relevant weather stations in the Rygge area.

Location	Operator	Distance to site[km]	Distance to coast[km]	Available variables
Rygge	MET	2.2	4.4	Temperature, Wind speed
Ås	UMB	35	8	Global, Diffuse, Temperature, Wind speed
Ås	Bioforsk	35	8	Global, Temperature, Wind speed
Øsaker	Bioforsk	18	15	Global, Temperature, Wind speed

The weather station in Rygge is located at the Rygge Airport close to the Roer Farm, and has been operated by the Norwegian Meteorological Institute (MET) since 1955. It is therefore considered to contain relevant temperature and wind data for the site. However, no irradiation measurements have been made at this station. The data from MET was collected at their online weather- and climate database called eKlima.

The weather station operated by the Norwegian University of Life Sciences (UMB) has been in operation since 1859, and data from this station have been used by MET since 1885. The irradiation data used in this thesis are monthly averages of data recorded between 1983 and 2012 and collected by Grimenes and Thue-Hansen[33].

The Bioforsk station in Ås has been in operation since August 1991 and hourly values for global irradiance, temperature and wind speed has been recorded since then. However, a significant amount of values are missing from the first years of operation. The irradiation data shown here is therefore recorded between 1993 and 2012. The Bioforsk station in Øsaker has been in operation since October 2004, and global irradiance, temperature and wind data has been recorded since then. The irradiation data shown here is recorded between 2005 and 2012. Data from the two Bioforsk stations were collected from the Bioforsk website[34].

A comparison of the annual global irradiation data from the different sources is shown in figure 43.

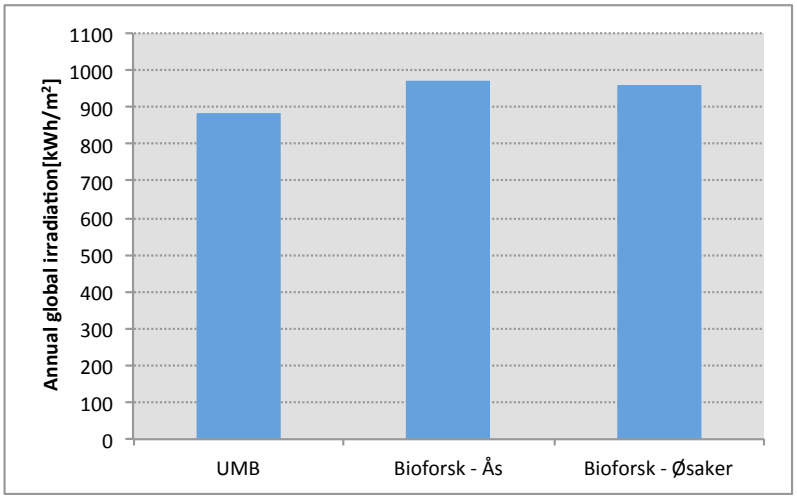

Figure 43: Measured values for annual global irradiation on the horizontal plane.

A comparison of the monthly global irradiation values for the different weather stations is shown in figure 44.

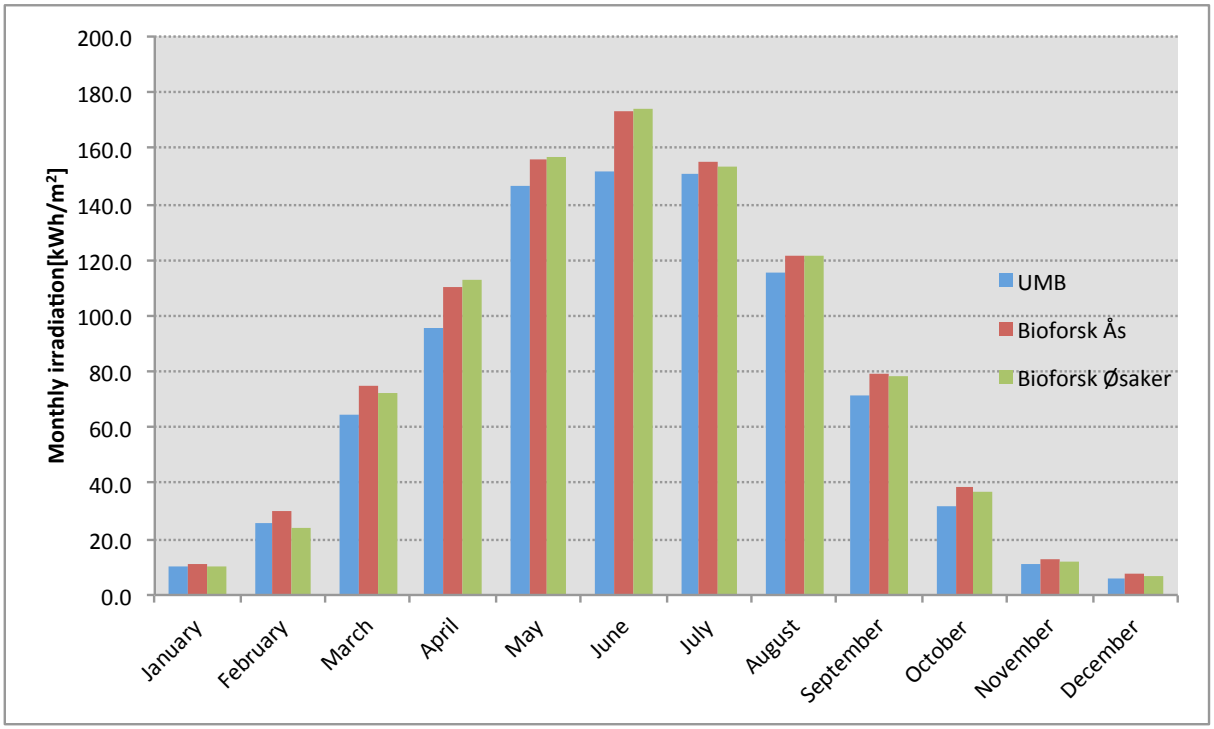

Figure 44: Measured values for monthly global irradiation on the horizontal plane.

Although the collected irradiation data show similar values during the winter and fall, there are relatively large variations in the irradiation data for the spring and summer months.

Table 6 shows the monthly average temperature and wind speed values from the different weather stations. The values from the MET station are averages of homogenized values recorded between 1961 and 1990. The values from UMB are also 1961-1990 averages for comparison with the MET values. The values for Bioforsk Øsaker are 2005-2012 averages, as this weather station was opened as late as in 2004.

Table 6: Average temperature and wind speed data.

	MET		UMB Ås		Bioforsk Øsaker	
	T[°C]	Wind[m/s]	T[°C]	Wind[m/s]	T[°C]	Wind[m/s]
Jan	-4.1	3.5	-4.8	2.6	-2.8	1.9
Feb	-4.2	3.2	-4.8	2.6	-3.6	1.6
Mar	-0.4	3.6	-0.7	2.6	-0.3	1.7
Apr	4.2	3.8	4.0	2.7	5.9	1.9
May	10.3	3.9	10.3	2.8	10.7	2
Jun	14.7	4.1	14.7	2.8	14.3	1.8
Jul	15.9	3.9	15.9	2.5	17	1.5
Aug	14.9	3.6	14.7	2.4	15.6	1.4
Sep	10.8	3.7	10.6	2.6	12.2	1.9
Oct	6.8	3.7	6.2	2.5	6.7	1.7
Nov	1.2	3.6	0.5	2.6	3.2	2.1
Dec	-2.5	3.5	-3.4	2.5	-2.4	1.5
Average	5.6	3.7	5.3	2.6	6.4	1.8

Table 7 shows average snow depth at the MET weather station between 1961 and 1990. Apparently, snow is present mainly during the winter months and in March. The average values for April, October and November are very low and most likely caused by extreme incidents during some years.

Table 7: Average snow depth in Rygge.

Month	Snow depth[cm]
January	12.0
February	17.7
March	13.4
April	2.7
May	0.0
June	0.0
July	0.0
August	0.0
September	0.0
October	0.1
November	2.0
December	5.7

4.3.3 Meteorological Data from Databases

An overview of the four databases that were consulted is shown in table 8. When meteorological data from databases were collected, the site coordinate of 59°21'58''N,10°44'57''E was used.

Table 8: Databases used to collect meteorological data for the site.

Database	Values	Source	Available variables
Meteonorm	Monthly	Interpolation between terrestrial stations	Global, Diffuse, Temperature, Wind speed
PVGiS	Monthly	Interpolation between terrestrial stations	Global, Diffuse, Temperature
Satellight	Hourly	Meteosat	Global
NASA SSE	Monthly	Transposition of satelitte data	Global, Temperature, Wind

The Meteonorm database contains measurements from about 1 200 different weather stations, and uses the stations closest to the site to construct weather data based on interpolation. The data collected for the Rygge area is based on measurements made between 1986 and 2009. The Meteonorm database is software that requires a license[35].

The PVGIS database contains measurements from 566 weather stations around Europe over the period 1981 to 1990. The PVGIS website can be used to create a monthly average data set for any location in Europe based on interpolation between the closest stations. Use of this database is free and does not require registration[14].

The Satellight database is based on hourly satellite data from Meteosat, measured in the time period 1996 – 2000. A dataset containing monthly means of daily sums can be constructed for any location in Europe. The Satellight database is free to use although registration is required.

The NASA SSE 6.0 database consists of NASA satellite data collected between 1983 and 2005. These data are hence extraterrestrial values which have been transposed to ground level by the use of transfer models taking into account cloud coverage and other atmospheric effects. The transfer models have then been validated by using data from ground stations[36].

A comparison of the annual global irradiation values collected from the databases is shown in figure 45.

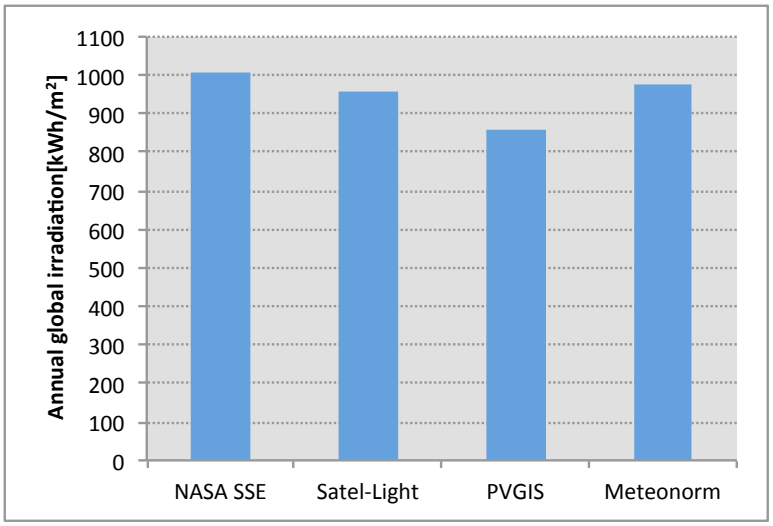

Figure 45: Annual global irradiation on the horizontal plane from different databases.

A comparison of the average monthly irradiation from the different databases is shown in figure 46.

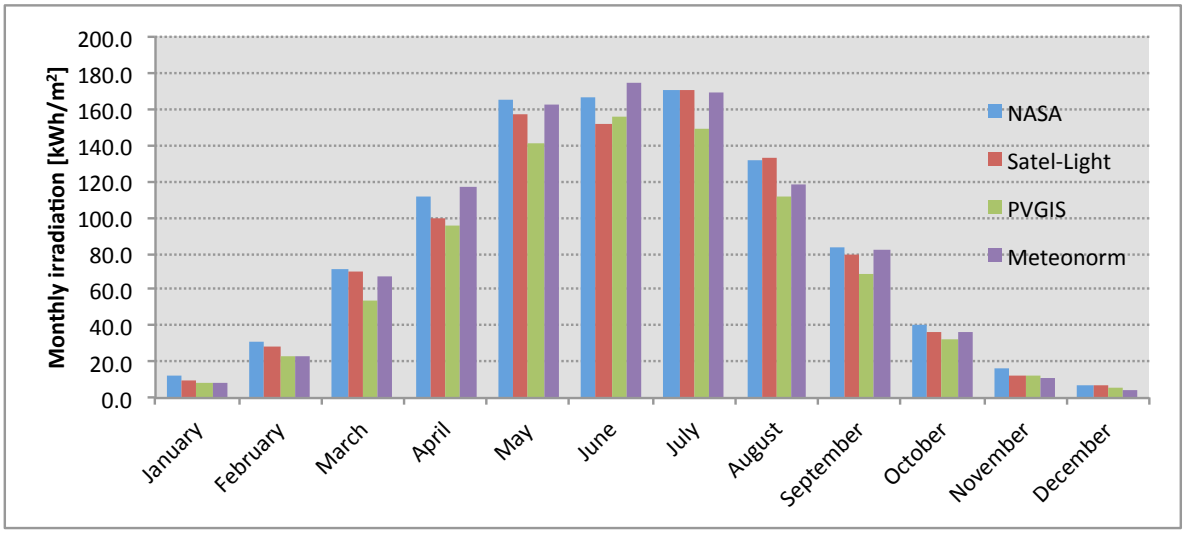

Figure 46: Monthly global irradiation on the horizontal plane from different databases.

4.3.4 Selection of Meteorological Data

The collected meteorological data shows variations in data concerning global irradiation, temperature and wind variables. There could be several reasons explaining some of the relatively large differences, including:

- Climatic distances between weather stations. The climatic distance is the vector sum of the ground distance and the difference in altitude between two stations. The weather stations are located at different sites and cannot be expected to hold identical data.
- Large differences in the length of the data series. The shortest data collection period is five years, while the longest is 30 years. This will significantly affect the data values due to statistical variations in the climate.
- Differences in methodology. For the weather stations, this will be how the data is recorded, the quality of the equipment used and differences in how homogenization of the data is done, and how the issue of missing data is treated.
  For the databases the differences in methodology could include the incorporation of micrometeorological effects, different interpolation methods and, obviously, the difference in the data used in the interpolations.

Considering these factors, it is difficult to determine the reliability of the different data sets. Due to the assumed importance of particularly the irradiation data for the performance of a PV system, three different meteorological data sets were created, and used in the simulations in order to further investigate the impact that these uncertainties have on the system yield.

As the MET station in Rygge is located closest to the site and has long, homogenized time series for temperature and wind data, the temperature and wind averages from this station was used in all the meteorological data sets.

The soiling loss settings evaluated in chapter 4.7.6 are also based on snow cower data from the MET station in Rygge.

Meteoset A was used in the main simulations. This dataset includes global and diffuse irradiation data from the UMB weather station in Ås, and temperature and wind data from MET. The climatic distance between the weather station and the site is low, and the UMB weather station has the longest time series of the weather stations considered.

Table 9: Meteoset A.

	Global [kWh/m^2]	Diffuse[kWh/m^2]	T[°C]	Wind speed[m/s]
January	9.9	6.8	-4.1	3.5
February	25.9	15.4	-4.2	3.2
March	64.7	31.2	-0.4	3.6
April	95.5	46.9	4.2	3.8
May	146.5	60.3	10.3	3.9
June	151.9	62.6	14.7	4.1
July	150.9	64.6	15.9	3.9
August	115.3	49.8	14.9	3.6
September	71.6	31.3	10.8	3.7
October	32.1	16.9	6.8	3.7
November	11.1	7.3	1.2	3.6
December	5.8	4.2	-2.5	3.5

Meteoset B consists of global and diffuse irradiation data from PVGIS, and temperature and wind data from MET. The PVGIS data set holds the lowest irradiation values of the considered databases. Use of these values could hence provide a possible worst-case scenario with regards to system yield.

Meteoset C consists of global and diffuse irradiation data from Meteonorm, and temperature and wind data from MET. The Meteonorm set is based on a long time period of measurements and also has some of the highest yearly irradiation values of the considered databases. Hence this dataset could provide a possible best-case scenario for annual system yield.

In order for PVsyst to take into account the effect of reflected diffuse radiation, the albedo values for the site must be given as an input. The albedo values, ρ, used in these simulations were based on the snow cover data shown in table 7, an evaluation of the system surroundings, and the general albedo values shown in table 2.

Table 10: Albedo values used in the simulations.

Month	Albedo value
January	0.70
February	0.70
March	0.60
April	0.20
May	0.20
June	0.20
July	0.20
August	0.20
September	0.20
October	0.20
November	0.20
December	0.60

The values in January, February, March and December was changed from the default value of 0.20 to reflect the likeliness of snow in the surrounding areas in those months. However, due to the small amounts of irradiation received during the winter months and the possibility of snow cover on the modules, the impact of these changes is assumed to be limited.

4.4 Module Orientation

The general impact of tilt and azimuth angle on PV system performance is described in chapter 3.3.

4.4.1 Tilt and azimuth angle in PVsyst

In the "Orientation" section of PVsyst, several configurations can be chosen including:

- Fixed tilted plane
- Seasonally adjusted plane
- Two axis tracking system
- One axis tracking system
- Two heterogeneous planes

The fixed tilted plane is the only relevant configuration in this case, and the tilt and azimuth angle of the array are the two main input parameters. The yearly irradiation value on the horizontal plane from the meteorological data is then transposed to the module plane, and the global irradiation on the module is shown.

PVsyst can be used to find the optimum tilt and azimuth angle. The software then uses equation 3.8 and calculates a set of transposition factors, R, in order to determine the maximum possible amount of irradiation on the array. The program will in any case show the transposition factor R for the given tilt and azimuth angle, and the percentage loss by respect to the optimum orientation of the array. The transposition mechanism then uses the monthly meteorological data and an evaluation of module orientation and latitude to create "Average days", where a "Clear day" profile is created for one day at the middle of each month. The amplitude of the clear day profile is fitted to the monthly irradiation. This day is used to represent all days in the given month. The transposition values could therefore deviate by a few per cents compared to the transposition done in the actual simulations, which uses the synthetic hourly data.

4.5.2 Tilt angle

As described in chapter 3.3 the impact of the system tilt angle is site-dependent and will also depend on whether the system is to be optimized for a maximum yearly yield, or a maximum seasonal yield. It will also be dependent on the ratio of diffuse irradiation to global irradiation, and thus vary depending on the meteorological data.

Using equation 3.7, the ideal tilt angle for a system at this site would be equal to:

$$\beta_{opt} \approx 59°$$

However, the PVsyst optimization tool suggest that the optimal tilt angle is within the range:

$$\beta_{opt} \approx 42° - 47°$$

Variations in tilt angle within this range will mainly affect the seasonal distribution of the yield.

Although some mounting systems exist that facilitates a difference between the roof angle and the module angle, these systems are rare and their suitability and effectiveness for the given area is highly uncertain. Hence the modules were in this case assumed to have a tilt angle equal to the roof tilt angle.

The tilt angles for the modules on the different roofs are shown in table 11.

Table 11: Module tilt angles for the different roofs.

Roof number	β
1	27°
2	22°
3	22°
4	27°
5	22°

4.4.3 Azimuth angle

The optimum azimuth angle is direct south. However, in this case the azimuth angle of the modules will be determined by the orientation of the buildings. The orientation of the buildings and hence the azimuth angle of the modules are shown in table 12.

Table 12: Azimuth angle for the different roofs.

Roof number	γ
1	13°
2	13°
3	13°
4	13°
5	13°

4.4.4 Evaluation of the Tilt and Azimuth angle

As observed in table 11 and table 12, neither the tilt nor the azimuth angle is optimal when a maximum yearly yield for the system is desirable. Using the transposition mechanism in PVsyst and Meteoset A, table 13 was created. This table shows the difference in R and thus the difference in yearly irradiation on the inclined plane for the different roof angles, and the loss with respect to a tilt angle of $\beta = 42°$ and $\gamma = 0°$.

Table 13: Irradiation losses with respect to optimum tilt and azimuth angle.

	H_G	β	γ	R(β,γ, D/G)	H_{plane} [kWh/m²/year]	Loss by respect to optimum[%]
Optimum	880	42	0	1.32	1162	0.00%
Building 1 and 4	880	27	13	1.26	1107	4.73%
Building 2,3 and 5	880	22	13	1.22	1077	7.31%

4.5 Shade Analysis

A shade analysis was conducted in order to evaluate the shading on the different roofs. As previously described, shading losses from a PV system can be divided into one irradiance loss component and one electrical mismatch loss component. For a tilted roof with a fixed orientation, there is not much that can be done about the irradiance losses caused by shading objects. However, if the string design is done properly, the shading can be limited to as few strings as possible and hence reduce the electrical mismatch losses.

4.5.1 Shade Analysis in PVsyst

In the "Near shadings" section of PVsyst a 3D-construction of the site can be made in order to perform a shade analysis of the array area. As described in chapter 3.4, the electrical effects of shading are complex and dependent on module layout, string configuration and the use of bypass-diodes.

PVsyst treats the three different irradiation components H_B, H_D og H_R differently, as only the shadow effect on the direct beam component H_B is dependent on the sun´s position. The shading of H_D and H_B is considered to be constant through the year and only dependent on the system geometry[18][Near shadings].

There are four options in the "Near Shadings" section of PVsyst:

- No shadings
- Linear shadings
- Accoring to module strings
- Detailed, according to module layout

The *no shadings* option simply means that no shading effects will be taken into account in the simulation and losses caused by shadings will be non-existent.

The *linear shadings* option will give a loss equal to the irradiance on the shaded fraction of the array. That is, if 50% of the array is shaded, only the irradiance loss due to this shading is considered, and the electrical losses due to mismatch between the modules are ignored. This is a non-accurate approach, as only limited shading on a string could cause severe reductions in the string output due to electrical mismatch effects.

Shading according to module strings provides an option to reduce the string output by a certain percentage as soon as a part of the string is shaded. The user determines what percentage fraction the software should apply in order to better represent the non-linear electrical losses caused by the shading.

In reality, neither the *linear shadings* option nor *shadings according to module strings* represents an accurate description of the total shading effects. However, the shading effects is likely to be somewhere in between *linear shadings* (best case) and *shading according to module strings* at 100%(worst case)[18][Partition in module strings].

Detailed, according to module layout considers the mechanical and electrical layout of the modules, which is given by the user in the "Module layout" section of PVsyst. Assuming that the modules have been accurately located and attributed correctly to their respective strings, this option will give an overview of the irradiance losses and the electrical mismatch losses separately at the end of the simulation[18][Shadings, Detailed electrical losses].

4.5.3 Evaluation of the Near Shadings

A shade analysis was made for the different roofs using the "Near shadings" feature in PVsyst. Figure 47 shows screen dumps from the shade analysis.

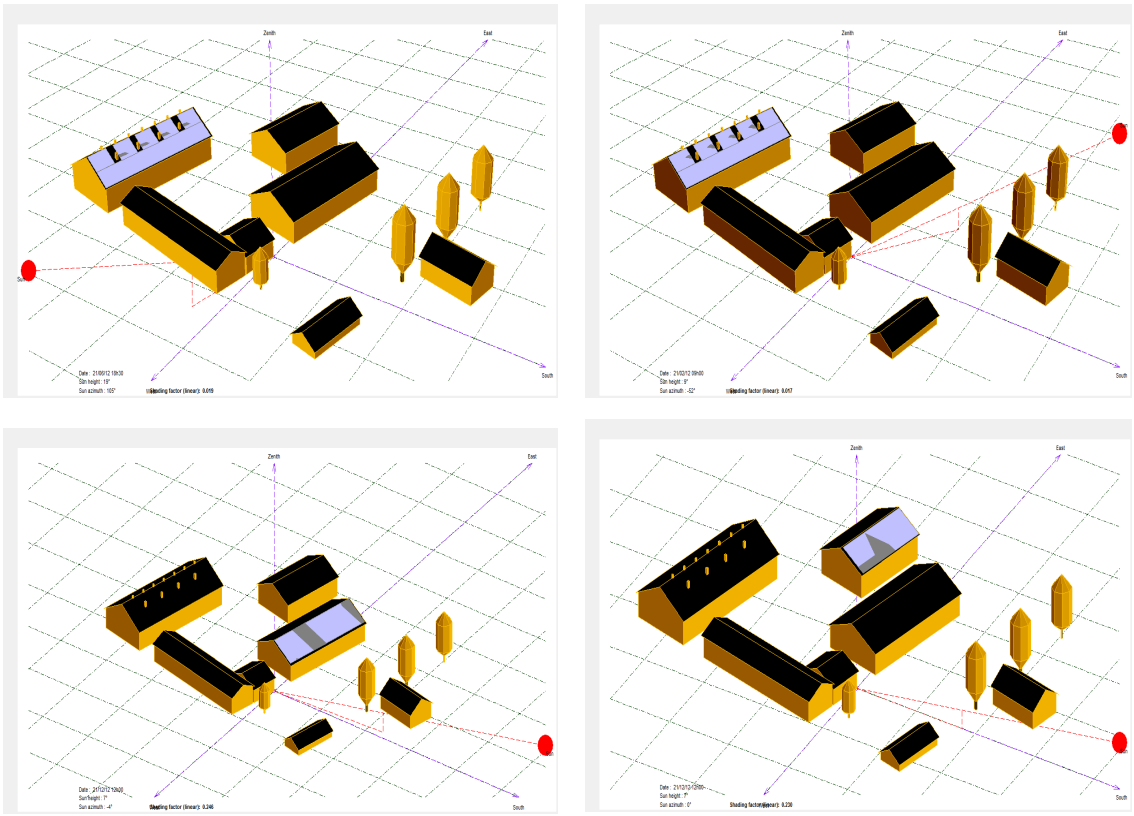

Figure 47: Screen dumps from the shade analysis in PVsyst.

Roof 1,3 and 5 were those considered in the shade analysis, as roofs 2 and 4 are relatively small and their potential for power production therefore limited.

The direct irradiation losses caused by shading at the different roofs were determined at December 21(winter solstice) and further for the 21st of each month until June 21(summer solstice). Table 14 shows the relative direct irradiation losses for each of the buildings on these dates.

Table 14: Percentage shading loss of direct irradiation for different dates.

	Building 1	Building 3	Building 5
December 21st	4.2%	24.2%	21.9%
January 21st	0.5%	18.8%	8.5%
February 21st	0.2%	1.6%	0.7%
March21st	0.2%	0.0%	0.0%
April 21st	0.3%	0.0%	0.0%
May21st	0.3%	0.0%	0.0%
June21st	0.3%	0.0%	0.0%

The meteorological data collected in chapter 4.3 showed that the amount of irradiation during the winter months are low and the diffuse fraction of the irradiation is large. Furthermore, the site snow data suggested that snow could be present on the modules during these months. Hence shading on the modules during the winter is not necessarily critical with regards to the yearly system yield.

PVsyst was also used to create iso-shading diagrams, which shows the percentage fraction of direct irradiance losses on a roof when the sun is located at different angles. The diagrams show the 1%, 10% and 20% iso-shading curves. The diagrams also show an estimated year-round

attenuation factor for the diffuse component of the irradiation, H_D, and the reflected irradiation, H_R.

Building 1 has low irradiation losses due to shading, although it is the only one of the three buildings that experiences irradiation losses during spring and summer. This can be observed in figure 48 where the 1% iso-shading curve is crossing the sun paths for the entire year. This shading is caused by the ventilators on the roof of the building, and is particularly high in the morning and evenings, as the sun is lower at these times of the day.

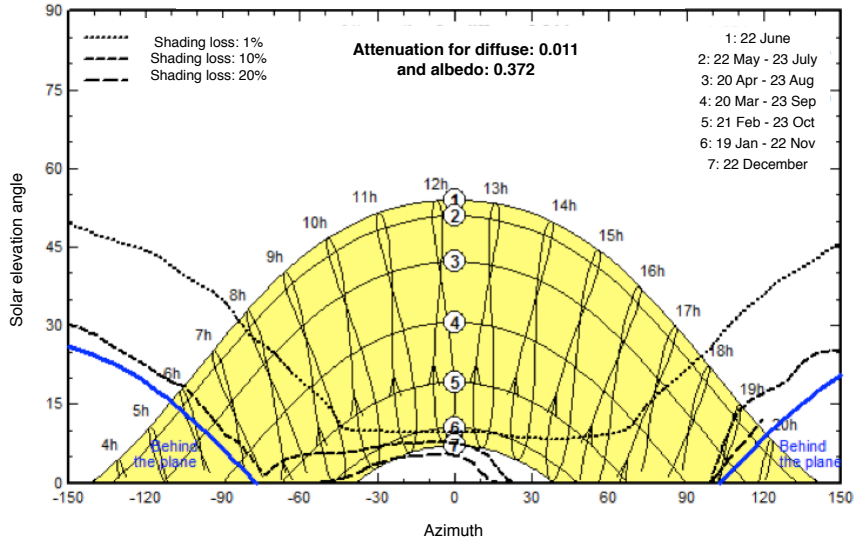

Figure 48: Iso-shading diagram for building 1 generated in PVsyst.

The shade on building 3 is mainly present during the winter months, and in figure 49 it can be observed that the 1% iso-shading curve does not cross the sun path at all between 20th of April and 23rd of August. The 10% and 20% iso-shading curves are present around the center of the sunpaths. Particularly between October 23 and February 21 the direct irradiance losses are more than 10% for many sun positions. Most of this shading is likely caused by the trees located directly south of the building.

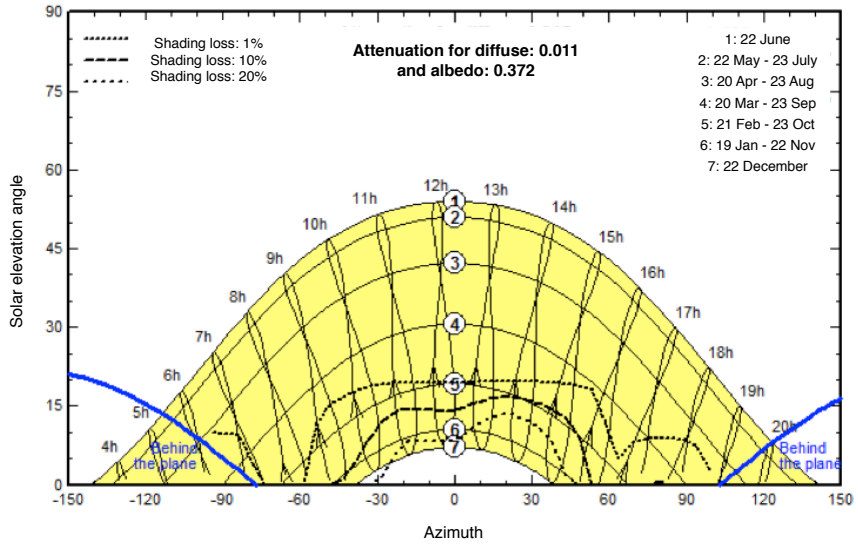

Figure 49: Iso-shading diagram for building 3 generated in PVsyst.

The shading curves for building 5 are similar to those of building 3. However, the curves for building 5 are lower as the distance to the southward trees are higher. Also, the attenuation factor for diffuse irradiation is higher for this building, most likely because building 3 is limiting the amount of reflected irradiation on building 5.

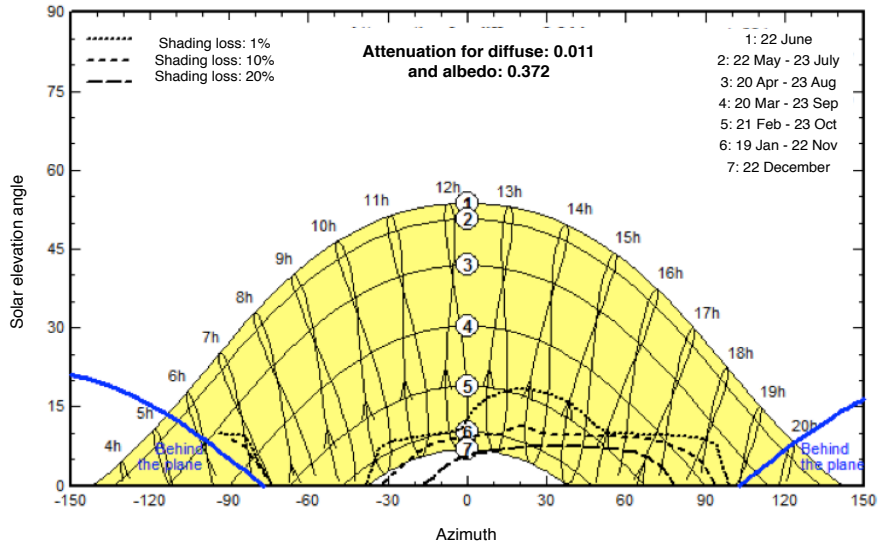

Figure 50: Iso-shading diagram for building 5 generated in PVsyst.

The initial shade analysis showed that the yearly shading patterns are different for the three largest buildings on the farm, although neither of the buildings was considered unsuitable for a PV system when evaluating the shading on the roofs. However, the string assignment for each roof took into account the different shading issues on the roofs, and was made in order to limit the shading to as few strings as possible.

4.5.4 Selection of Near Shadings settings

In the simulations made, the *"Detailed, according to module layout"* option for shading losses was used. This option gives the most realistic results with respect to shading losses, and also shows how the losses are distributed between irradiation losses and electrical mismatch losses.

The use of this option required that a detailed module layout was made for each of the simulated systems. This layout also had to show the string configuration of the modules in order to correctly calculate the electrical effect of the shading.

4.6 System Design and Component Selection

Meteorological data and shade are site- and roof specific sizes. When these were assessed, different systems were simulated in order to find the best-performing systems for different roofs. This chapter presents the selection of the two main components, the modules and the inverters, as well as methodology behind the string sizing and module layout.

4.6.1 System Design in PVsyst

The "System" section of PVsyst serves mainly two purposes:

1) Estimation of the necessary amount of modules and inverters given an available area or a desired power output.
2) String sizing and matching of array and inverter in accordance with the variations in voltage levels that occurs due to variations in array operating temperature.

PVsyst contains a wide selection of modules and inverters including the characteristics for each of the components. PVsyst uses the previously described one-diode model in order to characterize the module behaviour at different operating conditions. Data for modules and inverters are mainly provided by the manufacturers themselves[18].

As illustrated in chapter 3.5, the operating voltage of an array or a string will vary depending on the operating temperature and irradiance level. By defining site-specific temperatures for the system, PVsyst calculates the lower and upper voltage limit of a module and suggests a minimum and maximum amount of modules in one string for a given inverter.

The necessary design temperatures are:

- Absolute minimum operating temperature
- Winter operating temperature
- Usual operating temperature under 1000 W/m^2
- Maximum summer operating temperature

The absolute minimum operating temperature is used to determine the maximum operating voltage of the array, and is the lowest temperature that the array will experience. This value is equal to the lowest ambient temperature at the site.

PVsyst uses *the winter operating temperature* in order to ensure that the string voltage does not exceed the upper limit of the MPPT function of the inverter.

The *usual operating temperature under 1000 W/m^2* is not used by PVsyst as a design parameter, and is included to calculate the common operating voltage of the array. Since the inverter efficiency will change depending on the array voltage, the usual operating voltage should preferably be close to the maximum efficiency voltage of the inverter.

The *summer operating temperature* is used to prevent that the string voltage becomes lower than the lower limit of the inverter MPP tracking function during summer operation.

4.6.2 Selection of Modules

A wide selection of modules is available at the world market today. As modules are fairly easy to transport, most of these modules will also be available in the Norwegian market. Different technologies were used in the simulations for comparison. A site-specific set of criteria was made in order to narrow down the amount of possible modules for the simulations. These are shown in table 15.

Table 15: Module selection criteria.

	Technology	Requirement
Min. module efficiency @STC	Mono-Si	14%
	Poly-Si	14%
	CIS	12%
Mechanical strength	All technologies	Minimum 2400 Pa
Certifications	All technologies	IEC61646/IEC61215, IEC61701(salt mist corrosion test), ammonia resistance
Warranties	All technologies	5 years workmanship and 80% power output after 20 years
Tolerance	All technologies	3% or less

As the available roof area is a limiting factor for the PV system, the efficiency of the selected modules should be in the upper part of the efficiency range for their respective types.

Due to the possible snow loads at the site, the modules should be able to handle a mechanical load of minimum 2400 Pa, and preferably 5400 Pa, which is a common requirement in snowy areas[6][p.182].

Furthermore, the modules should be certified in accordance with the IEC61646 or IEC61215, which are the design qualification and type approval for thin film modules and crystalline modules, respectively. Finally, as the site is located near the coast in an agricultural district, the modules should be IEC61701 certified and also have a recognized ammonia resistance certification.

The selected warranty criteria are made in order to ensure an acceptable system output throughout the lifetime of the system. The module tolerance value should ideally be as low as possible, and 3% is set as an absolute maximum value in order to minimize the mismatch losses.

Based on the criteria given in table 15 and an evaluation of available modules, the following modules were selected for use in the simulations:

1) **REC Peak Energy series – REC250PE**
   The REC250PE is a polycrystalline silicon module from Norwegian manufacturer Renewable Energy Corporation (REC). This specific module has a nominal power of 250 W and meets all the given criteria.

2) **Suntech STP series – SPT250S – 20/Wd**
   The Suntech STP250S-20/Wd is a monocrystalline silicon module from Suntech, currently the world´s largest producer of solar modules. The module used in the simulations has a nominal power of 250 W and meets all the given criteria.

3) **Solar Frontier – SF165-S**
   Solar Frontier is a Japanese manufacturer which main focus is production of thin film CIS-modules. Thin film modules are, in general, known to perform well at low irradiance levels, and could therefore prove to be an interesting alternative in northern climates.

It should be underlined that the author has no indication that these modules are either better or worse than other, similar modules. Nevertheless, it would have been unfeasible to simulate all modules meeting the given requirements, and the availability of the selected modules were assumed to be good. Furthermore, the selected modules represented three different types of technologies, making it possible to compare the simulated performance of these.

4.6.3 Selection of Inverters

The selection of inverter differs from the selection of modules, as inverter selection should not only take into account the properties of the inverter. The inverter configuration must also be determined.

The following inverter types were be used in the simulations:

1) **SMA Solar – Sunny Tripower series**
   SMA Solar is the largest inverter manufacturer in the world and has a wide range of both string and central inverters. The tripower series are tri-phase inverters with a high number of DC-inputs and two MPPTs per inverter. These inverters also have a wide MPPT voltage operating range.

2) **Eltek Valere – Theia He-t series**
   Eltek Valere is a Norwegian inverter manufacturer and the availability of these inverters is hence assumed to be good. The Theia He-t series are one-phase inverters with one MPPT per inverter. They have a wide MPPT voltage range and very high efficiency within the MPPT-range.

Both these inverter types have Norwegian distributors which is considered an advantage with respect to availability and cost.

4.6.4 Matching of Array and Inverter

Firstly, the possible operating temperatures of the different modules were determined.

The *absolute minimum temperature* is in this case found from the absolute minimum temperature in the MET data set for Rygge, which is −31.5 °C registered in 1985. However, as PVsyst do not allow minimum temperatures below −30 °C, this was used as the absolute minimum operating temperature in the simulations.

Equation 3.9 was used to estimate the minimum winter operating temperature and the maximum summer operating temperature.

The average lower temperature during winter in the MET data set is −20 °C, and the synthetic hourly data generated by PVsyst shows that irradiance level typically takes values from 0 W/m² up to 400 W/m² on the horizontal plane during the same time period. The upper part of table 16 shows the operating temperatures for the selected modules when experiencing different irradiance levels at a constant ambient temperature of T_a = −20 °C. The NOCT values are given with an uncertainty from the manufacturer, and minimum and maximum values are therefore calculated for each situation.

The average maximum temperature during summer in the MET data set is 26.8 °C, while the absolute maximum temperature measured is 34.2 °C, registered in 1982. During the summer months, irradiance level typically varies between 0 W/m² and 800 W/m² on the horizontal plane, although higher irradiance values could also occur. The lower part of table 16 shows different operating temperatures for the selected modules at different irradiance levels and a constant ambient temperature of T_a = 25 °C.

Table 16: Cell temperatures for the selected modules under different operating conditions.

	NOCT[°C]		T(0 W, -20 °C)		T(200 W, -20 °C)		T(400 W, -20 °C)		T(600 W, -20 °C)	
Winter operation	**Min**	**Max**	**Min**	**Max**	**Min**	**Max**	**Min**	**Max**	**Min**	**Max**
REC PE series	43.7	47.7	-20.0	-20.0	-14.1	-13.1	-8.2	-6.2	-2.2	0.8
Suntech STP series	43.0	47.0	-20.0	-20.0	-14.3	-13.3	-8.5	-6.5	-2.8	0.2
Solar Frontier SF series	45.0	49.0	-20.0	-20.0	-13.8	-12.8	-7.5	-5.5	-1.3	1.8
	NOCT[°C]		**T(400 W, 25 °C)**		**T(600 W, 25 °C)**		**T(1000 W, 25 °C)**		**T(1200 W, 25 °C)**	
Summer operation	**Min**	**Max**	**Min**	**Max**	**Min**	**Max**	**Min**	**Max**	**Min**	**Max**
REC PE series	43.7	47.7	36.9	38.9	42.8	45.8	54.6	59.6	60.6	66.6
Suntech STP series	43.0	47.0	36.5	38.5	42.3	45.3	53.8	58.8	59.5	65.5
Solar Frontier SF series	45.0	49.0	37.5	39.5	43.8	46.8	56.3	61.3	62.5	68.5

Table 16 shows that operating temperatures for the PV array could vary from −20°C up to 69°C. Hence the MPPT function of the inverter should cover the voltage range associated with these temperatures. However, operation in −20°C will be rare, and will most likely occur in the winter months when the modules may be covered by snow and the shading effects are most severe. A MPPT range covering the voltages associated with an operating temperature range of 0°C to 70°C was therefore considered sufficient.

The PVsyst input values for the matching of array and inverter is shown in table 17. These values were used as input when matching the array and inverter in PVsyst.

Table 17: Input design temperatures for matching of array and inverter.

Absolute minimum operating temperature for V_{max} design	-30 °C
Lower winter operating temperature for $V_{mpp,max}$ design	0 °C
Usual operating temperature at 1000 W/m^2	50 °C
Upper summer operating temperature for $V_{mpp,\,min}$ design	70 °C

Equation 3.10 was used to calculate the module voltages associated with the given operating temperatures, in order to determine the minimum and maximum amount of modules in each string for the inverters. The voltage coefficients, γ_V, were found in the module product sheets.

Table 18: Voltage levels for the selected modules at different operating temperatures.

	V_{oc} -30 °C [V]	V_{mpp} 0 °C [V]	V_{mpp} 50 °C [V]	V_{mpp} 70 C [V]
REC PE series	43.0	32.2	28.2	26.5
Suntech STP series	44.4	33.3	28.1	26.0
Solar Frontier SF series	128.2	91.9	79.1	74.0

When the voltage levels for the design temperatures are calculated, these values were used to determine the minimum and maximum amount of modules in a string for the selected inverters.

By combining the calculated voltage levels of the modules shown in table 18 and the inverter specifications, equation 3.12 and 3.13 were used to calculate the minimum and maximum amount of modules in one string. The results from the calculations are shown in table 19.

Table 19: Minimum and maximum amount of modules in a string for different module/inverter combinations.

	SMA Tripower series		Eltek Valere Theia He-t	
	n_{min}	n_{max}	n_{min}	n_{max}
REC PE Series	6	23	9	13
Suntech STP series	6	22	9	13
Solar Frontier SF series	3	7	4	4

In table 19 it can be seen that the high voltage levels of the Solar Frontier modules limit the amount of modules that can be connected in one string, which mean that these modules will have to be distributed on a high number of strings. This could possibly increase the required amount of DC cables and thus the installation cost.

Systems were then designed and simulated for each of the three largest roofs on the farm. It would also be possible to simulate systems for the roofs on buildings 2 and 4. However, the three largest roofs account for more than 85% of the total southward-facing roof area, and designing and constructing systems for the two smallest roofs would be time consuming compared to the power gained.

Combinations of the selected modules and inverters were simulated in order to find the best-performing systems. The number of modules was determined from the available roof area on each roof. However, the amount of strings had to match the inverter specifications, and the length of each string had to match the voltage limits of the inverter.

In the cases where the possible maximum amount of modules did not match the inverter specifications, the amount of modules were reduced to the number closest to the maximum.

There are a total of six possible module/inverter-combinations. For each combination, two systems were constructed, one with slightly oversized inverters and one with slightly undersized inverters. Hence a total of 12 systems per roof were simulated, and a total of 36 systems for the entire farm.

Table 20: Combinations of modules and inverters used in the simulations.

System no.	Module	Modules	Strings	Modules per string	Module area [m^2]	P_{array}[kW]	Inverter	P_{nom}[kW]	# of inverters	$P_{array}/P_{inverter}$
Building 1										
1.1	REC PE250W	152	8	19	251	38.0	Tripower 10000TL	10.0	4	0.95
1.2	REC PE250W	152	8	19	251	38.0	Tripower 17000TL	17.0	2	1.12
1.3	REC PE250W	156	12	13	257	39.0	Theia 3.4 He-t	3.5	12	0.93
1.4	REC PE250W	156	12	13	257	39.0	Theia 2.9 He-t	2.9	12	1.12
1.5	Suntech STP250	156	12	13	257	39.0	Theia 3.4 He-t	3.5	12	0.93
1.6	Suntech STP250	156	12	13	257	39.0	Theia 2.9 He-t	2.9	12	1.12
1.7	Suntech ST250	152	8	19	247	38.0	Tripower 17000TL	17.0	2	1.12
1.8	Suntech ST250	152	8	19	247	38.0	Tripower 10000TL	10.0	4	0.95
1.9	Solar Frontier SF165	210	30	7	258	34.6	Tripower 17000TL	17.0	2	1.02
1.10	Solar Frontier SF165	210	30	7	258	34.6	Tripower 15000TL	15.0	2	1.15
1.11	Solar Frontier SF165	216	54	4	265	35.6	Theia 4.4 He-t	4.4	9	0.90
1.12	Solar Frontier SF165	216	54	4	265	35.6	Theia 3.8 He-t	3.8	9	1.04
Building 3										
3.1	REC PE250W	180	18	10	297	45.0	Theia 4.6 He-t	4.5	9	1.11
3.2	REC PE250W	180	18	10	297	45.0	Theia 4.4 He-t	4.4	9	1.14
3.3	REC PE250W	180	12	15	297	45.0	Tripower 15000TL	15.0	3	1.00
3.4	REC PE250W	180	12	15	297	45.0	Tripower 17000TL	17.0	3	0.88
3.5	Suntech STP250	180	18	10	297	45.0	Theia 4.6 He-t	4.5	9	1.11
3.6	Suntech STP250	180	18	10	297	45.0	Theia 4.4 He-t	4.4	9	1.14
3.7	Suntech STP250	180	12	15	297	45.0	Tripower15000TL	15.0	3	1.00
3.8	Suntech STP250	180	12	15	297	45.0	Tripower 17000TL	17.0	3	0.88
3.9	Solar Frontier SF165	216	36	6	265	35.6	Tripower TL12000	12.0	3	0.99
3.10	Solar Frontier SF165	216	36	6	265	35.6	Tripower TL10000	10.0	3	1.19
3.11	Solar Frontier SF165	216	54	4	265	35.6	Theia 4.4 He-t	4.4	9	0.90
3.12	Solar Frontier SF165	216	54	4	265	35.6	Theia 3.8 He-t	3.8	9	1.04
Building 5										
5.1	REC PE250W	90	9	10	149	22.5	Theia 2.9 He-t	2.9	9	0.86
5.2	REC PE250W	90	9	10	149	22.5	Theia 2.0 He-t	2.0	9	1.25
5.3	REC PE250W	88	4	22	145	22.0	Tripower TL12000	12.0	2	0.92
5.4	REC PE250W	88	4	22	145	22.0	Tripower TL10000	10.0	2	1.10
5.5	Suntech STP250	90	9	10	146	22.5	Theia 2.9 He-t	2.9	9	0.86
5.6	Suntech STP250	90	9	10	146	22.5	Theia 2.0 He-t	2.0	9	1.25
5.7	Suntech STP250	88	4	22	143	22.0	Tripower TL12000	12.0	2	0.92
5.8	Suntech STP250	88	4	22	143	22.0	Tripower TL10000	10.0	2	1.10
5.9	Solar Frontier SF165-S	112	16	7	138	18.5	Tripower TL8000	8.0	2	1.16
5.10	Solar Frontier SF165-S	112	16	7	138	18.5	Tripower TL10000	10.0	2	0.93
5.11	Solar Frontier SF165-S	108	27	4	133	17.8	Theia 2.9 He-t	2.9	9	0.68
5.12	Solar Frontier SF165-S	108	27	4	133	17.8	Theia 2.0 He-t	2.0	9	0.99

4.7 System Losses

Although some of the system losses described in chapter 3.6 are related to the selected modules and inverters, there are also loss parameters that are more or less independent on these components. This chapter discuss these system losses and the selection of loss parameters for the simulations.

4.7.1 System Losses in PVsyst

There are six tabs in the "Detailed losses" section in PVsyst. These are:

- Thermal parameter
- Ohmic losses
- Module quality – mismatch
- Soiling losses
- IAM losses
- Unavailability losses

These input parameters can be adjusted in order to reflect the operating conditions of the PV system.

4.7.2 Selection of Thermal Loss Parameter (U-value)

The theory concerning the thermal balance of a module and its influence on system performance is described in chapters 3.5 and 3.6 As all the parameters in equation 3.11 are available except for the module U-value, the U-value parameters from equation 3.16 are the input in this part of PVsyst.

The U-value is highly dependent on the mounting configuration, including the distance between the modules and the distance between the roof and the modules. Furthermore, local wind conditions including wind speed and direction would affect the U-value. No accurate model exist that can determine the U-value, although some suggestions have been made based on measured values from other PV-systems[18][Array thermal losses].

For semi-integrated modules with an air duct behind, the PVsyst default values are shown in table 21. These values were used in the main system simulations.

Table 21: U-value factors used in the main simulations.

Thermal Loss Factor		
Contant loss factor[U_c]	20	W/m^2K
Wind loss factor [U_v]	0	W/m^2K /m/s

4.7.3 Selection of Array Incidence Parameter

The "Array Incidence Parameter" determines how the module will respond to irradiance arriving at low incidence angles. The irradiance can either be absorbed or reflected of the module surface.

The ASHRAE model described in chapter 3.6.1 was used in the simulations, and the b_0-value in equation 3.15 was kept at the PVsyst default value of $b_0 = 0.05$.

The F_{IAM} as a function of the incindence angle for this value is shown in figure 51.

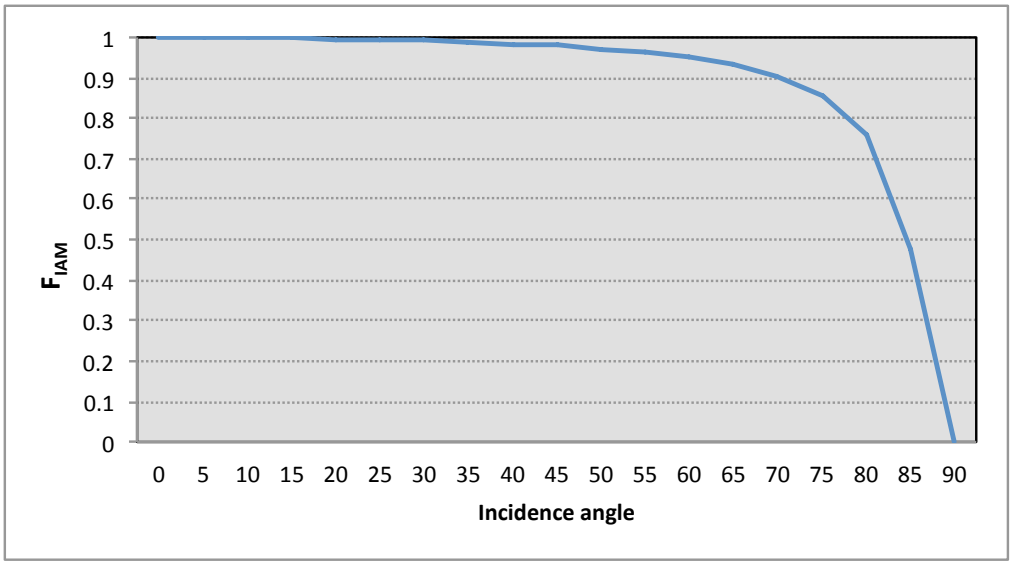

Figure 51: Incidence factor F as a function of incidence angle.

4.7.4 Selection of Ohmic Loss Parameters

There are several options available for the selection of ohmic loss parameters in PVsyst. The user can either define a maximum percentage loss in the DC-cabling and AC-cabling, or define the length and cross section area of the different cables. In the latter case PVsyst will calculate the ohmic losses using equation 3.17 and equation 3.18.

In [8][p.148], a maximum voltage drop of 1% is suggested on the DC-side as well as the AC-side of the system. In many countries there are specific requirements to a maximum voltage drop and ohmic losses, particularly on the AC-side. In Germany, the maximum voltage drop is set to 1%.

In practice, the amount of ohmic losses will be a compromise between a wish to reduce the losses to a minimum, while at the same time limit the cable cost. In these simulations, 1% is set as the maximum ohmic loss at STC on the DC-side, while 0.80% is used for the AC-side. The reason for the lower acceptance for losses on the AC-side is the previously mentioned requirements regarding voltage quality.

Table 22: DC and AC cable loss settings used in the simulations.

DC cable loss	1.00%	at STC
AC cable loss	0.80%	at STC

For the best-performing systems, the necessary cable diameter was calculated, assuming that the necessary cable length was two times the building length plus 10 meters.

4.7.5 Selection of Module Quality, LID and Mismatch Parameters

The module quality, LID and mismatch parameters are supposed to reflect the users confidence in the performance of the modules, and the different warranties provided by the module manufacturer.

The module quality loss parameter is the reduction in the performance of the module compared to the nameplate performance of the module. A negative value indicates that the module is expected to perform better than the nameplate specifications, which could typically be the case when a module manufacturer supplies modules with guarantied positive module tolerances[18][Module quality loss].

Light induced degradation (LID) is an effect that can be observed for crystalline modules during the first hours of operation. During this time a reduction in performance compared to the nameplate performance can sometimes be observed, depending on the quality of the wafer manufacturing[18][LID].

The mismatch parameter will also be a function of the module tolerance. The current in a string will be limited to the current of the weakest module, and high module tolerances could therefore give significant mismatch losses in a string and in the system as a whole.

There were limited data available regarding how to select these parameters, which will also be very specific to each module type and situation. In these simulations, the default values given in PVsyst were used. These are shown in table 23.

Table 23: Module quality, LID and mismatch parameters used in the simulations.

Module efficiency loss	According to manufacturer specifications	
LID	0.00%	
Mismatch losses	1.00%	at MPP

4.7.6 Selection of Soiling Loss Values

The soiling loss values should reflect the reduction in irradiation on the modules caused by dust, dirt, bird droppings, pollen and snow.

Table 7 shows that the site average snow depth is above 5 cm in January, February, March and December. Häberlin[6][p.183] suggests that it is safe to assume that snow sheding occur if the modules are mounted at a tilt angle of at least 60°.

In this case however, the module tilt angles span from 22° to 27° degrees. Furthermore, snow collectors on roof 1 and 5 further increase the likeliness of snow cover on the modules during the winter. Snow cover losses has been reported to be as high as 70% during the winter season in snowy locations like Minnesota[37]. This is not necessarily a representative value in this case, as temperature development, tilt angle and roof material will affect snow behaviour on the roof.

In 2010 and 2011, Townsend and Powers conducted a study of irradiation losses caused by snow in Truckey, California[38]. It was concluded that irradiation losses caused by snow will depend on several factors including snowfall quantity, array geometry, ground interference, and climatic factors such as temperature, radiation, relative humidity, wind speed and direction and snow moisture content.

The site is located in an agricultural district, which could be of importance for the soiling losses, particularly during summer and in dry periods. Many studies have been made concerning this phenomenon, although most of them have been site-specific. In dry, agricultural areas in California, soiling losses caused by dust and particles have been reported to be as high as 7% on a yearly basis, and up to 20% in certain months. In Malaga, a study performed by Casanova et.al. showed that average daily soiling losses were 4.4% for a site located near the University of Malaga[39].

No study considering soiling losses for PV systems in Scandinavia has been found. The monthly losses caused by soiling will hence be highly uncertain. For the main simulations, the monthly soiling loss values shown in table 24 were used.

Table 24: Monthly soiling loss values used in the main simulations.

Month	Soiling losses
January	70%
February	70%
March	30%
April	1%
May	1%
June	1%
July	1%
August	1%
September	1%
October	1%
November	1%
December	30%

4.7.7 Selection of Unavailability Loss Values

The unavailability losses are given to represent system downtime due to maintenance or grid-failure. Such losses are difficult to predict, although the relatively high reliability of the Norwegian power grid suggest that unavailability losses will mainly be caused by PV system failures. The unavailability losses in the simulations are assumed to be non-existent.

4.8 Sensitivity Analysis

The best-performing systems from each roof were used in further simulations to investigate the impact of uncertainties in three of the factors influencing system performance: Irradiation data, soiling losses and the U-value of the module (the thermal loss parameter).

The systems were simulated with settings different from those used in the main simulations. All other simulation settings were kept equal, and only one of the mentioned parameters was changed at once.

4.8.1 Sensitivity Analysis – Irradiation

The different meteorological data consulted in chapter 4.3 show relatively large differences, particularly with respect to irradiation values Several simulations were therefore made using Meteoset B and Meteoset C to investigate how this affected the system yield.

As the temperature and wind data used in Meteoset A, B and C are all the same, the sensitivity analysis is in essence used to investigate the impact of irradiation data uncertainties. As previously stated, Meteoset A include monthly average irradiation data from a weather station at UMB, while Meteoset B and C include irradiation data from PVGIS and Meteonorm, respectively.

4.8.2 Sensitivity Analysis – Soiling Losses

Due to the lack of reliable values for use in simulations, additional simulations were made using yearly average soiling loss values, in order to further investigate the possible impact of soiling and snow on the system performance.

The yearly average values used in the additional simulations are shown in table 25.

Table 25: Yearly average soiling losses used in the soiling loss sensitivity analysis.

Yearly average soiling loss parameters used in the sensitivity analysis		
Simulation setting I	3.0%	per year
Simulation setting II	1.0%	per year
Simulation setting III	0.0%	per year

4.8.3 Sensitivity Analysis – Module U-value

Due to the uncertainties in the selection of the thermal loss factors, and the fact that these parameters could be different between the roofs, additional simulations were performed in order to determine the impact of a change in the module U-value. The settings used in the additional simulations are shown in table 26

Table 26: Input parameters used in the module U-value sensitivity analysis.

Thermal loss factors used in the sensitivity analysis			
Simulation setting I - Low U	Contant loss factor[U_c]	15	W/m^2K
	Wind loss factor [U_v]	0	W/m^2K /m/s
Simulation setting II - High U	Contant loss factor[U_c]	29	W/m^2K
	Wind loss factor [U_v]	0	W/m^2K /m/s

4.9 Economical Evaluation

An economical evaluation of the best-performing roofs was performed, using both the NPV method and the LCOE method.

In order to determine the investment cost, system contractors in Norway, Sweden and Denmark were contacted and asked to provide information about the cost of similar systems. These also provided information about the approximate construction time for such facilities and some information about component prices.

Furthermore, suppliers of specific components like modules and inverters were contacted in order to better understand the cost distribution between the different components. However, Eltek Valere was the only component supplier who provided a useful response. Some internet-based suppliers were also consulted, and these are listed in the reference list as [40] and [41].

Some simplifications are also used regarding the price calculations:

- No adjustments have been made to the module prices collected from the different sources, although some of the prices are collected from sources outside the Norwegian market.
- Some prices have been extrapolated with respect to NOK/kWp. I.e. the cost of an Eltek inverter per kWp is assumed to be constant.
- Other BoS costs are assumed to be equal for each roof except in the cases of large differences in system size.
- The total labour cost per roof is assumed to be constant and independent of which system being installed.

4.9.1 The NPV Method

The assumptions used in the NPV calculations for the systems are shown in table 27.

Table 27: Financial assumptions used in the NPV calculations.

Financial assumptions		
Discount rate	6%	
Project lifetime	25	years
Investment support	0%	
Electricity spot price[NOK/kWh]	0.273	
Utility value, consumption[NOK/kWh]	0.166	
Utility value, export[NOK/kWh]	0.040	
One time certificate fee	(15 000)	
Residual value	0	
Operation and maintenance[NOK/kWh]	0.04	
System Degradation Rate(SDR)	0.5%	per year

The discount rate should reflect the project risk and the alternative rate of return that the investor could get from other projects. Several different examples have been observed with respect to the discount rate for PV systems. 6 % is used here as it represents a rate of return significantly higher than the current risk-free rate of return. This discount rate was also used by Good et.al when conducting LCOE calculations for PV systems[42]

The project lifetime of 25 years is determined from the module warranties and is a commonly assumed lifetime for PV-systems. It is assumed that all components must be replaced after 25 years and the residual value is hence assumed to be 0.

The electricity spot price is the average of Nordpool Spot Futures given at NASDAQ Commodities, from 2014 until 2018 in zone NO1, where Rygge is located[43].

The utility value is estimated using grid-tariffs provided by Hafslund, the utility company in this region[44]. In table 28, it can be observed that the customer´s utility expenses are divided into three parts: One fixed amount which is independent on the consumption and maximum power. The second part is calculated by multiplying the maximum power of the month by an amount that depends on the season. The third part is calculated by multiplying the monthly consumption with a season-dependent price.

Table 28: Utility grid tariff for Hafslund commercial customers[44].

Fixed tariff[NOK/month]	Power tariff[NOK/max. kW/month]		Energy tariff[NOK/kWh]	
	Summer(April - October)	Winter(November - March)	Summer	Winter
480	25	74	0.0425	0.064

As the power used at the farm is almost constant for most days, it is assumed that the PV-system will not affect the first two parts of the utility cost. This is due to the fact that the system will not produce any electricity at night. The third part will be reduced when the produced electricity is consumed at the farm, and the electricity produced is therefore given an added value. The exact value will be season-dependent, although an average is used here for simplicity. The utility tariff shown in table 29 does not include the electricity consumption fee of 0.116 NOK/kWh. For the electricity produced and consumed locally, the farmer will not have to pay this fee, since the generator size is less than 100 kVA.

If the consumer supplies electricity to the grid, it will receive compensation from the utility company which reflects the reduced marginal loss in the grid. The Hafslund tariffs for electricity supplied to the grid under the surplus-customer amendment is shown in table 29. Export of electricity to the grid will not give affect the electricity consumption fee, and the electricity that is exported will therefore have a lower utility value than the electricity consumed locally.

Table 29: Energy tariff for Hafslund surplus customers[45].

Energy tariff[NOK/kWh]			
	Summer(April -October)	Winter - day	Winter - night
Utility tariff	-0.0425	-0.064	-0.064
Electricity tariff	-Nordpool spot price		

No investment support scheme exists in Norway as of today. However, it is assumed that the customer will be allowed to participate in the green-certificate scheme and pay a one-time fee of 15 000 NOK to participate in this market. The certificate price is assumed to be 0.20 NOK/kWh which is close to the late 2012 price.

From a technical point of view, the maintenance cost and the system degradation rate (SDR) must be determined. The maintenance cost includes inspections and possible replacement of components, and was assumed to be 0.04 NOK/kWh per year. A properly installed roof mounted system should not require much maintenance, although inspections should be performed to ensure maximum system output. The SDR represents the expected loss in output from the system per year due to degradation. 0.5 % per year is used here. Both the maintenance cost and SDR value is taken from a sample calculation in [46].

It is assumed that the inverters would have to be changed one time during the lifetime of the system, in this case in year 12. The inverter price is then assumed to be equal to the initial inverter price.

The Norwegian organization ZERO has recently purposed a 40% investment support scheme for PV systems in Norway, similar to the system currently existing in Sweden[47]. Calculations of the NPV are also done considering such a support scheme.

4.9.2 The LCOE method

The LCOE is the necessary minimum value of the electricity for the NPV to be positive. Hence the assumptions used in the LCOE method should be equal to the assumptions used when calculating the NPV. However, as the LCOE method does not include any income variables, these are naturally not a part of the calculations. Table 30 shows the assumptions used in the LCOE calculations.

Table 30: Financial assumptions used in the LCOE calculations.

Financial assumptions		
Discount rate	6%	
Project lifetime	25	years
Residual value	0	
Operation and maintenance[NOK/kWh]	0.04	
System Degradation Rate(SDR)	0.5%	per year

The LCOE is highly sensitive to the assumptions made regarding discount rate, investment cost, maintenance cost and system yield. The yield sensitivity analysis performed for the different systems was used to make a sensitivity analysis of the LCOE. When discussing LCOE, it is common to distinguish between real and nominal LCOE, where the real LCOE is the minimum electricity price denoted in today´s currency.

Nominal LCOE also takes into account inflation and is hence higher than the real LCOE. In this case, the real LCOE is calculated to avoid making assumptions about future inflation rates.

5. Simulation Results and Economical Evaluation

This chapter presents the results from the main simulations, the sensitivity analysis, the comparison of production and consumption and the economical evaluation. Each simulation in PVsyst produces a report of four pages containing the results of the simulations. As it would not be feasible to present all reports here, key data from each report were collected and presented in tables and figures. Some figures were also directly exported from the PVsyst reports. Each chapter is concluded by a subchapter were the results from the simulations are discussed.

5.1 System Performance

This chapter presents the results from the main simulations considered the most interesting. Included is the system performance of all the systems simulated for each roof, roof-specific losses for each of the buildings and detailed results for the best-performing systems of each roof.

5.1.1 Main Simulation Results

Several of the losses in PV systems occur even before the irradiance hits the PV array. The module orientation, shading, incidence losses and soiling losses are all factors that affect the total amount of irradiation available for conversion in the modules.

These factors are determined mainly by the site meteorology and the roof orientation. In this case, they are therefore roof –specific sizes, and equal for all the systems on each roof. The influence of these factors in the main simulations is shown in table 31.

Table 31: Yearly effective irradiation the PV arrays.

	Global irradiation Horizontal plane [kWh/m^2]	R(β,Y,D/G)	Global irradiation Inclinded plane [kWh/m^2]	Shading Irradiance loss	Incidence angle(IAM) loss	Soiling loss	Effective irradiation PV array [kWh/m^2]
Building 1	880	1.183	1041	1.30%	3.40%	7.90%	913
Building 3	880	1.163	1023	1.90%	3.70%	7.40%	895
Building 5	880	1.163	1023	1.50%	3.70%	7.60%	899

The column on the left shows the yearly global irradiation on the site,. Then the transposition factor R and the resulting irradiation on each of the inclined roofs are shown. After the losses caused by shading, low incidence angle and soiling are deducted, the resulting effective irradiation on each roof is shown in the column to the right.

Table 32 shows the yearly yield, specific yield and performance ratio of the simulated systems. There are many different system losses in the simulated PV systems, and many of these are very similar for all the systems. The module efficiency losses and the inverter losses in each system are presented here, as those are the losses where the differences are largest between the systems.

The “Efficiency loss temperature” and the “Efficiency loss irradiance” columns show the losses in the modules due to reduced efficiency when the modules are operating at conditions different from STC conditions. These are identical for the systems using the same modules. The righter-most column shows the average percentage loss in the inverter. A value of 5.40% means that the average yearly inverter efficiency is 94.60%.

Table 32: System performance for the simulated systems.

System no.	Yearly yield [kWh]	Specific yield [kWh/kWp/year]	PR	Efficiency loss Irradiance	Efficiency loss Temperature	Inverter loss
Building 1						
1.1	31003	816	78.4%	1.70%	2.60%	5.40%
1.2	31594	831	79.9%	1.70%	2.60%	3.40%
1.3	32240	827	79.2%	1.70%	2.60%	4.30%
1.4	32331	829	79.5%	1.70%	2.60%	4.00%
1.5	31338	804	77.0%	4.30%	3.10%	4.30%
1.6	31434	806	77.3%	4.30%	3.10%	4.00%
1.7	30716	808	77.5%	4.30%	3.10%	3.40%
1.8	30112	792	76.0%	4.30%	3.10%	5.50%
1.9	27893	805	77.2%	2.20%	2.20%	3.60%
1.10	27640	798	76.5%	2.20%	2.20%	4.60%
1.11	28672	804	77.1%	2.20%	2.20%	3.70%
1.12	28670	804	77.1%	2.20%	2.20%	3.70%
Building 3						
3.1	36729	816	79.8%	1.70%	2.50%	3.40%
3.2	36696	815	79.7%	1.70%	2.50%	3.50%
3.3	36548	812	79.4%	1.70%	2.50%	4.30%
3.4	36424	809	79.1%	1.70%	2.50%	4.40%
3.5	35732	794	77.6%	4.40%	2.90%	3.40%
3.6	35702	793	77.5%	4.40%	2.90%	3.50%
3.7	35290	784	76.6%	4.40%	2.90%	4.40%
3.8	35423	787	76.9%	4.40%	2.90%	4.50%
3.9	27831	781	76.3%	2.20%	2.00%	5.00%
3.10	27764	779	76.1%	2.20%	2.00%	5.30%
3.11	28083	788	77.0%	2.20%	2.00%	3.70%
3.12	28081	788	77.0%	2.20%	2.00%	3.70%
Building 5						
5.1	18326	814	79.6%	1.70%	2.50%	4.40%
5.2	18318	814	79.6%	1.70%	2.50%	4.40%
5.3	17845	811	79.3%	1.70%	2.50%	5.00%
5.4	17864	812	79.3%	1.70%	2.50%	4.90%
5.5	17806	791	77.3%	4.40%	2.90%	4.40%
5.6	17837	793	77.5%	4.40%	2.90%	4.20%
5.7	17330	788	77.0%	4.40%	2.90%	5.10%
5.8	17383	790	77.0%	2.20%	2.00%	5.20%
5.9	14414	780	76.2%	2.20%	2.00%	5.20%
5.10	14354	777	75.9%	2.20%	2.00%	5.60%
5.11	13944	782	76.5%	2.20%	2.00%	4.90%
5.12	13979	784	76.6%	2.20%	2.00%	4.60%

For building 1, the system with the highest average PR was system 1.2. This system consisted of a 38 kWp module array of REC Peak Energy modules and two SMA Sunny Tripower 17000TL inverters. An overview of the systems yearly average performance from the PVsyst report is shown in figure 52. The upper part shows the losses previously described in table 31, and the resulting effective irradiation on the array. The effective irradiation is then converted at the STC efficiency of the module.

The modules will not usually operate at STC conditions. Hence additional losses caused by elevated temperatures, low irradiance levels, mismatch, quality and cable resistance are deducted. The resulting available power at the inverter input is then shown in the middle of the arrow. The inverter losses and AC cable loss are then accounted for and amount of electricity delivered at the system output is calculated.

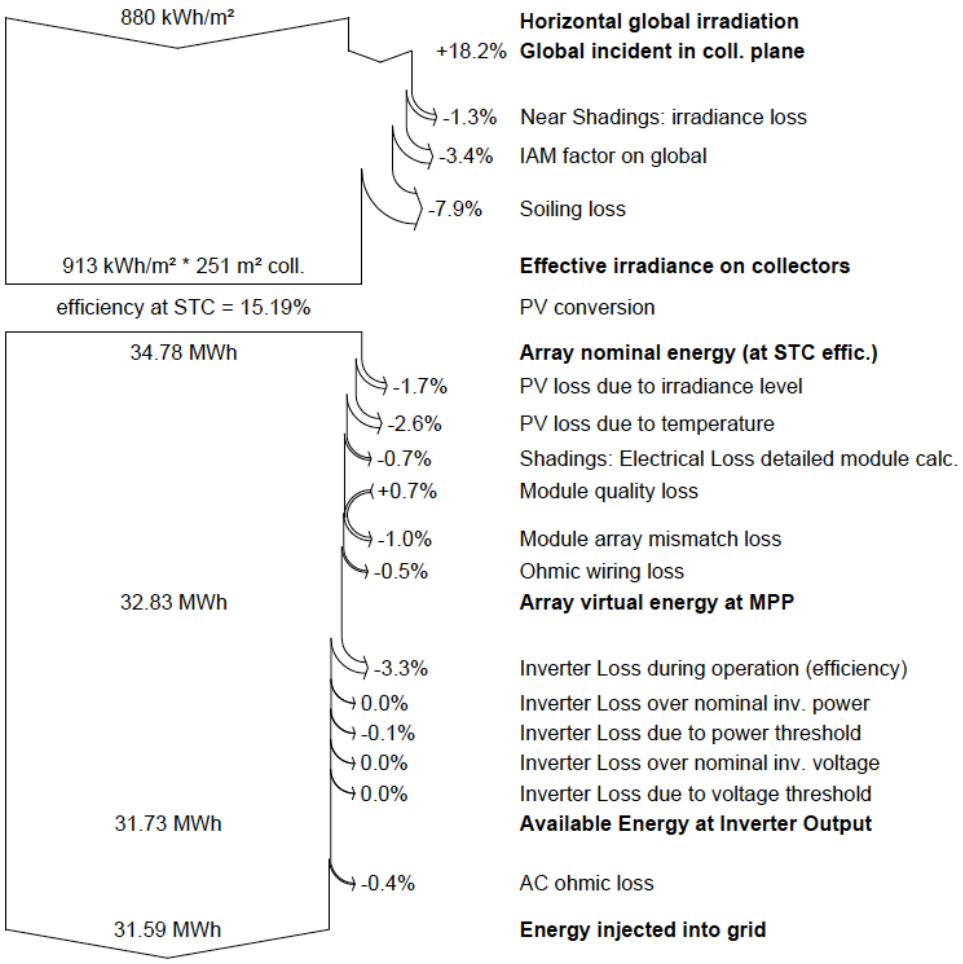

Figure 52: Yearly average performance of system 1.2 from PVsyst.

The monthly normalized production and the PR of the system is shown in figure 53. In the figure to the left, the purple coloured bars are collection losses occurring in the module array. These losses could be irradiance losses caused by i.e. shading or soiling, or conversion losses caused by elevated temperatures or low irradiance. The green part of the bars shows the inverter losses and the red part the output energy of the system. The figure to the right shows the PR of the system for each month.

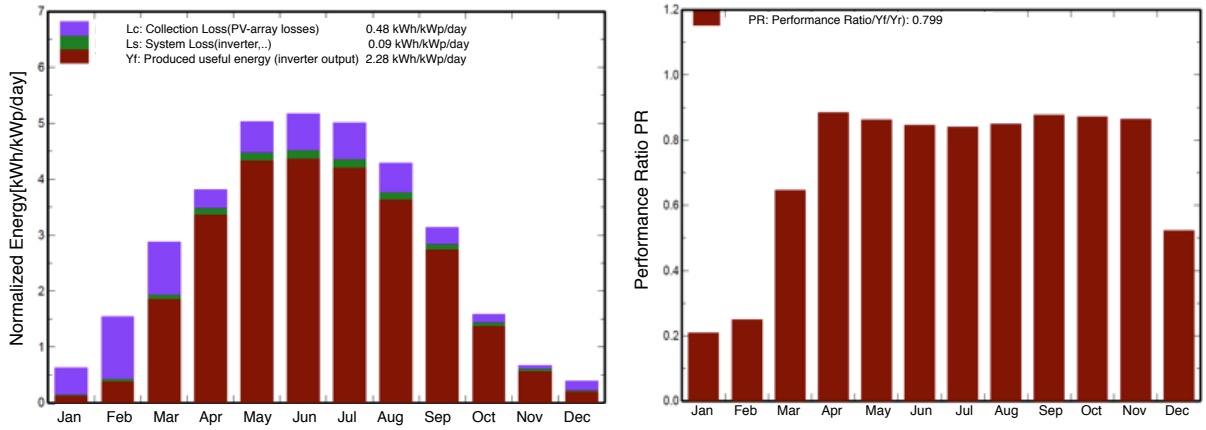

Figure 53: Normalized production and monthly average PR for system 1.2 from PVsyst.

For building 3, systems 3.1 and 3.2 have practically identical performance. However, as system 3.2 consists of smaller inverters, it is considered to be the best-performing system. System 3.2 consisted of a 45 kWp array of REC modules and nine Eltek Valere Theia 4.4 He-t inverters.

An overview of the systems yearly average performance from the PVsyst report is shown in figure 54.

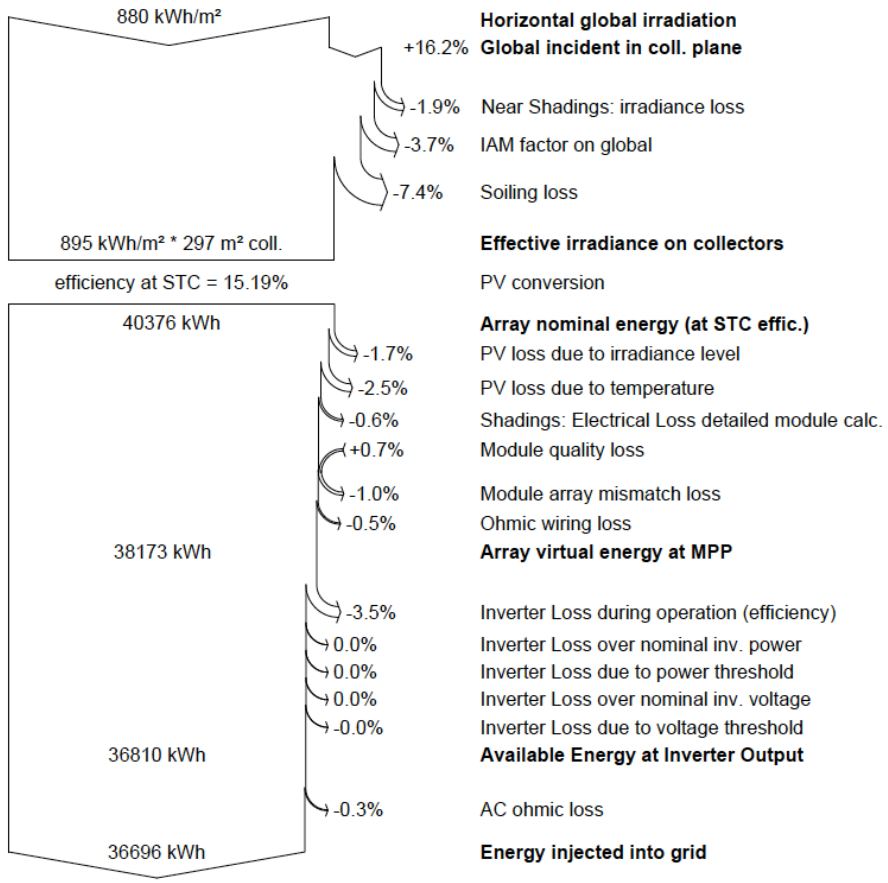

Figure 54: Yearly average performance of system 3.2 from PVsyst.

The normalized monthly production and the PR for this system are shown in figure 55.

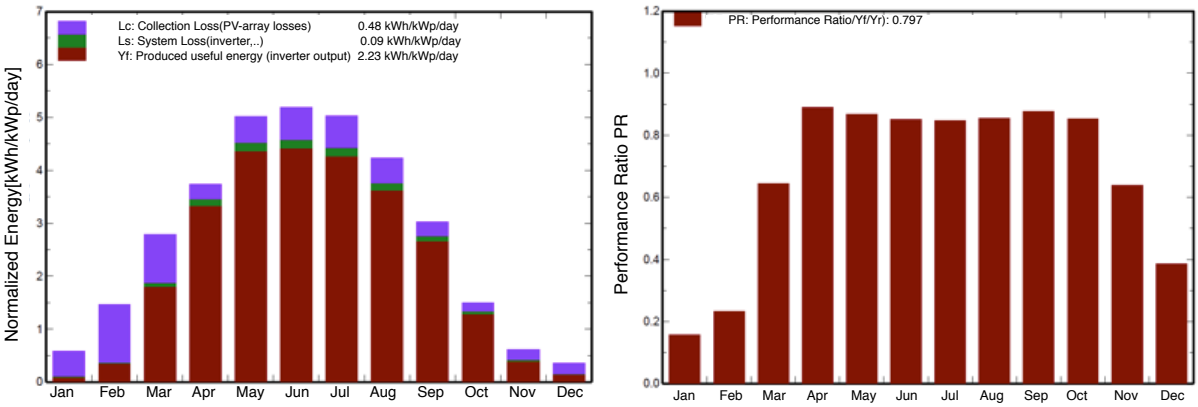

Figure 55: Normalized production and average monthly PR for system 3.2 from PVsyst.

For building 5, both systems 5.1 and 5.2 had a PR of 79.6%. However, system 5.2 consists of smaller inverters and is therefore assumed to be the best-performing system from an economical point of view. System 5.2 consisted of a 22.5 kWp array of REC modules and nine Eltek Valere Theia 2.0 He-t inverters.

An overview of the systems yearly average performance from the PVsyst report is shown in figure 56.

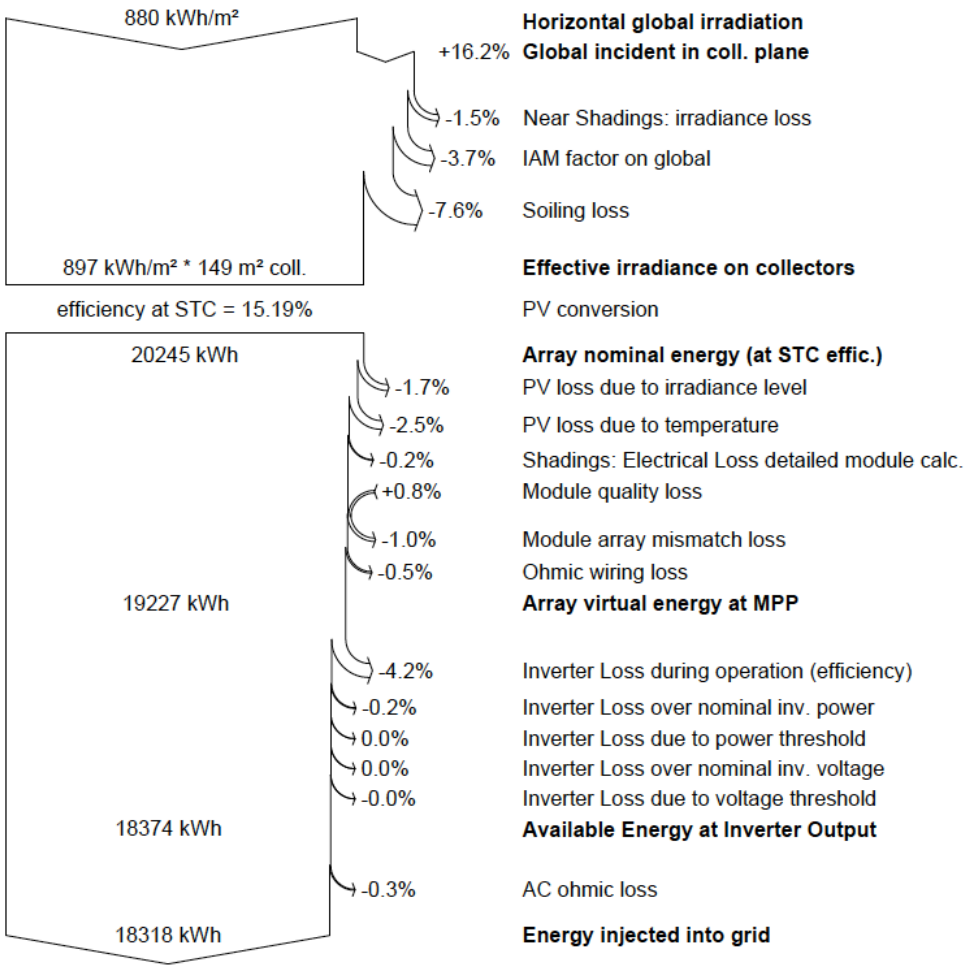

Figure 56: Yearly average performance of system 5.2 from PVsyst.

The normalized monthly production and the PR for this system are shown in figure 57.

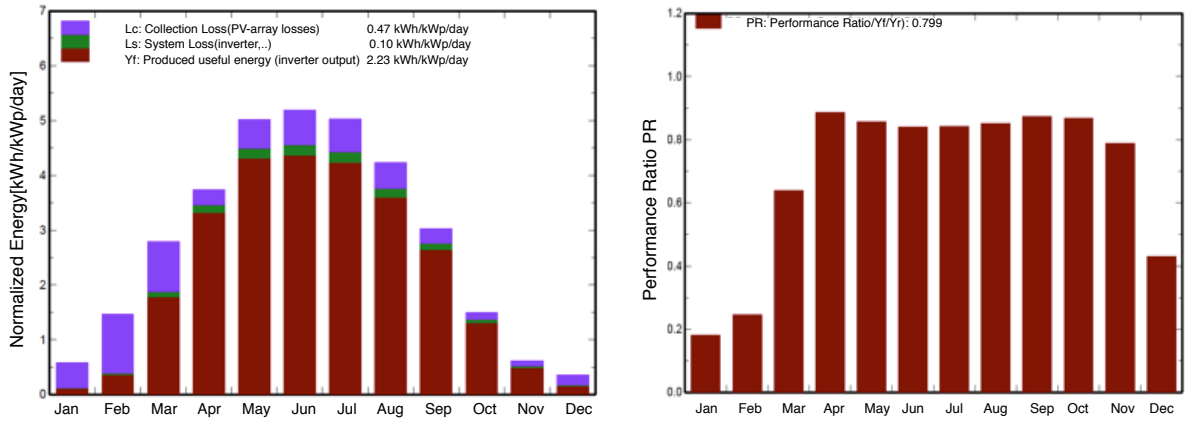

Figure 57: Normalized production and monthly performance ratio for system 5.2 from PVsyst.

5.1.2 String Configuration and Cable Sizing

In order to correctly calculate the electrical mismatch losses caused by shading, a string layout must be made that says where on the roof the modules are located, and to which string they are assigned.

Figure 58 shows the string configuration for system 1.2. As the shade on this roof was distributed because of the ventilators, the string design was made in order to limit the shading from each ventilator to one string.

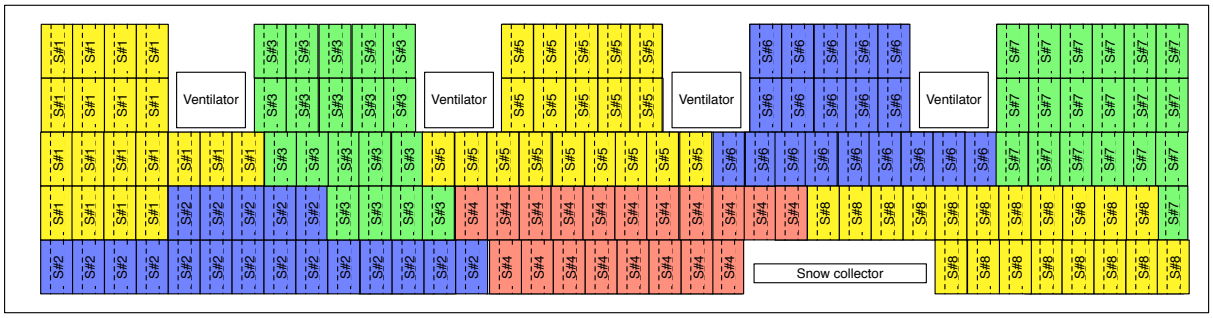

Figure 58: Suggested module layout and string configuration for system 1.2.

In the main simulations, the losses in DC and AC cables were treated by setting a maximum accepted value for the losses at STC. By using the same requirement, the necessary cable cross sectional area for each string was determined using equations 3.17 and 3.18. The results from the DC cable sizing when a maximum allowed ohmic loss of 1.0% was acceptable is shown in table 33.

Table 33: DC cable sizing for system 1.2.

Cross section[mm^2]	Array I_{mpp}[A]	Strings	String I_{mpp}[A]	L[m]	ρ[Ω mm^2/m]	P_{STC}[W]	Cable resistance[Ω]	Ohmic loss, $_{STC}$[W]	Loss at STC[%]
1.5 mm^2	66.20	8	8.28	90	0.0183	38	1.098	601	1.6%
2.5 mm^2	66.20	8	8.28	90	0.0183	38	0.659	361	0.9%
4.0 mm^2	66.20	8	8.28	90	0.0183	38	0.412	226	0.6%
6.0 mm^2	66.20	8	8.28	90	0.0183	38	0.275	150	0.4%

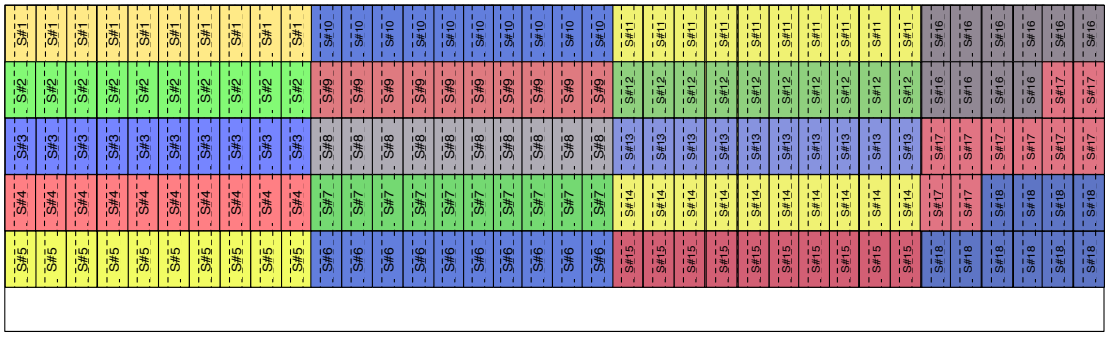

Figure 59: Suggested module layout and string configuration for system 3.2.

Figure 59 shows the suggested string configuration for system 3.2.

The results from the DC cable sizing when a maximum allowed ohmic loss of 1.0% was accepted is shown in table 34.

Table 34: DC cable sizing for system 3.2.

Cross section[mm²]	Array I_{mpp}[A]	Strings	String I_{mpp}[A]	L[m]	ρ[Ω mm²/m]	P_{STC}[W]	Cable resistance[Ω]	Ohmic loss, $_{STC}$[W]	Loss at STC[%]
1.5 mm²	149.00	18	8.28	82	0.0183	45	1.000	1234	2.7%
2.5 mm²	149.00	18	8.28	82	0.0183	45	0.600	740	1.6%
4.0 mm²	149.00	18	8.28	82	0.0183	45	0.375	463	1.0%
6.0 mm²	149.00	18	8.28	82	0.0183	45	0.250	308	0.7%

Figure 60 shows the suggested module layout for system 5.2.

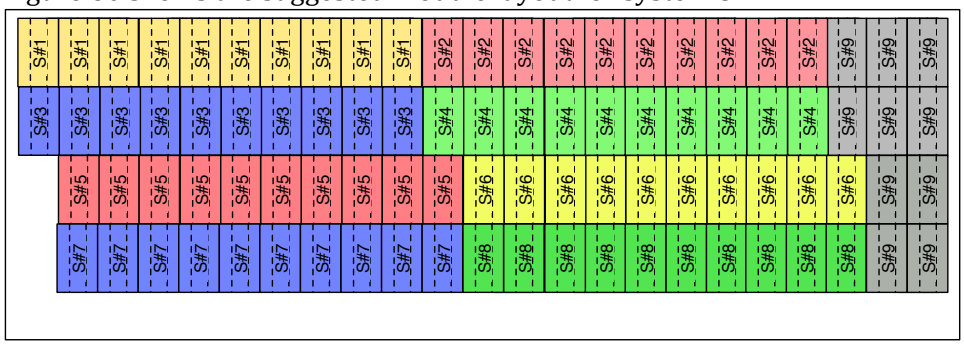

Figure 60: Suggested string configuration for system 5.2.

The results from the DC cable sizing when a maximum allowed ohmic loss of 1.0% was accepted is shown in table 35.

Table 35: DC-cable sizing for system 5.2.

Cross section[mm²]	Array I_{mpp}[A]	Strings	String I_{mpp}[A]	L[m]	ρ[Ω mm²/m]	P_{STC}[W]	Cable resistance[Ω]	Ohmic loss, $_{STC}$[W]	Loss at STC[%]
1.5 mm²	74.50	9	8.28	58	0.0183	22.5	0.708	436	1.9%
2.5 mm²	74.50	9	8.28	58	0.0183	22.5	0.425	262	1.2%
4.0 mm²	74.50	9	8.28	58	0.0183	22.5	0.265	164	0.7%
6.0 mm²	74.50	9	8.28	58	0.0183	22.5	0.177	109	0.5%

5.1.3 Discussion

The simulations show that there are several differences in the performance of the systems.

In table 32, three factors that had a significant impact on the system performance are shown: Efficiency loss due to irradiance levels different from STC, efficiency loss due to temperatures different from STC and inverter losses.

The module performance, and particularly module performance at low irradiance levels or high temperatures vary significantly between the different module types. The REC modules show the best performance with respect to low irradiance levels, as these losses are simulated to be 1.70%. The Solar Frontier modules have the best performance with respect to changes in temperature, and a 2.20% loss due to elevated temperatures is suggested from the simulations.

Recall from the irradiance spectrum shown in chapter 3 that the properties of sunlight changes through the atmosphere, and will appear different at different times of the day and year. Hence the modules that are able to absorb and utilize irradiance at a widest possible range of irradiance frequencies will show the best overall performance when the irradiance levels varies. This will depend on both the material properties of the module and the manufacturing process.

Thin film modules are recognized for their good performance at high temperatures, so the performance of the Solar Frontier modules are somewhat as expected. High performance in elevated operating temperatures requires that the electric field, and thus the voltage in the module, does not drop when the temperature increases. This is again affected by the module material and manufacturing process.

All the best-performing systems on each roof consist of REC-modules, illustrating the importance of careful selection of this component in PV system design. However, the selection of modules for a PV system is a balance between performance and cost, and it is therefore not obvious that the best-performing module will be the best choice from a cost/benefit perspective.

The average yearly PR spans from 75.9% up to 79.9%. It can be observed in table 32 that there is a close correlation between the specific yield and the PR, and between the module losses and the PR. Although the PR and specific yield for the systems using Solar Frontier modules are similar to those of the other systems, the yearly yield is significantly lower. The significantly lower STC efficiency for thin film modules means that less electricity will be produced on a given area, although the performance of the system is equal to those of crystalline modules. However, modules of low efficiency can be an issue when the available area is limited.

Most of the inverter losses could usually be attributed to "regular" inverter efficiency losses, as there always will be losses in the DC/AC-conversion. However, in some cases power from the PV array could also be lost due to the inverter power threshold, or when the array power is larger than the inverter nominal power. Nevertheless, the 36 simulated systems in general have limited variations in average inverter losses, as all the inverters used have high efficiency for a broad input range. Two of the best-performing systems on each roof are using Eltek inverters while the best-performing system on building 1 is using SMA inverters.

There are some general differences in the amount of irradiation received on each roof. As shown in table 31, the systems on building 1 receive more irradiation than the systems on buildings 3 and 5. This is also in accordance with known theory, as building 1 has a tilt angle closer to the optimum tilt angle than the other roofs. The higher tilt angle also causes lower annual incidence angle losses, as the modules on this roof to a lesser extent act as a mirror when the sun is low. The roof on building 1 also has the lowest yearly irradiation losses due to shading,

As previously stated in the shade analysis, the shading losses on buildings 3 and 5 are mainly caused by large trees located south of these buildings. Trees are not finite sizes and their impact on the system performance is hence subject to uncertainties. Although the irradiation losses caused by shading are significantly lower than those caused by soiling and low incidence angles, the irradiation losses are only one part of the shading losses; the electrical mismatch losses are accounted for after the conversion.

The seasonal soiling losses suggested in chapter 4.7.6 gives high yearly soiling losses between 7.4% and 7.9% for all the simulated systems. The uncertainties in the assumptions made with regards to the soiling loss settings will be further discussed in the sensitivity analysis.

The detailed simulation results for system 1.2 are shown in figures 52 and 53. Some of the losses, like module quality loss and mismatch loss, are determined by the predefined settings and therefore expected.

The module quality loss actually has a negative sign, indicating that it is actually a power gain of 0.7% rather than a power loss. The sign can be explained by the modules positive tolerances. That is, a 250 Wp module will never have a rating lower than 250 Wp, although some modules will have ratings above 250 Wp. This gain is offset by the mismatch between such modules, as the weakest module always will limit the power delivered from a string.

The ohmic losses are significantly lower than the pre-set values of 1.0% and 0.8% on the DC-side and AC-side respectively. The loss limits are defined for STC conditions, and for larger parts of the year the current in the cables will be lower than at these conditions. Since the cabling losses are proportional to the squared current value, these results are thus as expected.

The monthly average system PR for all systems is at its lowest in January and February, and is also lower in March and December than for the rest of the year. The low PR in these months can be directly attributed to the seasonal soiling losses, and the large fraction of collection losses in these months is shown in figures 53, 55 and 57.

The highest average system PR is observed to occur in April and September. In these months the average temperatures are relatively low, there are no snow on the modules and the sun path is high enough to prevent significant incidence- and low irradiance losses. The slightly reduced PR during the summer months is most likely caused by an increase in operating temperatures, which in turn reduces module efficiency.

The systems 3.2 and 5.2 show many similarities with system 1.2 with respect to system losses and PR. Nevertheless, two differences can be observed.

Firstly, by comparing the electrical losses due to shading for the three systems, it can be observed that the electrical losses are highest for system 1.2, although the shading irradiation losses are lower than for systems 3.2 and 5.2. Although the ventilators on the roof of building 1 are relatively small, their shadows are distributed over different parts of the roof, and the output from different strings is therefore reduced. The shading from the ventilators will be present more or less year-round, while the shading on buildings 3 and 5 are seasonal and mainly occurs during winter, when irradiance levels are low. Thus the amount of shading on a roof is not necessarily the most important for the system PR, the distribution on the roof and the time of occurrence can turn out to be just as important.

Secondly, the PR of system 1.2 is significantly higher in November than for systems 3.2 and 5.2 during the same month. The shading in this month rapidly becomes more severe on building 3 and 5 as the sun path is lowered, which could provide an explanation to these differences. Also, the incidence losses will become more significant for these buildings due to their lower roof tilt angle.

5.2 Sensitivity Analysis - Irradiation Data

5.2.1 Simulations Results

Table 36 shows the performance of different systems when using Meteoset A, Meteoset B and Meteoset C in the simulations. All other system parameters were kept equal to those used in the main simulations. The yearly yield for each system simulation is shown, as well as the PR of the systems. For Meteoset B and C, the percentage difference in yearly yield from the main simulations with Meteoset A is shown.

Table 36: Influence of meteorological data on simulated system performance.

	Main(Meteoset A)		Meteoset B			Meteoset C		
System no.	Yearly yield [kWh]	PR	Yearly yield [kWh]	PR	Yield difference from main	Yearly yield [kWh]	PR	Yield difference from main
Building 1								
1.2	31594	79.9%	31382	80.9%	-0.7%	36205	81.0%	14.6%
1.7	30716	77.5%	30446	78.5%	-0.9%	35186	78.8%	14.6%
1.9	27893	77.2%	27689	78.3%	-0.7%	32081	78.7%	15.0%
Building 3								
3.2	36696	79.7%	36296	80.5%	-1.1%	41939	81.0%	14.3%
3.6	35702	77.5%	35229	78.1%	-1.3%	40767	78.7%	14.2%
3.12	28081	77.0%	27764	77.8%	-1.1%	32175	78.5%	14.6%
Building 5								
5.2	18318	79.6%	18168	80.6%	-0.8%	20951	80.9%	14.4%
5.6	17837	77.5%	17633	78.2%	-1.1%	20365	78.7%	14.2%
5.9	14414	76.2%	14295	77.2%	-0.8%	16601	78.1%	15.2%

Figure 61 shows the difference in monthly production from system 3.2 when using the different meteorological datasets in the simulations.

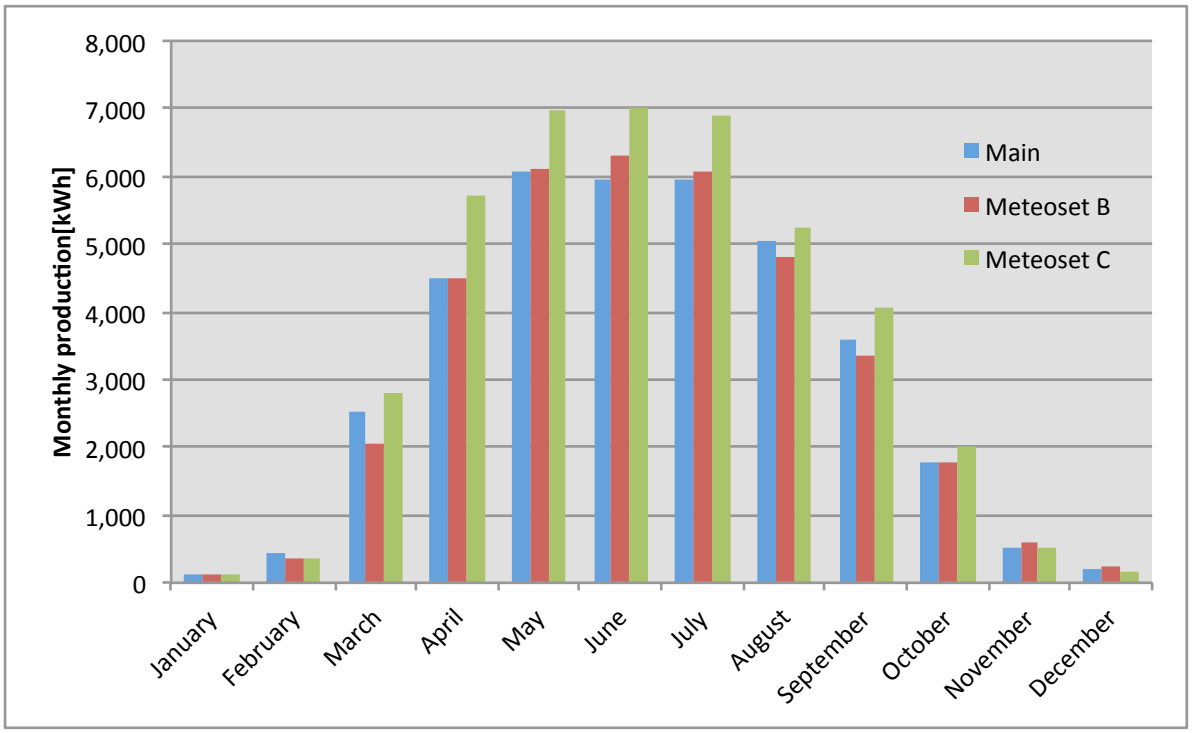

Figure 61: Monthly yield from system 3.2 for different meteorological datasets.

5.2.2 Discussion

In table 36, it can be observed that the selection of meteorological data could have a major impact on the expected performance of a PV-system.

Meteoset A and B gives results which on a yearly basis are consistent and within the margin of error for e.g. meteorological measurement equipment. However, as shown in figure 61, the results for system 3.2 vary when considering monthly system yield. Particularly in March there is a significant difference in system yield when the simulations of system 3.2 for Meteoset A and B are compared.

Seasonal differences in system yield could in many cases be important to the economical evaluation of the project, as electricity prices and the local consumption also have seasonal variances. A unit of electricity produced in March may in many cases have a different value than a unit produced in July. Using Meteoset C in the simulations gives a system yield that is consistently higher through the year, except for the winter months and November. The annual yield is about 15% higher than for Meteoset A, a significant difference.

Table 36 shows that the PR remains more or less equal for each system when different irradiation data is used. This result is in accordance with know theory, as the PR only shows the real performance of the system compared to an ideal system, and is independent from irradiation data. This is the reason why PR often is used to compare module and system performance for different sites. It should however be mentioned, that the PR is not independent of temperature and wind data, as these factors will influence the module efficiency.

The differences between Meteoset A, B and C could be explained by their fundamental differences in how the data is generated.

The irradiation data used in Meteoset A is recorded using a pyranometer located about 30 km away from the PV-system site at practically the same latitude. Meteorological parameters like temperature and wind are well correlated for the sites, although the distance to the coast for the two sites is different. The latter could have significant impact on cloud cover and thus the amount of irradiation and the irradiance spectrum.

Although measured data in many cases would be preferable, many factors exist that could severely reduce the value of such data. Measurement equipment of low quality and non-homogenized data could cause such measured data to be less reliable than other sources. It is also important that the equipment is properly cleaned and that snow is removed during winter.

Two of the meteorological data sources consulted in this thesis, UMB and Bioforsk Ås, are measurements made in the same town. Yet there is a 10 % difference in the measured yearly irradiation between the two sources. This serves as an example of how also meteorological data measurements can be highly uncertain.

Meteoset B consists of irradiation data from PVGIS, constructed using interpolation between different weather stations. The accuracy of such data will depend on the density of the weather stations used, and how well the interpolation mechanism manage to incorporate micrometeorological effects due to i.e. cloud cover. No information has been found that shows which weather stations the PVGIS database collects data from.

Meteoset C consists of irradiation data from Meteonorm, which also construct weather data using interpolations between weather stations located in Europe. However, relatively few of the weather stations in the Scandinavian part of the network include irradiation measurements. The interpolations have been made between stations relatively far away from the site, which makes it more challenging to incorporate meteorological factors influencing irradiance values. Furthermore, the stations in both the PVGIS network and the Meteonorm network will have the same measurement uncertainties as those related to the weather station used in Meteoset A.

5.3 Sensitivity Analysis - Soiling Losses

5.3.1 Simulation Results

The impact of uncertainties in soiling loss values has been evaluated by performing simulations using different soiling loss settings. Table 37 shows the system performance when yearly soiling losses of 3.0%, 1.0% and 0.0% were used. All other system parameters were kept equal to those used in the main simulation.

Table 37: Influence of soiling losses on the simulated system performance.

	Main simulations		Yearly soiling losses - 3.0%			Yearly soiling losses - 1.0%			No soiling losses		
	Yearly yield [kWh]	PR	Yearly yield [kWh]	PR	Yield difference from main	Yearly yield [kWh]	PR	Yield difference from main	Yearly yield [kWh]	PR	Yield difference from main
Building 1											
1.2	31594	79.9%	33603	84.8%	6.4%	34266	86.4%	8.5%	34563	87.2%	9.4%
1.7	30716	77.5%	32651	82.4%	6.3%	33305	84.0%	8.4%	33632	84.8%	9.5%
1.9	27893	77.2%	29642	82.0%	6.3%	30249	83.7%	8.4%	30551	84.5%	9.5%
Building 3											
3.2	36696	79.7%	38612	83.8%	5.2%	39369	85.5%	7.3%	39746	86.3%	8.3%
3.6	35702	77.5%	37531	81.5%	5.1%	38242	83.0%	7.1%	38649	83.9%	8.3%
3.12	28081	77.0%	29578	81.1%	5.3%	30177	82.7%	7.5%	30476	83.6%	8.5%
Building 5											
5.2	18318	79.6%	19357	84.1%	5.7%	19720	85.6%	7.7%	19891	86.4%	8.6%
5.6	17837	77.5%	18832	81.8%	5.6%	19208	83.4%	7.7%	19395	84.2%	8.7%
5.9	14414	76.2%	15272	80.8%	6.0%	15557	82.3%	7.9%	15699	83.0%	8.9%

Figure 62 shows the simulated monthly production from system 3.2 for different soiling loss settings.

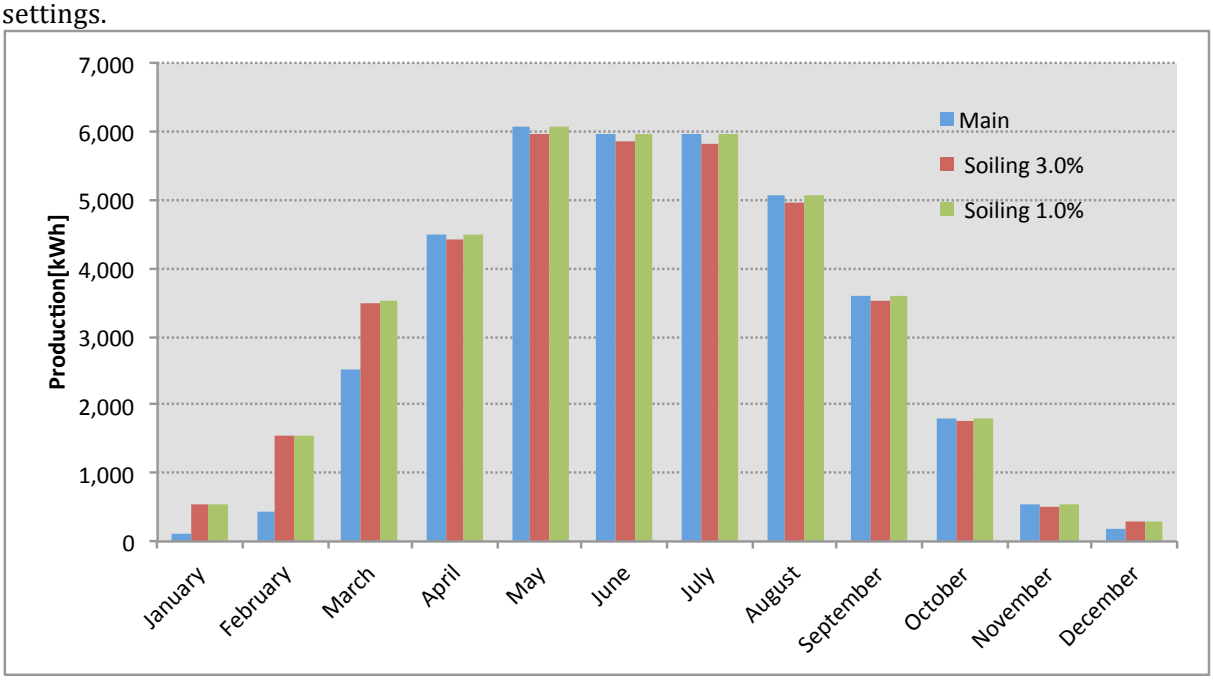

Figure 62: Monthly simulated production for system 3.2 for different soiling loss values.

5.3.2 Discussion

As shown in table 37, the selection of soiling loss parameters can have a major impact on both seasonal and yearly system performance.

The main soiling loss settings resulted in average soiling losses of 7.5 – 8.5% on a yearly basis. The reduction of the yearly average soiling losses to 3.0% gives an increase in system yield in the range 5.1% to 6.4%, and assuming no soiling losses increases the system yield by about 9.0% from the main simulations. The PR also increases steadily as the soiling losses are reduced, which is in accordance with the PR definition explained in chapter 3.

The soiling losses have a slightly larger impact on the systems on building 1 than on the other roofs. The roof on building one has a higher tilt angle than the others and thus a higher transposition factor, R. The higher soiling losses on this roof are therefore expected. Furthermore, building 3 and building 5 have larger shading losses during the winter months, and the effect of a reduction in soiling losses during winter will partially be offset by increased shading losses.

Figure 62 shows the monthly system yield for system 3.2 when different soiling loss settings were used. Naturally, the impact of soiling will be largest during the winter months when the seasonal soiling loss settings are used.

To estimate soiling losses caused by snow is a difficult task, as these losses are highly dependent on local conditions. Even though the meteorological data collected shows that presence of snow on the ground is likely during the winter months and March, there is no guarantee that the snow will also be present at the modules. Both the tilt angle of the modules and their smooth surface will cause snow shedding before the snow has completely melted on the ground. Daily temperature profiles and snow properties will also influence the soiling losses due to snow.

Furthermore, the site location in an agricultural area could cause soiling losses during spring, summer and fall. These losses could prove to be highly seasonal, evenly distributed through the

year or practically non-existent. As this is not a particularly dry climate, rainfall will contribute to a reduction in the soiling losses.

A total of 15 ventilators are located on building 1. The main purpose of these is to remove exhaust gas from the gas-fired heating system in the building. However, as this system is located inside the room where several thousand chickens are also present, dust and particles will inevitably be present in the exhaust. The farmer has also observed such dust collecting on the roof of building 1 and the risk of soiling losses on this roof is therefore higher than on the other roofs.

5.4 Sensitivity Analysis – Module U-value

5.4.1 Simulation Results

Table 38 shows the system performance for different systems when different module U-value settings were used in the simulations. All other system parameters were kept equal to those used in the main simulations. The module temperature loss parameter is also included in table 39.

Table 38: System performance for different module U-value simulation settings.

	Main			Low U-value				High U-value			
	Yearly yield [kWh]	PR	Temperature loss	Yearly yield [kWh]	PR	Temperature loss	Yield difference from main	Yearly yield [kWh]	PR	Temperature loss	Yield difference from main
Building 1											
1.2	31594	79.9%	2.6%	30761	77.6%	5.2%	-2.6%	32196	81.2%	0.3%	1.9%
1.7	30716	77.5%	3.1%	29728	75.0%	6.1%	-3.2%	31430	79.3%	0.4%	2.3%
1.9	27893	77.2%	2.2%	27280	75.5%	4.2%	-2.2%	28409	78.6%	0.2%	1.8%
Building 3											
3.2	36696	79.7%	2.5%	35749	77.6%	5.0%	-2.6%	37521	81.5%	0.2%	2.2%
3.6	35702	77.5%	2.9%	34574	75.1%	5.8%	-3.2%	36641	79.6%	0.2%	2.6%
3.12	28081	77.0%	2.0%	27489	75.4%	4.1%	-2.1%	28630	78.5%	0.1%	2.0%
Building 5											
5.2	18318	79.6%	2.5%	17884	77.7%	5.0%	-2.4%	18572	80.7%	0.2%	1.4%
5.6	17837	77.5%	2.9%	17295	75.1%	5.8%	-3.0%	18186	79.0%	0.2%	2.0%
5.9	14414	76.2%	2.0%	14132	74.7%	4.1%	-2.0%	14717	77.8%	0.1%	2.1%

Figure 63 shows the monthly system yield from system 3.2 when different module U-value settings were used in the simulations.

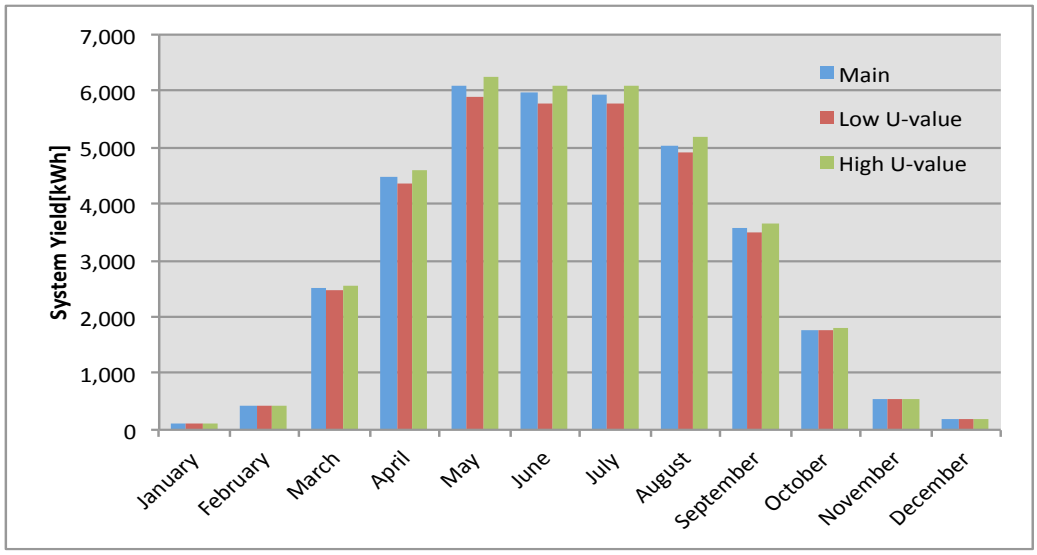

Figure 63: Monthly system yield from system 3.2 using different module U-values.

5.4.2 Discussion

Table 38 show the differences in system yield when different U-value settings were used in the simulations

There is a consistent, yet relatively low difference between the different settings. It should be noted however, that for e.g. system 3.6 the difference in system yield when using a low U-value instead of the main U-value is 3.2%. The importance of a highest possible U-value should therefore not be underrated.

The systems using Suntech modules in general have a larger sensitivity to the module U-value, while the Solar Frontier modules show the lowest change in output for the different U-values. These results are in accordance with previous results shown in table 32, where the Suntech modules were most sensitive to high temperatures and the Solar Frontier modules were affected the least.

In figure 63 it can also be observed that the systems are more sensitive to a change in the U-value during the summer months when the ambient temperature is high. During the months from September until April the ambient temperature is low and the U-value becomes less significant for the module operating temperature.

A highest possible U-value could be obtained by constructing a system that allows air to circulate as freely as possible around the modules. This includes leaving a largest possible gap between the roof and the back of the module, and also allow some space between the modules in both the vertical and horizontal direction of the roof.

5.5 Comparison of Production and Consumption

5.5.1 Results

Table 39 shows the monthly production from the best-performing systems on building 1,3 and 5, and their combined production. The production is also compared to the 2012 consumption on the farm.

Table 39: Monthly production from the best-performing systems.

	System 1.2 [kWh]	% of 2012 consumption	System 3.2 [kWh]	% of 2012 consumption	System 5.2 [kWh]	% of 2012 consumption	Sum [kWh]	% of 2012 consumption
January	154	0.8%	128	0.6%	73	0.4%	355	1.8%
February	409	2.4%	429	2.5%	227	1.3%	1 065	6.3%
March	2 192	18.2%	2 512	20.8%	1 242	10.3%	5 946	49.3%
April	3 842	27.0%	4 496	31.6%	2 237	15.7%	10 576	74.4%
May	5 108	38.5%	6 079	45.9%	3 004	22.7%	14 192	107.1%
June	4 986	97.9%	5 961	117.1%	2 945	57.8%	13 894	272.9%
July	4 960	99.2%	5 944	118.9%	2 955	59.1%	13 861	277.2%
August	4 295	73.7%	5 051	86.6%	2 511	43.1%	11 859	203.4%
September	3 131	18.6%	3 586	21.3%	1 782	10.6%	8 499	50.6%
October	1 623	7.4%	1 784	8.1%	906	4.1%	4 313	19.6%
November	655	3.4%	532	2.7%	328	1.7%	1 515	7.8%
December	240	1.1%	193	0.9%	107	0.5%	540	2.4%
Sum	31 595	18.3%	36 695	21.3%	18 317	10.6%	86 607	50.2%

Figure 64 shows the combined monthly production of systems 1.2, 3.2 and 5.2 and the 2012 consumption.

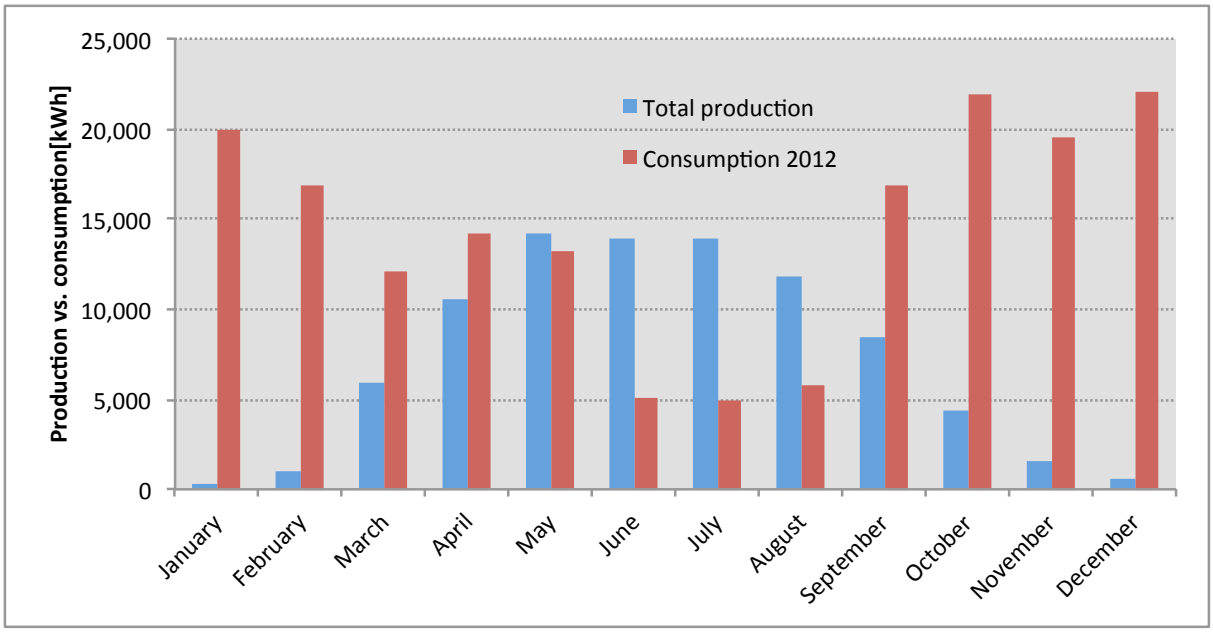

Figure 64: Combined simulated production and consumption.

5.5.2 Discussion

As shown in table 39, the three best-performing systems would produce an amount of electricity equal to roughly 50% of the local consumption in 2012.

If only the system on the smallest of the three roofs were constructed, it would provide a self-supply rate of 10.6%. The highest and lowest monthly self-supply rate from this system would be 59.1% in July and 0.4% in January. As the nominal power this system is 22.5 kW and the average consumed power in July 2012 was 6.7 kW, it is very likely that this system would supply power to the grid for parts of the year. It would hence become a part of the surplus-customer arrangement.

As systems 3.2 and 1.2 are larger than system 5.2, the construction of any of these systems would also cause an export situation for certain parts of the year. However, as the self-supply rate would remain below 100%, the customer could still connect the systems to the grid under the surplus customer arrangement.

The production from the system is not very well correlated with the local consumption. While the local consumption is particularly high during the fall and winter months, the larger fraction of the system production occurs during in the spring- and summer months.

An increase in the module tilt angle would results in a higher production during the fall- and winter months. However, as the roof tilt angle is fixed this is not easy to obtain. One option could be to mount the modules on the façade of one or several buildings, although shading would be a challenge and the yearly yield would be lower than for the systems suggested here.

As a gross metering solution would have to be installed anyway due to the large production during summer, supplying electricity to the grid is not a major technical issue. However, it as already been explained in chapter 4.9 that the electricity will have a higher economical value when being consumed on the farm.

5.6 Economical Evaluation

5.6.1 NPV and LCOE Calcuations

Table 40 shows the results from the calculation of NPV and LCOE for three of the best-performing systems simulated on building 1. Numbers in parenthesis are negative. For NPV calculations, it was assumed from the comparison of production and consumption that 20% of the produced electricity would be exported, while the rest would be consumed on the farm.

Table 40: LCOE and NPV calculations for three of the systems on building 1.

	System 1.2		System 1.7		System 1.9	
	Cost[NOK]	NOK/kWp	Cost[NOK]	NOK/kWp	Cost[NOK]	NOK/kWp
Modules	250 800	6 600	246 240	6 480	220 500	6 373
Inverter	62 000	1 632	62 000	1 632	62 000	1 792
Mounting system	60 000	1 579	60 000	1 579	60 000	1 734
Cable	32 000	842	32 000	842	32 000	925
Other BoS	10 000	263	10 000	263	10 000	289
Labour	112 500	2 961	112 500	2 961	112 500	3 251
Sum	527 300	13 876	522 740	13 756	497 000	14 364
LCOE[NOK/kWh]	1.49		1.52		1.59	
NPV[NOK]	(351 729)		(353 297)		(372 012)	

Table 41 shows the results from the calculations of LCOE and NPV for three of the systems on building 3. For the NPV calculations, it was assumed from the comparison of production and consumption that 25% of the electricity would be exported and the rest consumed on the farm.

Table 41:LCOE and NPV calculations for three of the systems on building 3.

	System 3.2		System 3.6		System 3.12	
	Cost[NOK]	NOK/kWp	Cost[NOK]	NOK/kWp	Cost[NOK]	NOK/kWp
Modules	297 000	6 600	291 600	6 480	226 800	6 371
Inverter	70 200	1 560	70 200	1 560	60 300	1 694
Mounting system	70 000	1 556	70 000	1 556	60 000	1 685
Cable	48 000	1 067	48 000	1 067	32 000	899
Other BoS	10 000	222	10 000	222	10 000	281
Labour	112 500	2 500	112 500	2 500	112 500	3 160
Sum	607 700	13 504	602 300	13 384	501 600	14 090
LCOE[NOK/kWh]	1.47		1.50		1.59	
NPV[NOK]	(403 295)		(405 632)		(352 059)	

Table 42 shows the results from the LCOE and NPV calculations for three of the systems on building 5. For the NPV calculations, it was assumed from the comparison of production and consumption that 10% of the produced electricity was exported and the rest consumed on the farm.

Table 42: NPV and LCOE calculations for three of the systems on building 5.

	System 5.2		System 5.6		System 5.9	
	Cost[NOK]	NOK/kWp	Cost[NOK]	NOK/kWp	Cost[NOK]	NOK/kWp
Modules	148 500	6 600	145 800	6 480	117 600	6 357
Inverter	36 000	1 600	36 000	1 600	38 000	2 054
Mounting system	40 000	1 778	40 000	1 778	40 000	2 162
Cable	18 000	800	18 000	800	18 000	973
Other BoS	10 000	444	10 000	444	10 000	541
Labour	67 500	3 000	67 500	3 000	67 500	3 649
Sum	320 000	14 222	317 300	14 102	291 100	15 735
LCOE[NOK/kWh]	1.55		1.58		1.80	
NPV[NOK]	(221 670)		(222 355)		(221 599)	

Table 43 shows the NPV of system 3.2 considering different support schemes.

Table 43: NPV of system 3.2 for different support schemes.

NPV of system 3.2	
Green-certificates only	(403 295)
40% Investment support only	(233 665)
Certificates + 40% investment support	(159 015)

Figure 65 shows how a change in different parameters would affect the estimated LCOE for system 3.2. Four of the parameters are sensitivities with respect to the assumptions made in the economical analysis, while the last three parameters are the technical parameters for which a technical sensitivity analysis was performed in the simulations.

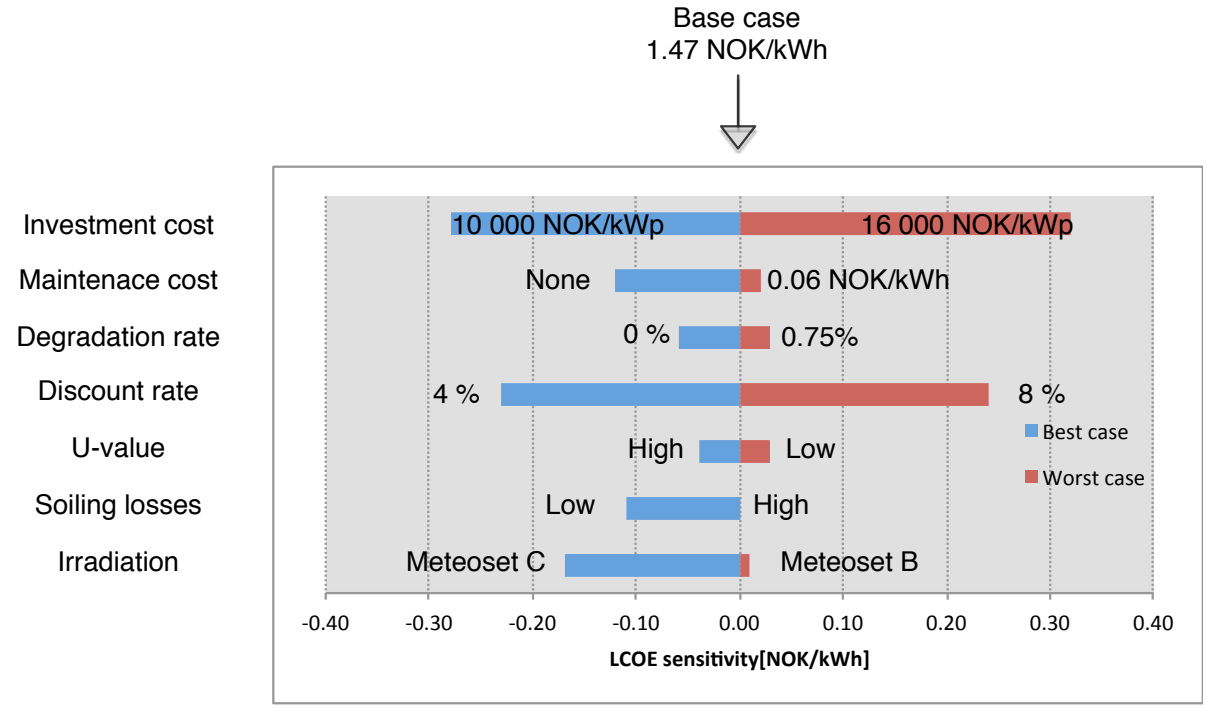

Figure 65: Sensitivity in LCOE for system 3.2.

5.6.2 Discussion

The economical evaluation shows that the NPV is negative for all systems, and that the NPV is negative for system 3.2 when including a 40% support scheme.

The lowest LCOE is calculated to 1.47 NOK/kWh for system 3.2. The LCOE is similar for many of the systems, as the module costs seem to be somewhat levelled according to their expected yield. It should however be mentioned that the module prices used come from different sources, and both Suntech and Solar Frontier prices are from foreign sources. The price in the Norwegian market could therefore be different depending on taxes and transportation costs. The REC modules gave a higher yearly yield in the simulations, and are also the most expensive.

The module cost account for almost half of the total system cost, and the price development on PV modules will be important for the future of these systems in Norway. The labour cost is also an important factor. Here it is assumed that the time spent on each roof is independent on which system is installed. The assumption disfavours the Solar Frontier modules as they have a lower power rating, and therefore an increased labour cost in NOK/kWp.

Practically all assumptions used in the economical evaluation are highly debatable. As for the component prices, these could change rapidly, and will also depend on volumes and market competition. BoS-components are often sold as complete systems, and there is hence limited data showing the exact distribution of costs between the different components, particularly in the Norwegian market.

The labour costs are estimated from an assumed amount of hours necessary in order to mount the systems. It is likely that the farmer would be able to reduce this cost by doing parts of the mounting job, or by assisting in the construction process. This would in turn lower the LCOE. The prices on modules and BoS components have been steadily dropping in recent years, and a continuation of this trend will increase the competitiveness of PV also in Norway.

As for the NPV estimations, these are highly dependent on future electricity prices, certificate prices and utility costs. Particularly the utility costs become very low with the assumptions made here, and it could be argued that the construction of a PV-system could also lower the monthly peak power, and hence reduce the utility cost even further. Such an assumption would require a scenario where the peak power was concentrated around daytime, which is not the case for this farm.

Most households in Norway have a utility price distribution were the energy tariff is between 0.30 NOK/kWh and 0.40 NOK/kWh, and such an arrangement would clearly improve the NPV of these systems. Nevertheless, such an arrangement would cause an increase in the farmer´s overall utility cost.

Figure 65 shows how a change in one of the assumptions made in the calculations could affect the calculated LCOE. Changes in the investment cost of the system will have a large influence on the LCOE, as will the selected discount rate. As previously mentioned, the investment cost could be reduced by doing some of the construction work, although the limited competition in the Norwegian market could also cause a investment cost higher than estimated.

In the base case, a discount rate of 6% was assumed. However, some would argue that this is to low for a long-term investment where the value of electricity is highly uncertain. Others would claim that the current low risk-free rate of return makes 4% an acceptable discount rate.

Maintenance costs are assumed to be equal at 0.04 NOK/kWhfor each year, except for year 12 when a replacement of inverters is expected. However, maintenance costs are not likely to be constant for each year, and should be limited during the first years of operation. Furthermore,

increased quality of inverters could also mean that replacement of inverters will be unnecessary, or could be done later than expected. The sensitivity analysis therefore shows a best-case where no maintenance costs and no inverter replacement is assumed, and a worst-case where the maintenance cost is 0.06 NOK/kWh and the inverters are replaced in year 12.

The degradation rate is set a 0.50%, which is mainly linked to an assumed reduction in the performance of the modules. As a large fraction of the PV systems existing today is less than ten years old, there are limited data available about how the performance of PV systems develops in time, and this value is therefore also highly uncertain.

The sensitivities regarding system performance like meteorology, soiling losses and the module U-value has already been discussed, and these factors also have an influence on the sensitivity of the LCOE calculations. Particularly the differences in irradiation data stand out as a large uncertainty concerning the system yield. It could be argued that the irradiation values could also become significantly lower than assumed, and soiling losses significantly higher. However, the settings used in the simulations are conservative when comparing them to collected data. The LCOE estimation can thus be considered to be a conservative estimate with respect to the technical performance of the system.

6. Conclusion

There are large uncertainties related to the solar resource at the site considered in this thesis. The different sources consulted suggest that the global irradiation on the horizontal plane is between 861 kWh/m^2 and 1005 kWh/m^2 at this site.

The combined maximum array power of the best-performing system from each of the three roofs are 105.5 kWp, which would give a yearly yield of 86 607 kWh, and an average specific yield of 821 kWh/kWp. However, the yearly system yield is sensitive to uncertainties in irradiation data, soiling losses caused by snow and particles, and the module U-value.

Different systems have been suggested for the three largest roofs on the Roer farm. All the best-performing systems consist of REC modules. Two of the systems include Eltek Valere inverters, while one system includes SMA inverters.

The production is concentrated around the spring and summer months, while the consumption is largest during fall and winter. The farm is expected to export electricity for some times of the year, even if only one of the suggested systems is constructed. The farmer would then become a surplus customer, as the farm would remain a net-consumer of electricity when considering the entire year.

The NPV is negative for all the suggested systems, also when a possible 40% investment support was considered. The lowest calculated LCOE was 1.47 NOK/kWh, although this number is uncertain and sensitive to the assumptions made in the calculations.

7. Further Work

This thesis is a feasibility study, and some details with respect to PV system design is not included here. If any of the systems suggested in this thesis were to be built, further work would be necessary with respect to mechanical dimensioning of the mounting system, as well electrical dimensioning of an earthing system, in order to prevent damage to the equipment in case of lightning strikes.

Also, the amount of modules and inverters used in the simulations are highly limited compared to the amount available on the market today, and other systems should also be evaluated and compared with respect to system yield and cost.

The thesis has shown that there are uncertainties related to several of the key factors influencing system performance, particularly with respect to irradiation data and snow shedding. No literature has been found that addresses these issues in Scandinavia, and it would be interesting to learn more about why different data sources provide such different results with respect to irradiation data. With respect to the influence of snow cover, a data collection process from PV systems installed in Norway and Sweden combined with weather data from the sites could provide useful information about this issue.

Also, the uncertainties in the economical estimations done here could be further addressed by collecting more information from a larger number of market actors. As the Norwegian market structure gives an incentive to consume the produced electricity locally, it could be interesting to evaluate the possibility of adapting the consumption to the production from the PV system. Such an adaption could improve the economics of a PV system installation in Norway, and bring the project closer to a positive NPV.

Finally, a roll out of PV systems in Norway of scale could have both positive and negative effects from a power system point of view, i.e. related to possible reduced marginal losses in the grid and the effect of a roll out on voltage quality and grid stability. An assessment of these could also be an interesting continuation of this thesis.

8. References

[1] The Ministry of Petroleum and Energy. (2011, April 25th). *Target of 67.5 percent for Norway´s renewable energy share by 2020*. Available: http://www.regjeringen.no/en/dep/oed/press-center/press-releases/2011/target-of-675-percent-for-norways-renewa.html?id=651715

[2] R. T. Paynter and B. J. T. Boydell, *Electronics Technology Fundamentals*. New Jersey: Pearson Prentice Hall, 2009.

[3] J. Twidell and T. Weir, *Renewable Energy Sources*. New York: Taylor & Francis Ltd., 2006.

[4] C. J. Chen, *Physics of Solar Energy*. New Jersey: John Wiley & Sons, Inc, 2011.

[5] T. Markvart, Ed., *Solar Electricity* (Energy Engineering Learning Package. John Wiley & Sons Inc., 2000, p.^pp. Pages.

[6] H. Häberlin, *Photovoltaics System Design and Practice* vol. 1. United Kingdom: John Wiley & Sons, Ltd, 2012.

[7] A. Mermoud, "PVsyst - Components database: PV Modules," U. o. Geneva, Ed., ed, 2013.

[8] G. Stapleton and S. Neill, *Grid-connected Solar Electric Systems - The Earthscan Expert Handbook for Planning, Design and Installation*. New York: Earthscan, 2012.

[9] Europe Solar. (2012, April 29th). *Price Trend PV modules*. Available: http://www.europe-solar.de/catalog/index.php?main_page=page_3

[10] SolarServer. (2013, April 29th). *PVX spot market price index solar PV modules*. Available: http://www.solarserver.com/service/pvx-spot-market-price-index-solar-pv-modules.html

[11] SMA Solar Technology AG, "Intensive Seminar - Inverters," S. S. Technology, Ed., ed: SMA Solar Technology AG, 2012.

[12] Schüco, "Premium Line MSE500 Mounting Systems," ed. Germany, 2013.

[13] American Society for Testing and Materials(ASTM), "Standard Tables for Reference Solar Spectral Irradiances: Direct Normal and Hemispherical on 37 Tilted Surface," ed: ASTM, 2003.

[14] M. Súri, T. A. Huld, E. D. Dunlop, and H. A. Ossenbrink, "Potential of solar electricity generation in the European Union member states and candidate countries," vol. 81, 2007.

[15] G. Howell, "Utility-Intertied Solar Electric Houses - Characteristics, Benefits, Limitations and Potential Barrieres," in *The Canadian Renewable Energy Guide*, ed: Tyrell Press Ltd, 1999.

[16] H. S. S.Beringer, I.Lohse, G. Seckmeyer, "Case study showing that the tilt angle of photovolatic plants is nearly irrelevant," Institute of Meteorology and Climatology, Hannover2010.

[17] A. Woyte, J. Nijs, and R. Belmans, "Partial shadowing of photovoltaic arrays with differen system configurations: Litterature review and field test results," *Solar Energy,* vol. 74, p. 17, 2003.

[18] A. Mermoud, "PVsyst contextual help," vol. 6.04, ed. University of Geneva: PVSyst, 2013.

[19] S. Canada, "Impacts of Soiling on Utility-Scale PV System Performance," *Solar Professional,* 2013.

[20] D. Thevenard, "Uncertainty in long-term photovolatic yield predictions," Quebec2010.
[21] M. G. Tamizhmani, A. Mikonowicz, and J. Kuitche, "Nameplate, Datasheet and Sampling Requirements for PV modules," Arizona2011.
[22] NVE. (2013, February 20th). *Plusskunder*. Available: http://www.nve.no/no/Kraftmarked/Nettleie1/Beregning-av-tariffer-for-innmating-fra-produksjon/Plusskunder/
[23] K. Ryen and S. Kvikstad, "Tilknytning av produksjonsanlegg 230 - 400 V," Hafslund Nett AS2006.
[24] P. E. Morthorst, P. Helby, J. Twidell, O. Hohmeyer, D. Mora, H. Auer*, et al.*, "Support Schemes for Renewable Energy - A Comparative Analysis of Payment Mechanisms in the EU," 2002.
[25] The Ministry of Petroleum and Energy. (2012, February 19th). *Electricity certificates*. Available: http://www.regjeringen.no/en/dep/oed/Subject/energy-in-norway/electricity-certificates.html?id=517462
[26] Norwegian Water Resources and Energy Directorate. (2012, February 19th). *Electricity certificates*. Available: http://www.nve.no/en/Electricity-market/Electricity-certificates/
[27] ENOVA, "Hjelp til deg som skal kjøpe solfanger," ed. Trondheim: ENOVA, 2010.
[28] Innovasjon Norge, "Miljøteknologiordningen," ed. Oslo: Innovasjon Norge, 2012.
[29] M. Helbæk and S. Lindset, *Finansiering og investering - Kort og godt*. Trondheim: Universitetsforlaget, 2007.
[30] S. B.Darling, F. You, T. Veselka, and A. Velosa, "Assumptions and the Levelized Cost of Energy for Photovoltaics," 2011.
[31] B. Veatch, "Levelized cost of Energy Calculation - Methodology and Sensitivity."
[32] P. O. Roer, "Information about the buildings on the Roer Farm," A. Størdal, Ed., ed, 2013.
[33] V. Thue-Hansen and A. A. Grimenes, "Meteorologiske data for Ås 1950-2012," UMB, Ås2012.
[34] Bioforsk. (2013, February 25th). *Bioforsk weather data - Landbruksmeteorologisk tjeneste*.
[35] Meteotest, "Meteonorm report for Rygge," Switzerland2013.
[36] NASA, "Surface meteorology and Solar Energy(SSE) Release 6.0 Methodology," NASA2013.
[37] National Renewable Energy Laboratory. (2012, April 1st). *How to change parameters in PVWatts*.
[38] T. Townsend and L. Powers, "Photovoltaics and snow: An update from two winters of measurements in the Sierra," San Ramon, CA2011.
[39] J. Z. Casanova, M.Piliougine, J. Carretero, P.Bernaola, P.Carpena, L.Mora-López*, et al.*, "Analysis of dust losses in photovoltaic modules," Universidad dé Malaga, Malaga2011.
[40] W. Sun. (2013, April 25th). *Wind & Sun - Products*. Available: http://www.windandsun.co.uk
[41] Bright Green Energy. (2013, April 25th). *Bright Green Energy*. Available: http://www.wirefreedirect.com
[42] C.Good, H.Persson, Ø.Kleven, M.Norton, and T.Boström, "Towards cost-efficient grid-connected PV power plants in Northern Scandinavia," presented at the 26th European Photovoltaic Solar Energy Conference and Exhibition, 2011.
[43] NASDAQ Commodities. (2013). *Nordpool Futures* Available: http://www.nasdaqomx.com/commodities/markets/marketprices/

[44] Hafslund. (2013, April 25th). *Nettleiepriser for bedrifter og næringsliv*. Available: http://www.hafslundnett.no/nett/artikler/les_artikkel.asp?artikkelid=239
[45] E. Grudic, "Egenproduksjon Roer Gård," Contact through e-mail ed, 2013.
[46] A. Hazlehurst, "Economic Analysis of Solar Power: Achieving Grid Parity," Stanford Graduate School of Business2008.
[47] E. Wilhelmsen, "Diskusjonsnotat: Når kommer solcellerevolusjonen til Norge?," Zero Emission Resource Organisation(ZERO)2013.

Appendix A: Meteorological Data

Meteorological data were collected from four different weather stations and four different databases. As it was considered unpractical to present all the data collected in the thesis, additional information about the meteorological data is shown in this appendix. Figure A.1 shows the location of the farm and the local weather stations consulted in the thesis.

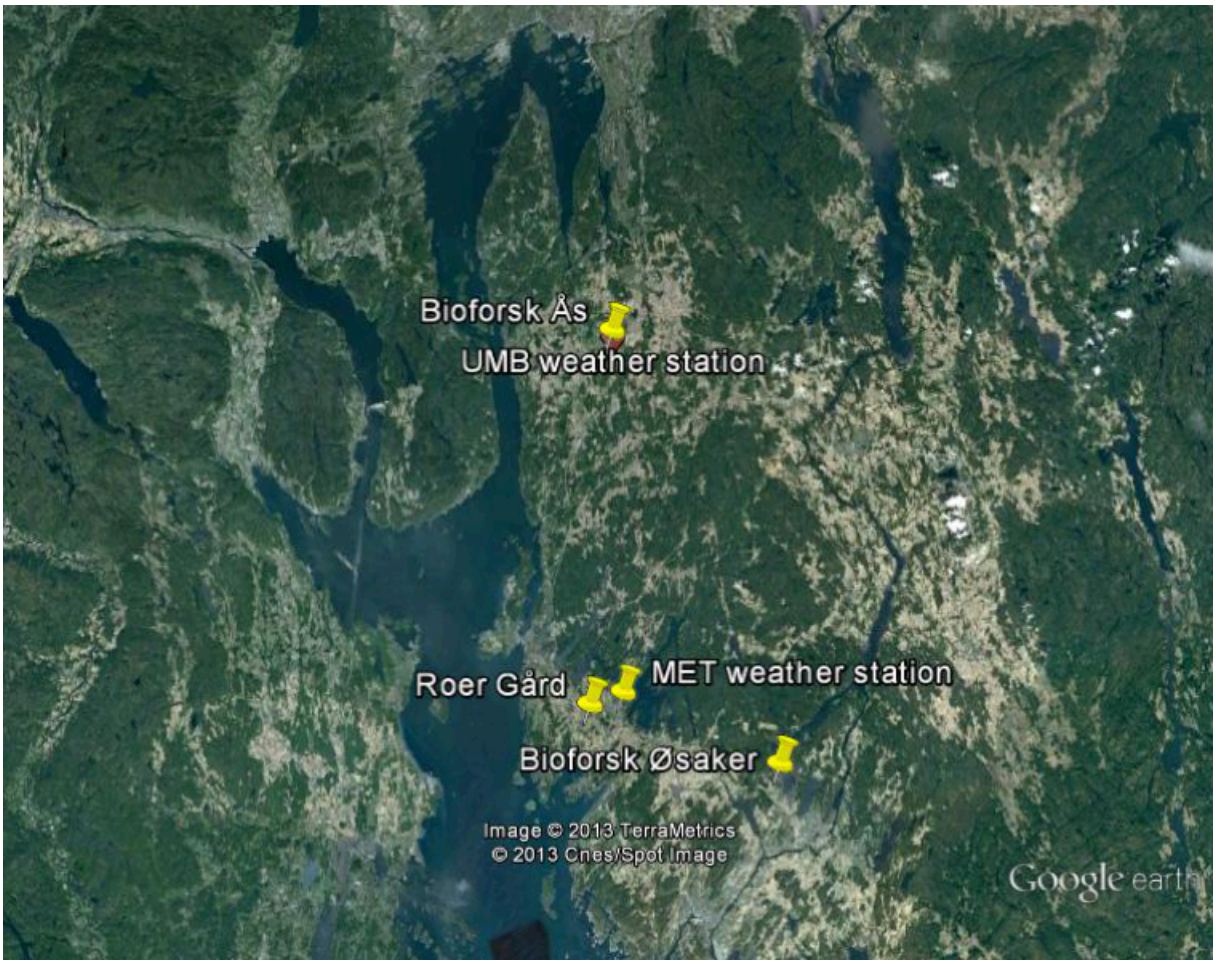

FigureA 1: Map from Google Earth showing the different weather stations used and Roer Gård.

Table A.1 shows the average global average irradiance values from each of the three weather stations performing irradiance measurements.

.

	UMB Global[kWh/m^2]	Bioforsk - Ås Global [kWh/m^2]	Bioforsk - Øsaker Global [kWh/m^2]
January	9.9	11.5	10.3
February	25.9	26.8	24.2
March	64.7	73.3	72.2
April	95.5	110.4	112.5
May	146.5	155.7	156.7
June	151.9	173.3	174.4
July	150.9	155.5	153.3
August	115.3	121.9	121.8
September	71.6	79.1	78.1
October	32.1	38.3	37.2
November	11.1	12.8	11.6
December	5.8	7.2	7.1
Sum	**881**	**966**	**959**

Table A1: Average global irradiation measurements collected from three weather stations.

Table A.2 shows the average global irradiance measurements collected from four different databases. The databases do not necessarily provide the irradiation data in the unit shown in the table, some databases also use Wh/m^2/day. In these cases, the numbers have been multiplied by the number of days in order to get values with the same unit.

	RETScreen Global[kWh/m^2]	Satel-Light Global[kWh/m^2]	PVGIS Global[kWh/m^2]	Meteonorm Global[kWh/m^2]
January	12.1	10.3	8.6	9.0
February	30.5	28.4	22.9	23.0
March	71.6	69.9	54.6	68.0
April	111.0	98.9	96.0	117.0
May	164.9	156.6	141.7	162.0
June	166.2	152.4	156.0	174.0
July	170.8	170.9	149.4	169.0
August	131.1	133.5	111.6	118.0
September	82.8	79.6	68.7	82.0
October	40.3	36.6	32.9	36.0
November	16.2	12.5	12.3	11.0
December	7.4	7.2	6.3	5.0
Sum	**1005**	**957**	**861**	**974**

Table A 2: Global irradiation values collected from four different weather stations.

Tabele A.3 shows the input data in Meteoset B, which was used in the sensitivity analysis. Meteoset B consists of irradiance data from PVGIS, and

	Global [kWh/m^2]	Diffuse[kWh/m^2]	T[°C]	Wind speed[m/s]
January	8.6	6.6	-4.1	3.5
February	22.9	15.8	-4.2	3.2
March	54.6	34.3	-0.4	3.6
April	96.0	53.1	4.2	3.8
May	141.7	68.0	10.3	3.9
June	156.0	74.1	14.7	4.1
July	149.4	76.5	15.9	3.9
August	111.6	61.6	14.9	3.6
September	68.7	38.6	10.8	3.7
October	32.9	22.3	6.8	3.7
November	12.3	9.0	1.2	3.6
December	6.3	5.1	-2.5	3.5

Table A 3: Meteoset B.

Table A.4 shows Meteoset C, which was used in the sensitivity analysis. Meteoset C consists of irradiance data from Meteonorm, and temperature and wind data from MET.

	Global [kWh/m^2]	Diffuse[kWh/m^2]	T[°C]	Wind speed[m/s]
January	9.0	6.0	-4.1	3.5
February	23.0	14.0	-4.2	3.2
March	68.0	33.0	-0.4	3.6
April	117.0	49.0	4.2	3.8
May	162.0	69.0	10.3	3.9
June	174.0	76.0	14.7	4.1
July	169.0	79.0	15.9	3.9
August	118.0	61.0	14.9	3.6
September	82.0	45.0	10.8	3.7
October	36.0	21.0	6.8	3.7
November	11.0	8.0	1.2	3.6
December	5.0	4.0	-2.5	3.5

Table A 4: Meteoset C.

Table A.5 shows the collected monthly values for irradiation data at the UMB weather station in Ås. The data is collected from Grimenes, Thue-Hansen "Meteorologiske data for Ås", UMB, 1950-2012.

UMB, Ås

Global

	1983(kWt/m²)	1984(kWt/m²)	1985(kWt/m²)	1986(kWt/m²)	1987(kWt/m²)	1988(kWt/m²)	1989(kWt/m²)	1990(kWt/m²)	1991(kWt/m²)	1992(kWt/m²)	1993(kWt/m²)	1994(kWt/m²)	1995(kWt/m²)	1996(kWt/m²)	1997(kWt/m²)	1998(kWt/m²)	1999(kWt/m²)	2000(kWt/m²)	2001(kWt/m²)	2002(kWt/m²)	2003(kWt/m²)	2004(kWt/m²)	2005(kWt/m²)	2006(kWt/m²)	2007(kWt/m²)	2008(kWt/m²)	2009(kWt/m²)	2010(kWt/m²)	2011(kWt/m²)	2012(kWt/m²)	Global average(1983-2012)(kWt/m²)	Global
Januar		36.27	37.68	39.1	38.4		35.9	28.0	36.7	37.5	40.0	40.6	37.91		33.34	41.39	34.86	32.86	38.64	27.92	32.43	37.45	27.70	36.32	30.65	34.85	32.08	31.00	40.27	43.83	34.96	35.7
Februar		71.28	86.75	112.5	94.0		76.0		95.7	83.0	84.4	103.77	90.88		110.50	89.35	82.22	108.32	93.01	105.32	91.65	85.35	115.40	91.72	90.33	59.44	93.11	102.30	93.99	96.79	102.30	93.2
März	132.99		189.60	170.3	221.4		179.4	128.8	133.3	171.9	284.5	208.86	213.51		173.72	191.10	246.65	173.84	269.86	240.61	246.50	235.66	260.23	261.19	267.13	227.01	233.18	228.08	233.84	277.60	277.86	232.9
April	265.77	271.77	336.04	313.5	357.9		265.3	336.8	332.3	314.5	366.8	336.21	373.46		377.26	438.12	244.40	327.12	290.15	302.65	316.84	400.30	335.62	404.25	338.10	408.34	344.83	407.91	400.88	446.99	399.17	343.7
Mai	362.10	390.00	421.75	440.7	461.4	493.0	376.0	616.1	509.1	601.6	573.0	652.28	588.10		438.38	495.37	594.11	575.75	590.00	574.96	508.94	434.60	572.67	460.72	500.17	482.67	619.27	601.95	545.09	561.43	598.16	527.5
Juni	395.27	433.65	476.56	500.5	373.9	538.9	586.5	514.4	361.8		577.5	638.82	598.38		537.92	550.94	462.54	471.63	532.19	592.52	617.66	575.12	557.69	574.08	622.15	670.12	655.50	682.31	627.86	598.99	538.72	546.9
Juli	632.04	406.02	427.75	498.3	595.1	446.0	507.8	559.6			486.3	418.6	375.78	570.19	422.72	485.69	401.59	472.79	451.76	408.34	472.54	479.92	435.20	419.62	355.32	418.35	393.12	424.08	391.99	405.69	437.07	415.1
August	534.46	357.00		233.9	338.0	384.1	347.5	425.5	382.9		288.2	228.37	203.23		295.96	306.31	235.33	246.48	273.24	229.80	232.20	265.07	269.12	261.34	260.88	289.29	228.64	300.85	274.18	294.45	288.84	257.8
September	192.07	197.89	231.86	208.0	269.9	228.3	257.2	234.8	277.2		233.2	228.37	203.23		195.96	306.31	235.33	246.48	273.24	229.80	232.20	265.07	269.12	261.34	260.88	289.29	228.64	300.85	274.18	294.45	288.84	257.8
Oktober	104.80	122.30	133.41	119.0	56.9	90.8	121.9	94.7	105.7	116.0	111.3	133.50	107.82		106.20	145.10	117.71	128.55	77.95	100.95	101.70	169.77	102.13	114.31	88.97	142.24	134.72	148.73	122.59	122.08	122.05	115.5
November	52.65	21.60	45.21	39.3		53.9	29.3	38.5	34.7	34.7	24.0	42.00	30.35		45.78	39.00	30.73	44.40	24.40	50.28	41.15	33.94	48.38	35.89	47.86	48.87	54.08	22.44	50.98	30.91	34.28		40.0
Desember	18.74	14.71	21.44	17.6		24.0	21.9		24.1	22.7	21.4	18.49	21.38		23.70	13.50	22.12	20.81	16.22	23.15	21.30	20.63	20.21	19.11	20.78	20.89	20.45	21.38	28.29	24.37	23.27		21.0

Diffuse

	1983(kWt/m²)	1984(kWt/m²)	1985(kWt/m²)	1986(kWt/m²)	1987(kWt/m²)	1988(kWt/m²)	1989(kWt/m²)	1990(kWt/m²)	1991(kWt/m²)	1992(kWt/m²)	1993(kWt/m²)	1994(kWt/m²)	1995(kWt/m²)	1996(kWt/m²)	1997(kWt/m²)	1998(kWt/m²)	1999(kWt/m²)	2000(kWt/m²)	2001(kWt/m²)	2002(kWt/m²)	2003(kWt/m²)	2004(kWt/m²)	2005(kWt/m²)	2006(kWt/m²)	2007(kWt/m²)	2008(kWt/m²)	2009(kWt/m²)	2010(kWt/m²)	2011(kWt/m²)	2012(kWt/m²)	Diffuse average(1983-2012)(kWt/m²)	Diffuse
Januar				25.50	24.70		23.80	26.10	22.80	28.50	23.10		22.38		21.70	23.67	23.64	24.71	24.00	23.08	24.36	25.83	25.16	25.38	22.63	24.70	20.25	23.42	30.85	27.21	28.51	24.6	
Februar			82.52	90.00	111.50		106.50	88.30	51.70	52.00	45.30	62.73	49.82		136.41	112.53	127.26	111.02	108.46	104.11	116.44	119.68	120.80	116.46	116.38	99.49	118.11	135.80	138.40	132.41	119.83	112.2	
März	81.65			136.50	146.30		153.50	198.30	155.20	159.70		156.21	160.60		182.67	201.81	161.16	192.59	167.51	170.01	171.7	143.98	177.59	154.49	171.69	144.16	160.13	186.00	181.92	180.57	170.23	168.8	
April	165.53			173.20	181.70	150.00	178.60	256.70	211.60	213.90		185.92			232.87		240.94	219.57	208.08	215.47	244.72	218.87	227.70	194.11	207.70	257.28	237.02	266.53	265.57	221.76	241.72	227.2	
Mai	209.40			195.10	196.00		186.90		199.50			197.92			236.63	221.09	240.94	227.67	208.08	236.71	221.87	219.20	253.21	227.70	284.11	225.56	221.76	277.15	270.89	242.88	238.50	270.39	225.4	
Juni	225.72	103.53		189.60	199.70	211.00	188.50			256.10		198.08			262.32	240.11	272.07	228.07	248.06	223.94	228.37	228.13	232.06	246.82	229.02	247.57	217.57	264.94	249.49	245.67	278.02	232.5	
Juli	226.28			229.50	247.30	154.80	168.70	170.60	155.70		157.20		142.07		173.75	158.41	207.55	168.41	211.42	190.88	188.30	176.27	198.96	206.24	176.02	183.57	200.86	198.14	221.63	206.97	204.75	179.3	
August	156.55			91.00	154.80	147.45	168.70	170.60	155.70			94.65	92.82		104.68	119.25	111.34	119.76	118.16	130.61	135.14	169.37	112.38	117.23	120.07	109.53	138.77	141.31	109.93	130.73	119.21	112.8	
September	104.31		87.15	94.50	88.70	87.80	83.60	113.80	94.70		124.80	55.02	56.99		66.60	68.05	71.82	70.49	58.73	64.28	70.07	58.65	72.20	63.52	65.97	63.69	71.81	66.70	63.33	70.91	66.29	61.0	
Oktober	46.61	58.41	55.52	56.20	30.90	53.80	44.20	49.20	54.40	72.80	53.10	32.53	24.96		28.11	20.88	22.82	27.82	25.19	21.49	28.75	23.58		27.18	22.22	34.99		31.80	25.96	30.44		26.4	
November	31.89	17.81			34.40	16.70		21.90	23.00	18.80	27.15	30.38			31.53	24.96	28.11	16.85	13.14	17.35	16.90	14.88	17.01	14.63		14.14	18.16	16.74		17.14	17.32		
Desember	14.26	0.35	15.95	11.50		15.40	14.20		17.60	15.00	15.90	12.57	9.15		17.78	12.24	16.62															15.2	

Table A 5: Global and diffuse monthly irradiation data from UMB(1983-2012).

Table A.6 shows the monthly irradiation data collected from the Bioforsk Agromet service for Ås.

Global, Bioforsk Ås

	2003	2004	2005	2006	2007	2008	2009	2010	2011	2012	Average[MJ/m²]	Average[kWh/m²]
January	47.1	29.9	40.5	38.6	40.9	36.3	36.1	48.4	56.6	39.3	41.4	11.5
February	106.7	129.2	103.6	107.4		93.3	107.2	99.4	108.6	110	107.3	29.8
March	260.7	287	289.8	301.1		236.6	231	243.6	288.6	292.2	270.1	75.0
April	438.3	362.9	443.3	348.2	411.2	343	415.2	416.4	463	334.5	397.6	110.4
May	460.9	616.9	500.4	547.9	507.1	622.6	609	552.5	571.6	617.9	560.7	155.7
June	615.4	600.4	619.9	676.1	622.9	659.5	685.9	639.1	554.2	563.9	623.7	173.3
July	613.1	577.7	586.1	674.4	462.2	656.3	477.7	539.5	521.6	490.7	559.9	155.5
August	517	459.7	456	440	460.8	347.9	430.2	401.5	420.6	452.9	438.7	121.9
September	284.9	292.8	285.5	288.3	296.1	229.3	305.6	308	259.2	297.5	284.7	79.1
October	190.3	111	127.5	98.5	160.9	137.6	155.9	134.4	129.6	133.2	137.9	38.3
November	37.5	60.3	42.2	58.3	54.4	57.2	23.8	57.9	32.5	34.9	45.9	12.8
December	24.6	24.1	23	26.8	24.9	14	26	38.5	28.9	29.7	26.1	7.2
												970.5

Table A6: Monthly global irradiation values collected from Bioforsk Ås(2003-2012).

Table A.7 shows the monthly irradiation data collected from the Bioforsk Agromet service for Øsaker.

	2005	2006	2007	2008	2009	2010	2011	2012	Average[MJ/m²]	Average[kWh/m²]
January	38	32.9	31.3	35.2	32.1	43.8	47.5	35.5	37.0	10.3
February	98.3	96.1	50.9	82.4	63.5	90.5	106.2	107.9	87.0	24.2
March	297.7	300	244.6	217.3	223.2	236.2	270.6	290.2	260.0	72.2
April	423.6	348.5	468.9	356.6	428.2	418.3	454.8	340.6	404.9	112.5
May	492.6	541.4	480.5	627.2	617.7	562.1	571.9	618.6	564.0	156.7
June	605.5	662	611.5	673.1	682.5	655.8	594.9	537	627.8	174.4
July	602.3	668.6	442.8	661.7	486.3	528.9	517.6	506.5	551.8	153.3
August	439.7	467.3	445.7	407.7	439.8	422.8	437.1	449.1	438.7	121.8
September	289.3	294.3	286.8	235.1	299.6	308.2	252.2	283.3	281.1	78.1
October	140.3	97.7	147	137.4	154.3	131.6	129.8	132.2	133.8	37.2
November	41.9	52.5	44.8	55.5	23	52.4	33.2	32.2	41.9	11.6
December	24.2	23.7	13.9	18.4	26.9	40.1	25.2	31.2	25.5	7.1
Average	291.1	298.8	272.4	292.3	289.8	290.9	286.8	280.4	287.8	959.3

Table A7: Monthly global irradiation values collect from Bioforsk Øsaker(2005-2012).

Table A.8 shows the minimum temperature observed at Rygge for each month during the years between 1961 and 1990, while table A.9 shows the maximum observed temperature for the same time period. The data is collected from MET´s online service eKlima.

17150 RYGGE, Minimum temperature (TAN)

Year	Jan	Feb	Mar	Apr	May	Jun	Jul	Aug	Sep	Oct	Nov	Dec	Total	Mean
1961	-22,1	-17,6	-5,7	-8,6	-0,4	6,7	7,0	4,5	2,0	1,1	-8,8	-19,4		-5,1
1962	-21,0	-13,6	-28,4	-4,4	-1,6	0,1	5,6	5,0	0,0	-3,6	-11,5	-20,4		-7,8
1963	-24,6	-29,1	-22,0	-8,0	2,4	7,5	4,1	6,0	-1,6	-3,0	-8,2	-19,1		-8,0
1964	-18,1	-21,4	-11,2	-7,5	0,0	0,6	5,4	3,9	-1,0	-4,6	-4,9	-18,2		-6,4
1965	-17,4	-14,9	-21,2	-4,1	-1,5	4,9	5,0	3,4	1,3	-2,0	-19,5	-24,4		-7,5
1966	-25,4	-30,8	-16,5	-11,3	-1,1	3,3	7,6	4,2	-3,9	-6,0	-5,7	-16,5		-8,5
1967	-22,5	-17,8	-4,9	-6,1	-1,5	3,1	5,2	5,6	2,0	-3,1	-2,6	-22,6		-5,4
1968	-27,2	-21,4	-14,9	-9,5	-1,7	3,9	5,4	4,1	-4,5	-6,5	-15,1	-18,4		-8,8
1969	-20,8	-25,7	-20,3	-3,9	-0,1	0,3	7,4	5,6	0,6	-4,7	-19,2	-17,3		-8,2
1970	-21,0	-28,5	-14,9	-9,8	-0,6	4,9	6,3	5,7	-3,4	-5,0	-13,0	-14,1		-7,8
1971	-20,2	-19,0	-19,6	-5,1	-4,4	2,7	3,9	3,2	-2,0	-7,5	-14,8	-12,2		-7,9
1972	-17,0	-13,0	-18,9	-3,9	-0,6	5,0	8,5	3,4	-3,4	-5,6	-12,2	-7,5		-5,4
1973	-11,7	-10,7	-8,0	-5,9	-1,4	2,4	8,2	1,8	0,6	-9,3	-18,7	-20,6		-6,1
1974	-7,6	-14,4	-9,6	-7,9	-3,0	2,0	5,7	5,0	3,3	-3,5	-7,8	-11,6		-4,1
1975	-12,0	-17,9	-9,3	-5,6	-1,0	-0,3	7,5	6,9	1,8	-8,4	-9,2	-18,0		-5,5
1976	-17,4	-15,9	-15,0	-4,4	-2,5	6,0	7,8	5,2	-0,7	-3,7	-10,5	-22,3		-6,1
1977	-23,9	-23,6	-15,1	-8,2	-0,3	4,8	5,7	3,7	-2,1	-1,1	-12,6	-10,6		-6,9
1978	-14,5	-26,0	-23,6	-5,6	-3,6	5,8	6,2	0,7	-2,1	-2,2	-12,0	-22,2		-8,3
1979	-23,9	-25,1	-20,8	-5,4	-0,9	6,3	3,6	4,1	-3,0	-5,1	-7,0	-16,7		-7,8
1980	-25,1	-25,5	-21,7	-6,5	-0,5	5,5	8,0	4,1	1,0	-9,7	-12,5	-14,4		-8,1
1981	-17,0	-19,3	-17,1	-6,0	-4,9	1,4	7,9	2,4	3,4	-4,5	-6,4	-24,0		-7,0
1982	-27,5	-17,6	-9,9	-3,5	0,4	4,0	7,0	4,0	0,5	-3,2	-6,4	-11,6		-5,3
1983	-11,5	-17,2	-15,0	-3,2	0,4	3,6	4,7	5,0	-2,6	-4,9	-15,4	-15,7		-6,0
1984	-18,0	-14,2	-12,4	-6,9	-2,1	5,2	7,0	6,5	0,1	-2,0	-6,5	-7,0		-4,2
1985	-22,8	-31,5	-10,3	-11,6	-0,3	5,5	7,4	3,5	-3,0	-4,8	-15,3	-22,0		-8,8
1986	-25,1	-27,2	-18,2	-7,2	0,8	5,2	6,5	2,9	-3,0	-5,5	-6,2	-15,6		-7,7
1987	-27,7	-22,0	-23,3	-5,2	-0,4	3,7	4,3	2,7	-1,9	-2,6	-10,8	-16,3		-8,3
1988	-10,2	-13,3	-14,9	-6,7	-1,6	4,2	7,9	5,1	3,1	-9,1	-17,2	-17,9		-5,9
1989	-7,3	-6,3	-6,7	-7,4	-0,6	0,6	4,6	2,5	-0,7	-5,0	-11,4	-18,7		-4,7
1990	-7,8	-4,1	-4,9	-8,2	0,0	6,0	6,5	3,5	-5,1	-5,5	-12,0	-15,0		-3,9
Number of	30	30	30	30	30	30	30	30	30	30	30	30		
Minimum	-27,7	-31,5	-28,4	-11,6	-4,9	-0,3	3,6	0,7	-5,1	-9,7	-19,5	-24,4		
Year	1987	1985	1962	1985	1981	1975	1979	1978	1990	1980	1965	1965		
Highest	-7,3	-4,1	-4,9	-3,2	2,4	7,5	8,5	6,9	3,4	1,1	-2,6	-7,0		
Year	1989	1990	1967	1983	1963	1963	1972	1975	1981	1961	1967	1984		
Total														
Mean	-18,9	-19,5	-15,1	-6,6	-1,1	3,8	6,3	4,1	-0,8	-4,7	-11,1	-17,0		

Table A8: Monthly minimum temperatures observed at Rygge(1961-1990).

17150 RYGGE, Maximum temperature (TAX)

Year	Jan	Feb	Mar	Apr	May	Jun	Jul	Aug	Sep	Oct	Nov	Dec	Total	Mean
1961	6,5	9,5	14,2	19,7	23,5	26,2	24,2	21,6	20,1	16,6	11,7	2,7		16,4
1962	5,7	8,0	4,5	15,5	16,7	22,8	22,9	22,3	18,9	17,8	9,0	6,1		14,2
1963	2,1	2,3	8,0	15,5	25,3	26,6	25,8	23,5	19,6	14,0	8,5	6,0		14,8
1964	6,2	10,2	11,0	17,2	24,0	27,6	24,5	25,5	20,3	14,9	9,3	8,9		16,6
1965	5,5	9,8	13,8	17,6	17,9	24,6	26,0	22,4	20,8	16,0	10,8	1,2		15,5
1966	3,5	1,7	9,0	13,5	20,0	30,6	28,9	23,2	20,6	13,7	9,4	8,0		15,2
1967	6,5	7,6	14,6	15,0	24,5	24,3	24,5	24,4	21,3	15,4	11,7	10,9		16,7
1968	6,5	4,3	11,9	18,8	21,6	26,0	25,7	27,0	25,0	14,4	7,1	2,8		15,9
1969	2,5	2,9	7,5	14,4	21,2	28,8	28,7	29,3	22,0	17,3	12,0	5,7		16,0
1970	0,6	-1,1	8,0	11,0	22,5	31,0	26,6	24,7	19,0	14,9	8,9	8,5		14,6
1971	6,5	9,3	8,2	14,7	25,7	26,6	28,6	25,0	22,0	20,0	13,4	11,0		17,6
1972	2,9	1,6	10,8	14,6	21,5	26,3	28,7	22,6	23,8	19,3	11,0	8,8		16,0
1973	11,1	10,2	13,5	16,0	22,4	26,0	29,8	24,0	22,4	19,6	12,0	6,8		17,8
1974	6,8	7,0	14,8	19,1	21,0	27,2	23,0	23,6	24,7	12,4	9,2	7,3		16,3
1975	11,1	5,8	9,9	15,7	24,5	27,4	27,4	33,2	22,4	15,4	11,3	12,1		18,0
1976	8,0	12,8	9,2	14,6	23,5	25,0	27,8	28,6	20,6	15,4	8,9	5,0		16,6
1977	4,8	1,9	7,0	14,1	25,9	30,0	30,4	25,6	19,2	16,1	11,2	6,3		16,0
1978	5,6	3,5	9,5	15,4	26,3	26,0	28,5	29,7	17,5	16,7	14,7	3,3		16,4
1979	5,1	6,7	6,3	16,2	26,9	28,4	23,6	25,8	19,8	13,1	9,8	9,4		15,9
1980	2,6	5,5	7,0	17,6	25,9	26,6	27,6	24,6	18,7	15,6	10,0	8,0		15,8
1981	10,2	8,1	13,2	18,1	26,2	22,3	26,0	23,0	20,0	14,5	10,7	7,1		16,6
1982	3,0	3,0	13,3	14,6	21,0	27,0	29,2	34,2	20,6	13,6	11,4	6,8		16,5
1983	9,5	3,1	9,6	16,5	18,6	27,8	30,1	27,3	22,7	16,6	14,0	8,4		17,0
1984	8,4	5,2	8,5	21,0	25,0	25,5	24,6	25,5	17,6	14,6	11,5	8,1		16,3
1985	0,2	2,6	6,6	12,5	23,9	24,4	25,9	24,4	18,1	18,9	9,0	7,0		14,5
1986	2,5	1,6	7,0	15,0	23,6	28,9	25,2	22,7	18,3	16,3	10,9	9,3		15,1
1987	6,7	6,6	9,2	17,7	27,0	20,5	28,6	22,7	19,2	14,8	9,0	8,5		15,9
1988	6,4	4,3	4,4	14,8	26,6	31,2	24,6	23,6	20,6	14,3	11,3	9,9		16,0
1989	11,2	9,3	12,2	21,8	21,6	27,6	30,0	23,8	21,7	16,8	11,8	9,8		18,1
1990	7,9	9,9	18,1	21,9	26,3	24,7	27,2	25,3	19,8	14,4	7,7	9,3		17,7
Number of	30	30	30	30	30	30	30	30	30	30	30	30		
Minimum	0,2	-1,1	4,4	11,0	16,7	20,5	22,9	21,6	17,5	12,4	7,1	1,2		
Year	1985	1970	1988	1970	1962	1987	1962	1961	1978	1974	1968	1965		
Highest	11,2	12,8	18,1	21,9	27,0	31,2	30,4	34,2	25,0	20,0	14,7	12,1		
Year	1989	1976	1990	1990	1987	1988	1977	1982	1968	1971	1978	1975		
Total														
Mean	5,9	5,8	10,0	16,3	23,4	26,6	26,8	25,3	20,6	15,8	10,6	7,4		

Table A9: Monthly maximum temperatures observed at Rygge(1961-1990).

Appendix B: Shade Analysis

The first step of a shade analysis in PVsyst is to draw a 3D scene that is as equal as possible to the real scene. During the site assessment, attention was therefore paid to the orientation of the buildings and the tilt angles, as well as the length, width and height of the buildings. If there are elements that are unlikely to cause any shade at the array, these should be left out of the 3D sketch in order to make the processing faster.

Figure B.1 shows the "Near shadings" dialog in PVsyst.

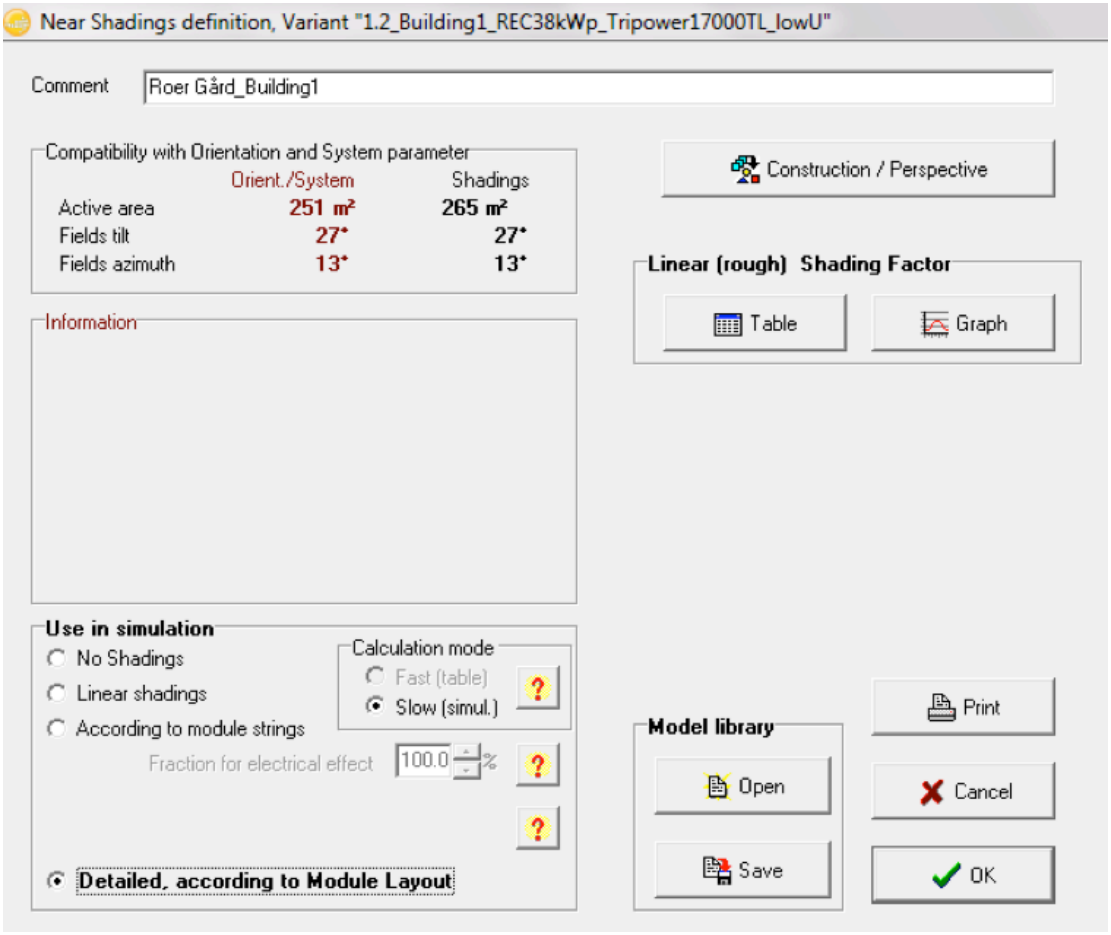

FigureB 2: The "Near Shadings" dialog in PVsyst.

When the scene is drawn and the array is located, a table showing the irradiance fraction which is lost at different positions. If the sun is located at a height of 30° and an azimuth angle of -100°, a table value of 0.019 indicates that 1.9% of the direct irradiance is lost when the sun is located at this position.

Figure B.2 shows how the PV module area was located at building 1 in the shade analysis and the simulations. Note that the ventilators and snow collectors occupy some of the roof area at building.

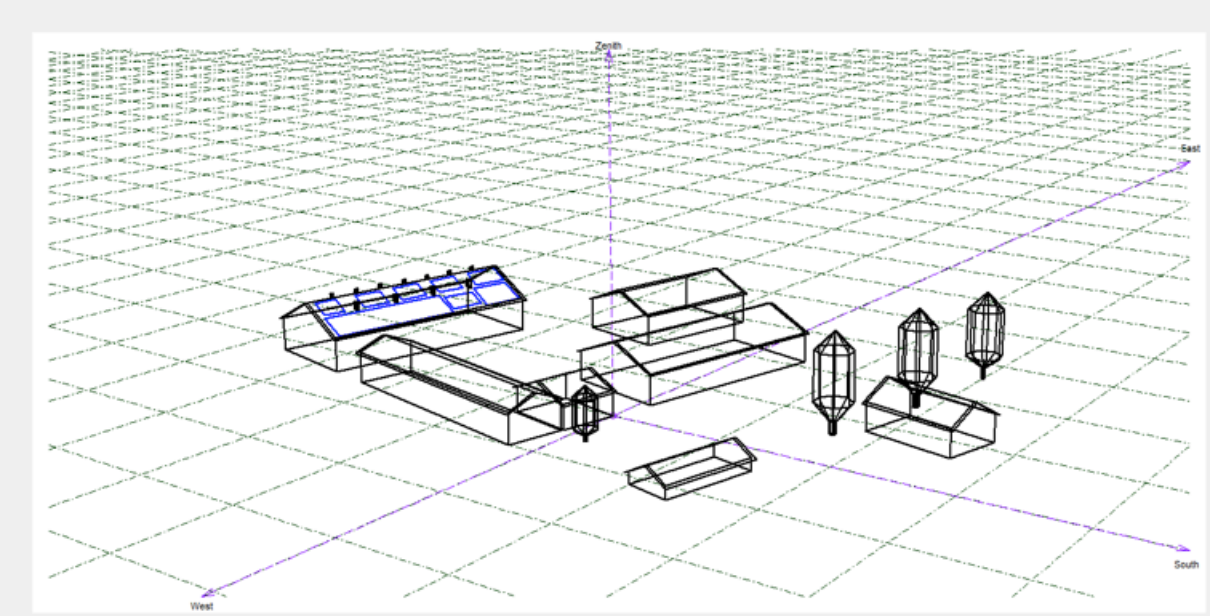

FigureB 3: The PV array location and 3D scene used in the simulations for building 1. From PVsyst.

Table B.1 shows the direct irradiance losses for building 1 at different angles between the building and the sun. In the bottom of the table, the shading factors for diffuse irradiance and reflected diffuse irradiance are shown. These are not dependent on the sun´s position, and therefore only one yearly factor is generated for each parameter, based on the geometry of the scene. It can be observed that the highest irradiance losses due to shading are experienced when the sun is low on the horizon and located at azimuth angles far from zero. There are practically no shading losses when the sun is high on the horizon.

Shading factor table (linear), for the beam component

Azimuth / Height	-180°	-160°	-140°	-120°	-100°	-80°	-60°	-40°	-20°	0°	20°	40°	60°	80°	100°	120°	140°	160°	180°
90°	0.000	0.000	0.000	0.000	0.000	0.000	0.000	0.000	0.000	0.000	0.000	0.000	0.000	0.000	0.000	0.000	0.000	0.000	0.000
80°	0.000	0.000	0.000	0.000	0.000	0.000	0.000	0.000	0.000	0.000	0.000	0.000	0.000	0.000	0.000	0.000	0.000	0.000	0.000
70°	0.000	0.000	0.000	0.000	0.000	0.000	0.000	0.000	0.000	0.000	0.000	0.000	0.000	0.000	0.000	0.000	0.000	0.000	0.000
60°	0.001	0.001	0.000	0.000	0.000	0.000	0.000	0.000	0.000	0.000	0.000	0.000	0.000	0.000	0.000	0.000	0.000	0.000	0.001
50°	0.010	0.011	0.007	0.003	0.002	0.000	0.000	0.000	0.000	0.000	0.000	0.000	0.000	0.000	0.000	0.002	0.003	0.006	0.010
40°	0.034	0.034	0.018	0.016	0.007	0.003	0.002	0.000	0.000	0.000	0.000	0.000	0.000	0.001	0.003	0.006	0.013	0.024	0.034
30°	0.103	0.118	0.089	0.039	0.021	0.008	0.004	0.001	0.000	0.000	0.000	0.000	0.000	0.003	0.007	0.016	0.040	0.081	0.103
20°	0.173	0.201	0.159	0.063	0.058	0.018	0.009	0.003	0.000	0.000	0.000	0.000	0.002	0.008	0.014	0.044	0.155	0.139	0.173
10°	Behind	Behind	Behind	Behind	0.095	0.046	0.020	0.008	0.001	0.000	0.000	0.000	0.006	0.016	0.034	0.247	0.270	Behind	Behind
2°	Behind	Behind	Behind	Behind	Behind	0.075	0.192	0.225	0.409	0.451	0.086	0.052	0.061	0.058	0.073	0.449	Behind	Behind	Behind

Shading factor on diffuse: 0.011 and for albedo: 0.372

Table B 10: Direct irradiance losses caused by shading on building 1. From PVsyst.

Figure B.3 shows how the PV module area was located on building 3 in the shade analysis and the simulations.

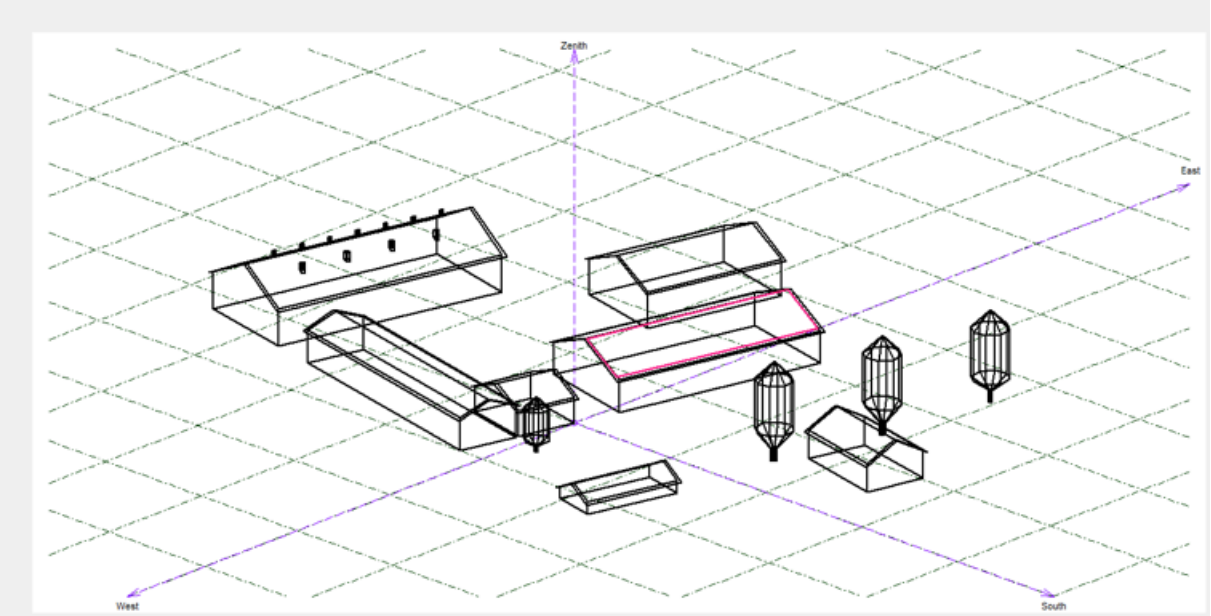

FigureB 4: The location of the PV array used in the shade analysis and simulations for building 3.From PVsyst.

Table B.2 shows the direct irradiance losses for the roof on building 3 for different solar angles. In the bottom of the table, the constant loss factors for diffuse irradiance and reflected diffuse irradiance are shown. Due to the trees located south of the building, the shading losses are relatively high for low angles. However, at solar angles above 20 degrees the shading losses are practically zero.

Shading factor table (linear), for the beam component

Azimuth / Height	-180°	-160°	-140°	-120°	-100°	-80°	-60°	-40°	-20°	0°	20°	40°	60°	80°	100°	120°	140°	160°	180°
90°	0.000	0.000	0.000	0.000	0.000	0.000	0.000	0.000	0.000	0.000	0.000	0.000	0.000	0.000	0.000	0.000	0.000	0.000	0.000
80°	0.000	0.000	0.000	0.000	0.000	0.000	0.000	0.000	0.000	0.000	0.000	0.000	0.000	0.000	0.000	0.000	0.000	0.000	0.000
70°	0.000	0.000	0.000	0.000	0.000	0.000	0.000	0.000	0.000	0.000	0.000	0.000	0.000	0.000	0.000	0.000	0.000	0.000	0.000
60°	0.000	0.000	0.000	0.000	0.000	0.000	0.000	0.000	0.000	0.000	0.000	0.000	0.000	0.000	0.000	0.000	0.000	0.000	0.000
50°	0.000	0.000	0.000	0.000	0.000	0.000	0.000	0.000	0.000	0.000	0.000	0.000	0.000	0.000	0.000	0.000	0.000	0.000	0.000
40°	0.000	0.000	0.000	0.000	0.000	0.000	0.000	0.000	0.000	0.000	0.000	0.000	0.000	0.000	0.000	0.000	0.000	0.000	0.000
30°	0.000	0.000	0.000	0.000	0.000	0.000	0.000	0.000	0.000	0.000	0.000	0.000	0.000	0.000	0.000	0.000	0.000	0.000	0.000
20°	0.000	0.000	0.000	0.000	0.000	0.000	0.000	0.000	0.000	0.000	0.003	0.000	0.000	0.000	0.000	0.000	0.000	0.000	0.000
10°	Behind	Behind	Behind	0.000	0.000	0.000	0.000	0.037	0.188	0.162	0.324	0.164	0.000	0.000	0.000	0.000	0.000	0.000	Behind
2°	Behind	Behind	Behind	Behind	Behind	0.000	0.000	0.131	0.270	0.384	0.516	0.255	0.000	0.112	0.010	0.000	Behind	Behind	Behind

Shading factor on diffuse: 0.015 and for albedo: 0.376

Table B 11: Direct irradiance losses caused by shading on building 3 for different solar angles. From PVsyst.

Figure B.4 shows how the PV module area was located on building 5 during the shade analysis and the simulations.

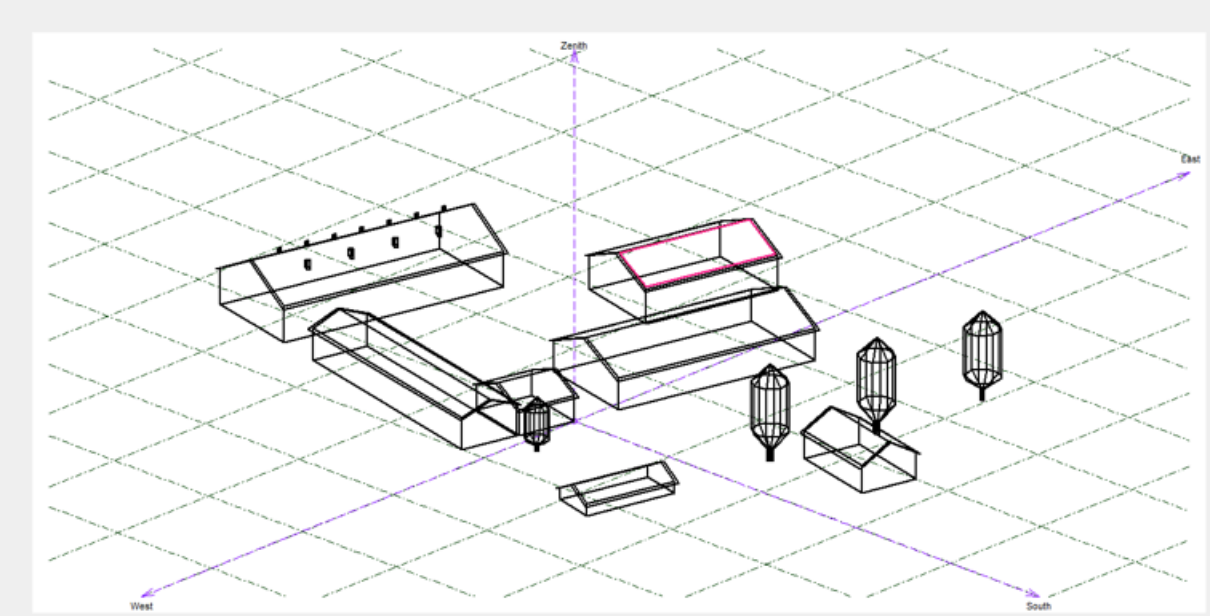

FigureB 5: Location of the PV array on building 5 used in the shade analysis and the simulations. From PVsyst.

Table B.3. shows the direct irradiance losses for the roof on building 5 for different solar angles. The shading on this roof is mainly caused by the trees located south of the building, and also by building 3, which is located almost directly south of the building.

Shading factor table (linear), for the beam component

Azimuth / Height	-180°	-160°	-140°	-120°	-100°	-80°	-60°	-40°	-20°	0°	20°	40°	60°	80°	100°	120°	140°	160°	180°
90°	0.000	0.000	0.000	0.000	0.000	0.000	0.000	0.000	0.000	0.000	0.000	0.000	0.000	0.000	0.000	0.000	0.000	0.000	0.000
80°	0.000	0.000	0.000	0.000	0.000	0.000	0.000	0.000	0.000	0.000	0.000	0.000	0.000	0.000	0.000	0.000	0.000	0.000	0.000
70°	0.000	0.000	0.000	0.000	0.000	0.000	0.000	0.000	0.000	0.000	0.000	0.000	0.000	0.000	0.000	0.000	0.000	0.000	0.000
60°	0.000	0.000	0.000	0.000	0.000	0.000	0.000	0.000	0.000	0.000	0.000	0.000	0.000	0.000	0.000	0.000	0.000	0.000	0.000
50°	0.000	0.000	0.000	0.000	0.000	0.000	0.000	0.000	0.000	0.000	0.000	0.000	0.000	0.000	0.000	0.000	0.000	0.000	0.000
40°	0.000	0.000	0.000	0.000	0.000	0.000	0.000	0.000	0.000	0.000	0.000	0.000	0.000	0.000	0.000	0.000	0.000	0.000	0.000
30°	0.000	0.000	0.000	0.000	0.000	0.000	0.000	0.000	0.000	0.000	0.000	0.000	0.000	0.000	0.000	0.000	0.000	0.000	0.000
20°	0.000	0.000	0.000	0.000	0.000	0.000	0.000	0.000	0.000	0.000	0.000	0.000	0.000	0.000	0.000	0.000	0.000	0.000	0.000
10°	Behind	Behind	Behind	0.000	0.000	0.000	0.000	0.000	0.000	0.012	0.063	0.020	0.000	0.000	0.000	0.000	0.000	0.000	Behind
2°	Behind	Behind	Behind	Behind	Behind	0.000	0.000	0.000	0.108	0.466	0.584	0.778	0.623	0.163	0.000	0.000	Behind	Behind	Behind

Shading factor on diffuse: 0.011 and for albedo: 0.643

Table B 12: Direct irradiance losses caused by shading on building 3 for different solar angles. From PVsyst.

Appendix C: Component Specifications

In this appendix, the product sheets of the modules and inverters used in the simulations are shown. The product sheets are collected from the manufacturers websites.

As manufacturers are continuously working to improve their products, the component specifications may have changed since the time they were collected. The manufacturer should therefore always be contacted directly in order to get product sheets that are up to date.

The order of the product sheets on the next pages is the following:

1) REC PE series
2) Suntech STP series
3) Solar Frontier SF series
4) SMA Tripower series
5) Eltek Valere Theia He-t series

ENERGIZING LIFE TOGETHER

REC

HIGH PERFORMANCE SOLAR MODULES

REC PEAK ENERGY SERIES

REC Peak Energy Series modules are the perfect choice for building solar systems that combine long lasting product quality with reliable power output. REC combines high quality design and manufacturing standards to produce high-performance solar modules with uncompromising quality.

MORE POWER PER M²

ROBUST AND DURABLE DESIGN

ENERGY PAYBACK TIME OF ONE YEAR

OPTIMIZED FOR ALL SUNLIGHT CONDITIONS

REC PEAK ENERGY SERIES

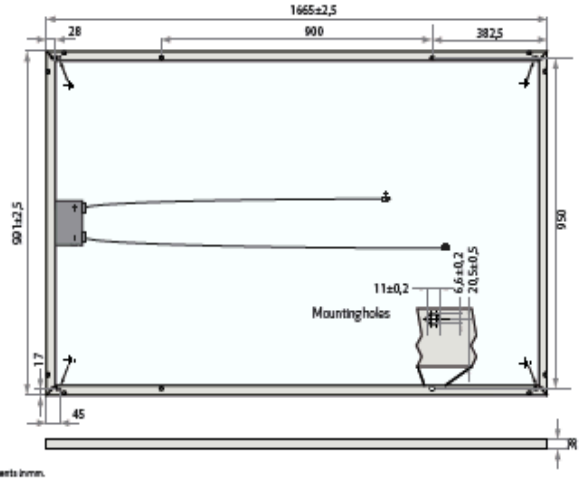

Measurements in mm.

15.8% EFFICIENCY

10 YEAR PRODUCT WARRANTY

25 YEAR LINEAR POWER OUTPUT WARRANTY

TEMPERATURE RATINGS	
Nominal Operating Cell Temperature (NOCT)	45.7°C (±2°C)
Temperature Coefficient of P_{MPP}	-0.40 %/°C
Temperature Coefficient of V_{OC}	-0.27 %/°C
Temperature Coefficient of I_{SC}	0.024 %/°C

ELECTRICAL DATA @STC	REC235PE	REC240PE	REC245PE	REC250PE	REC255PE	REC260PE
Nominal Power - P_{MPP} (Wp)	235	240	245	250	255	260
Watt Class Sorting - (W)	0/+5	0/+5	0/+5	0/+5	0/+5	0/+5
Nominal Power Voltage - V_{MPP} (V)	29.5	29.7	30.1	30.2	30.5	30.7
Nominal Power Current - I_{MPP} (A)	8.06	8.17	8.23	8.30	8.42	8.50
Open Circuit Voltage - V_{OC} (V)	36.6	36.8	37.1	37.4	37.6	37.8
Short Circuit Current - I_{SC} (A)	8.66	8.75	8.80	8.86	8.95	9.01
Module Efficiency (%)	14.2	14.5	14.8	15.1	15.5	15.8

Analysed data demonstrates that 99.7 % of modules produced have current and voltage tolerance of ±3% from nominal values.
Values at standard test conditions STC (airmass AM 1.5, irradiance 1000 W/m², cell temperature 25°C).
At low irradiance of 200 W/m² (AM 1.5 and cell temperature 25°C) at least 97 % of the STC module efficiency will be achieved.

GENERAL DATA	
Cell Type:	60 REC PE multi-crystalline 3 strings of 20 cells with bypass diodes
Glass:	3.2 mm solar glass with anti-reflection surface treatment
Back Sheet:	Double layer highly resistant polyester
Frame:	Anodized aluminium (silver)
Junction Box:	IP67 rated 4 mm² solar cable, 0.9 m + 1.2 m
Connectors:	MC4 (4 mm²) MC4 connectable (4 mm²) Radox twist lock (4 mm²)

ELECTRICAL DATA @NOCT	REC235PE	REC240PE	REC245PE	REC250PE	REC255PE	REC260PE
Nominal Power - P_{MPP} (Wp)	179	183	187	189	193	197
Nominal Power Voltage - V_{MPP} (V)	27.5	27.7	28.1	28.3	28.5	29.0
Nominal Power Current - I_{MPP} (A)	6.51	6.58	6.64	6.68	6.77	6.81
Open Circuit Voltage - V_{OC} (V)	34.2	34.4	34.7	35.0	35.3	35.7
Short Circuit Current - I_{SC} (A)	6.96	7.03	7.08	7.12	7.21	7.24

Nominal operating cell temperature NOCT (800 W/m², AM 1.5, windspeed 1 m/s, ambient temperature 20°C).

MAXIMUM RATINGS	
Operational Temperature:	-40 ... +80°C
Maximum System Voltage:	1000 V
Maximum Snow Load:	550 kg/m² (5400 Pa)
Maximum Wind Load:	244 kg/m² (2400 Pa)
Max Series Fuse Rating:	25 A
Max Reverse Current:	25 A

CERTIFICATION

IEC 61215 & IEC 61730, IEC 62716 (ammonia resistance) & IEC 61701 (salt mist - severity level 6).

Member of PV Cycle

WARRANTY

10 year product warranty
25 year linear power output warranty
(max. degression in performance of 0.7 % p.a.)

See warranty conditions for further details.

MECHANICAL DATA	
Dimensions:	1665 x 991 x 38 mm
Area:	1.65 m²
Weight:	18 kg

Note! Specifications subject to change without notice.

Rev P - 01.2013 This data sheet is EN 50380 compliant

REC is a leading global provider of solar electricity solutions. With nearly two decades of expertise, we offer sustainable, high-performing products, services and investment opportunities for the solar and electronics industries. Together with our partners, we create value by providing solutions that better meet the world's growing electricity needs. Our 2,300 employees worldwide generated revenues of more than NOK 7 billion in 2012, approximately EUR 1 billion.

REC

www.recgroup.com

STP250S - 20/Wd
STP245S - 20/Wd
STP240S - 20/Wd

SUNTECH

250 Watt
MONOCRYSTALLINE SOLAR MODULE

Features

High module conversion efficiency
Module efficiency up to 15.4% achieved through advanced cell technology and manufacturing capabilities

Excellent weak light performance
Excellent performance under low light conditions

Positive tolerance
Positive tolerance of up to 5% delivers higher outputs reliablity

Suntech current sorting process
System output maximized by reducing mismatch losses up to 2% with modules sorted & packaged by amperage

Extended wind and snow load tests
Module certified to withstand extreme wind (3800 Pascal) and snow loads (5400 Pascal) *

Withstanding harsh environment
Reliable quality leads to a better sustainability even in harsh environment like desert, farm and coastline

Certifications and standards:
IEC 61215, IEC 61730, conformity to CE

Trust Suntech to Deliver Reliable Performance Over Time

- World-class manufacturer of crystalline silicon photovoltaic modules
- Unrivaled manufacturing capacity and world-class technology
- Rigorous quality control meeting the highest international standards: ISO 9001: 2008, ISO 14001: 2004 and ISO17025: 2005
- Regular independently checked production process from international accredited institute/company
- Tested for harsh environments (salt mist, ammonia corrosion and sand blowing testing: IEC 61701, DIN 50916:1985 T2, DIN EN 60068-2-68)***

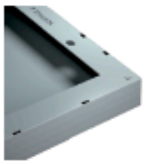

Compact and Durable Frame Design

Suntech`s new compact frame design is light-weight and easier to handle during installation. The rigid and durable hollow chamber guarantees the same long-term and reliable performance.

Industry-leading Warranty based on nominal power

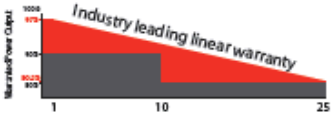

- 97% in the first year, thereafter, for years two (2) through twenty-five (25), 0.7% maximum decrease from MODULE's nominal power output per year, ending with the 80.2% in the 25th year after the defined WARRANTY STARTING DATE.****
- 10-year material and workmanship warranty

IP67 Rated Junction Box

Supports installations in multiple orientations. High reliable performance, low resistance connectors ensure maximum output for the highest energy production.

* Please refer to Suntech Standard Module Installation Manual for details. **PV Cycle only for EU market.
*** Please refer to Suntech Product Near-coast Installation Manual for details. **** Please refer to Suntech Product Warranty for details.

STP250S - 20/Wd
STP245S - 20/Wd
STP240S - 20/Wd

SUNTECH

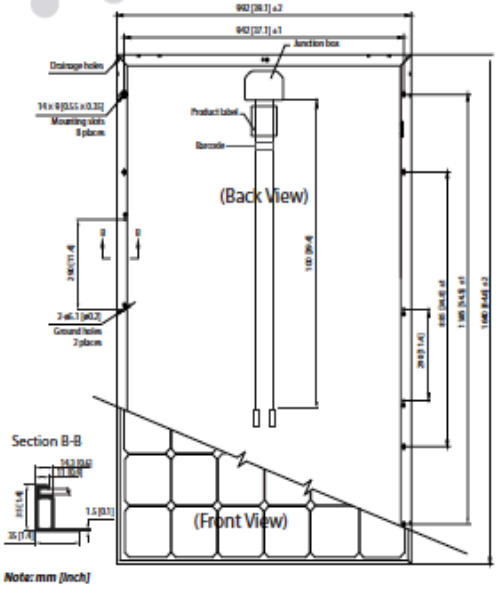

Note: mm (inch)

Electrical Characteristics

STC	STP250S-20/Wd	STP245S-20/Wd	STP240S-20/Wd
Maximum Power at STC (Pmax)	250 W	245 W	240 W
Optimum Operating Voltage (Vmp)	30.7 V	30.5 V	30.2 V
Optimum Operating Current (Imp)	8.15 A	8.04 A	7.95 A
Open Circuit Voltage (Voc)	37.4 V	37.3 V	37.2 V
Short Circuit Current (Isc)	8.63 A	8.52 A	8.43 A
Module Efficiency	15.4%	15.1%	14.8%
Operating Module Temperature	-40 °C to +85 °C		
Maximum System Voltage	1000 V DC (IEC)		
Maximum Series Fuse Rating	20 A		
Power Tolerance	0/+5 %		

STC: Irradiance 1000 W/m², module temperature 25 °C, AM=1.5;
Best in Class AAA solar simulator (IEC 60904-9) used, power measurement uncertainty is within +/- 3%

NOCT	STP250S-20/Wd	STP245S-20/Wd	STP240S-20/Wd
Maximum Power at NOCT (Pmax)	183 W	180 W	177 W
Optimum Operating Voltage (Vmp)	27.9 V	27.8 V	27.7 V
Optimum Operating Current (Imp)	6.56 A	6.47 A	6.40 A
Open Circuit Voltage (Voc)	34.4 V	34.3 V	34.2 V
Short Circuit Current (Isc)	6.98 A	6.91 A	6.83 A

NOCT: Irradiance 800 W/m², ambient temperature 20 °C, AM=1.5, wind speed 1 m/s;
Best in Class AAA solar simulator (IEC 60904-9) used, power measurement uncertainty is within +/- 3%

Current-Voltage & Power-Voltage Curve (240S-20)

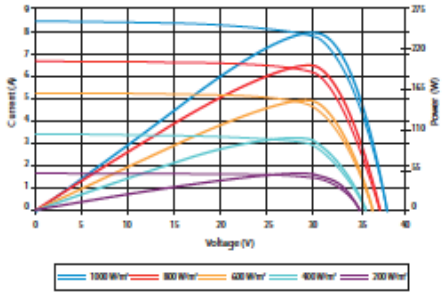

Excellent performance under weak light conditions: at an irradiation intensity of 200 W/m² (AM 1.5, 25 °C), 95.5% or higher of the STC efficiency (1000 W/m²) is achieved

Temperature Characteristics

Nominal Operating Cell Temperature (**NOCT**)	45±2°C
Temperature Coefficient of Pmax	-0.44 %/°C
Temperature Coefficient of Voc	-0.34 %/°C
Temperature Coefficient of Isc	0.060 %/°C

Mechanical Characteristics

Solar Cell	Monocrystalline silicon 156 x 156 mm (6 inches)
No. of Cells	60 (6 x 10)
Dimensions	1640 x 992 x 35mm (64.6 x 39.1 x 1.4 inches)
Weight	18.2 kgs (40.1 lbs.)
Front Glass	3.2 mm (0.13 inches) tempered glass
Frame	Anodized aluminium alloy
Junction Box	IP67 rated (3 bypass diodes)
Output Cables	TUV (2Pfg1169:2007)
	4.0 mm² (0.006 inches²), symmetrical lengths (-) 1000mm (39.4 inches) and (+) 1000 mm (39.4 inches)
Connectors	MC4 connectors

Dealer Information

Packing Configuration

Container	20' GP	40' HC
Pieces per pallet	30	30
Pallets per container	6	28
Pieces per container	180	840

Information on how to install and operate this product is available in the installation instruction. All values indicated in this data sheet are subject to change without prior announcement. The specifications may vary slightly. All specifications are in accordance with standard EN 50380. Color differences of the modules relative to the figures as well as discolorations of/in the modules which do not impair their proper functioning are possible and do not constitute a deviation from the specification.

E-mail: sales@suntech-power.com

Products > CIS Modules > SF145-165-S Series

Detail

Price： >> Contact Us

About CIS Module

Solar Frontier's SF145-165-S module series offers among the highest conversion efficiencies of any mass-produced thin-film module - from 11.8% to 13.4%. All modules are RoHS compliant and cadmium- and lead-free. Fewer production steps and raw materials also mean shorter energy payback time compared to crystalline silicon technologies. SF145-165S modules are shipped in cardboard-free packaging and use recyclable packaging materials.

STC* Characteristics

		SF145-S	SF150-S	SF155-S	SF160-S	SF165-S
Maximum power	Pmax	145 W	150 W	155 W	160 W	165 W
Module efficiency		11.8%	12.2%	12.6%	13.0%	13.4%
Tolerance of Pmax		+10%/-5%				
Factory binning		2.5W				
Open circuit voltage	Voc	107.0 V	108.0 V	109.0 V	110.0 V	110.0 V
Short circuit current	Isc	2.20 A	2.20 A	2.20 A	2.20 A	2.20 A
Voltage at maximum power	Vmpp	81.0 V	81.5 V	82.5 V	84.0 V	85.5 V
Current at maximum power	Impp	1.80 A	1.85 A	1.88 A	1.91 A	1.93 A

*STC (Standard Test Conditions)
1,000 W/m2 irradiance, module temperature 25 °C (77 °F), air mass 1.5. Isc and Voc are ±10% tolerance of STC rated values. Module output may rise after light soaking due to its unique characteristics.

NOCT** Characteristics

		SF145-S	SF150-S	SF155-S	SF160-S	SF165-S
Maximum power	Pmax	108 W	111 W	115 W	119 W	123 W
Open circuit voltage	Voc	97.4 V	98.3 V	99.2 V	100.0 V	100.0 V
Short circuit current	Isc	1.73 A	1.76 A	1.76 A	1.76 A	1.76 A
Voltage at maximum power	Vmpp	76.0 V	76.4 V	77.4 V	78.8 V	80.2 V
Current at maximum power	Impp	1.43 A	1.47 A	1.49 A	1.51 A	1.53 A

**NOCT (Nominal Operating Cell Temperature Conditions)
Module operating temperature at 800 W/m2 irradiance, air temperature 20 °C (68 °F), wind speed 1 m/s and open circuit condition.

Performance at Low Irradiance

Efficiency reduction of maximum power from an irradiance of 1,000 W/m2 to 200 W/m2 at 25 °C (77°F) is typically 2.0%. The standard deviation for the reduction of efficiency is 1.9%.

Temperature Characteristics

NOCT	47 °C (116°F)	
Temperature coefficient of Isc	α	+0.01%/K
Temperature coefficient of Voc	β	-0.30%/K
Temperature coefficient of Pmax	δ	-0.31%/K

Mechanical

Dimensions (L x W x H)	1,257 x 977 x 35 mm (49.5 x 38.5 x 1.4 in.)
Weight	20 kg (44.1 lbs)
Application class (IEC 61730)	A
Fire rating (IEC 61730)	Class C
Safety class (IEC 61140)	II
Snow/wind load*	2,400 Pa (IEC 61646) / 1,600 Pa design load (UL 1703)
Cell type	CIS glass substrate (cadmium free)
Front cover	Clear tempered glass, 3.2 mm
Encapsulant	EVA
Back sheet	Weatherproof plastic film (color: black & silver)
Frame	Anodized aluminum alloy (color: black)
Edge sealant	Butyl rubber
Junction box	Protection rating: IP 67 (with bypass diode)
Adhesive	Silicone
Output cables (conductor)	2.5 mm2 /14 AWG (halogen free)
Cable lengths (symmetrical)	1,200 mm (47.2 in.)
Packing information	25 panels/pallet • 36 pallets/40' container (900 panels)

*UL: 1.5 x design load is applied to the module, i.e., 2,400 Pa (50.1 lbs/ft2) is applied to meet the 1,600 a UL design load standard

SUNNY TRIPOWER
8000TL / 10000TL / 12000TL / 15000TL / 17000TL

Economical
- Maximum efficiency of 98.2 %
- SMA OptiTrac Global Peak MPP tracking for best MPP tracking efficiency
- *Bluetooth*® communication

Reliable
- Triple protection with Optiprotect:
- Electronic string fuse
- Self-learning string failure detection
- DC surge arrester (Type II) can be integrated

Flexible
- DC input voltage up to 1000 V
- Integrated grid management functions
- Custom plant design with Optiflex

Simple
- Three-phase feed-in
- Cable connection without tools
- SUNCLIX DC plug-in system
- Easily accessible connection area

SUNNY TRIPOWER
8000TL / 10000TL / 12000TL / 15000TL / 17000TL

The three-phase inverter for easy plant design

Full of pioneering technology: highly flexible plant design with the three-phase Sunny Tripower inverter. Thanks to Optiflex technology, two MPP inputs and a broad input voltage range, it is suited to almost any module configuration. It meets any requirement such as reactive power supply, grid support thus reliably participating in grid management. The safety concept Optiprotect with its self-learning string-failure detection, electronic string fuse and integrable DC surge arrester type II, ensures maximum availability.

SUNNY TRIPOWER
8000TL / 10000TL / 12000TL / 15000TL / 17000TL

Technical Data	Sunny Tripower 8000TL
Input (DC)	
Max. DC power (@ cos φ=1)	8200 W
Max. input voltage	1000 V
MPP voltage range / rated input voltage	320 V – 800 V / 600 V
Min. input voltage / initial input voltage	150 V / 188 V
Max. input current input A / input B	22 A / 11 A
Max. input current per string input A* / input B*	33 A / 12.5 A
Number of independent MPP inputs / strings per MPP input	2 / A:4; B:1
Output (AC)	
Rated power (@ 230 V, 50 Hz)	8000 W
Max. apparent AC power	8000 VA
Nominal AC voltage	3 / N / PE; 220 / 380 V 3 / N / PE; 230 / 400 V 3 / N / PE; 240 / 415 V
Nominal AC voltage range	160 V – 280 V
AC power frequency / range	50 Hz, 60 Hz / –6 Hz ... +5 Hz
Rated grid frequency / rated grid voltage	50 Hz / 230 V
Max. output current	16 A
Power factor at rated power	1
Adjustable displacement factor	0.8 overexited... 0.8 underexited
Phase conductors / connection phases	3 / 3
Efficiency	
Max. efficiency / European efficiency	98.1 % / 97.5 %
Protection	
Input-side disconnection device	●
Ground-fault monitoring / grid monitoring	● / ●
DC surge arrester Type II, can be integrated	o
DC reverse-polarity protection / AC short-circuit current capability / galvanically isolated	● / ● / –
All-pole sensitive residual current monitoring unit	●
Protection class (according to IEC 62103) / overvoltage category (according to IEC 60664-1)	I / III
General Data	
Dimensions (W / H / D)	665 / 690 / 265 mm (26.2 / 27.2 / 10.4 in)
Weight	59 kg (130,07 lb)
Operating temperature range	–25 °C ... +60 °C (–13 °F ... +140 °F)
Noise emission (typical)	51 dB(A)
Self-consumption at night	1 W
Topology / cooling concept	Transformerless / OptiCool
Degree of protection (according to IEC 60529)	IP65
Climatic category (according to IEC 60721-3-4)	4K4H
Maximum permissible value for relative humidity (non-condensing)	100 %
Features	
DC terminal / AC terminal	SUNCLIX / Spring-type terminal
Display	Graphic
Interface: RS485 / Bluetooth / Webconnect / Speedwire[2]	o / ● / o / o
Multi-function relay / Power Control Module	o / o
Warranty: 5 / 10 / 15 / 20 / 25 years	● / o / o / o / o
Certificates and approvals (more available on request)	CE, VDE0126-1-1, RD 661/2007, G59/2, PPC, AS4777, SI4777, EN 50438[1], C10/11, PPDS, IEC 61727, UTE C15-712-1, VDE-AR-N 4105, RD 1699, CEI 0-21
● Standard features o Optional features – Not available Data at nominal conditions	
Type designation	STP 8000TL-10

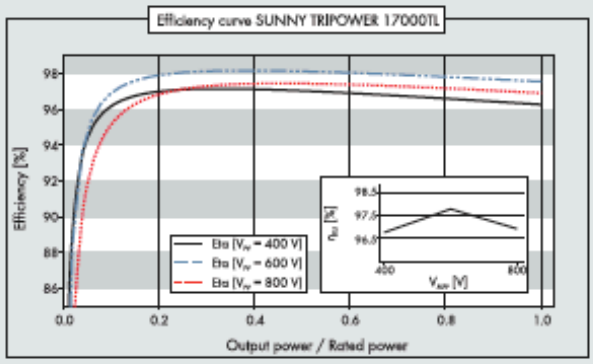

Accessories


RS485 interface
DM-485CB-10


DC surge arrester (Type II), input A
DCSPD KIT1-10


DC surge arrester (Type II), inputs A and B
DCSPD KIT2-10


Power Control Module
PWCMOD-10


Multi-function relay
MFR01-10


Webconnect interface
SWDM-10

[1] Does not apply to all national deviations of EN 50438
[2] To be observed in case of a short circuit in the electronic string fuse
[3] Planned (certificates, approvals, accessories)
Provisional data, as of September 2012

Sunny Tripower 10000TL	Sunny Tripower 12000TL	Sunny Tripower 15000TL	Sunny Tripower 17000TL
10200 W	12250 W	15340 W	17410 W
1000 V	1000 V	1000 V	1000 V
320 V – 800 V / 600 V	380 V – 800 V / 600 V	360 V – 800 V / 600 V	400 V – 800 V / 600 V
150 V / 188 V	150 V / 188 V	150 V / 188 V	150 V / 188 V
22 A / 11 A	22 A / 11 A	33 A / 11 A	33 A / 11 A
33 A / 12.5 A	33 A / 12.5 A	40 A / 12.5 A	40 A / 12.5 A
2 / A:4; B:1	2 / A:4; B:1	2 / A:5; B:1	2 / A:5; B:1
10000 W	12000 W	15000 W	17000 W
10000 VA	12000 VA	15000 VA	17000 VA
3 / N / PE; 220 / 380 V	3 / N / PE; 220 / 380 V	3 / N / PE; 220 / 380 V	3 / N / PE; 220 / 380 V
3 / N / PE; 230 / 400 V	3 / N / PE; 230 / 400 V	3 / N / PE; 230 / 400 V	3 / N / PE; 230 / 400 V
3 / N / PE; 240 / 415 V	3 / N / PE; 240 / 415 V	3 / N / PE; 240 / 415 V	3 / N / PE; 240 / 415 V
160 V – 280 V	160 V – 280 V	160 V – 280 V	160 V – 280 V
50 Hz, 60 Hz / –6 Hz … +5 Hz	50 Hz, 60 Hz / –6 Hz … +5 Hz	50 Hz, 60 Hz / –6 Hz … +5 Hz	50 Hz, 60 Hz / –6 Hz … +5 Hz
50 Hz / 230 V	50 Hz / 230 V	50 Hz / 230 V	50 Hz / 230 V
16 A	19.2 A	24 A	24.6 A
1	1	1	1
0.8 overexited… 0.8 underexited	0.8 overexited… 0.8 underexited	0.8 overexited… 0.8 underexited	0.8 overexited… 0.8 underexited
3 / 3	3 / 3	3 / 3	3 / 3
98.1 % / 97.7 %	98.1 % / 97.7 %	98.2 % / 97.8 %	98.2 % / 97.8 %
●	●	●	●
● / ●	● / ●	● / ●	● / ●
○	○	○	○
● / ● / –	● / ● / –	● / ● / –	● / ● / –
●	●	●	●
I / III	I / III	I / III	I / III
665 / 690 / 265 mm (26.2 / 27.2 / 10.4 in)	665 / 690 / 265 mm (26.2 / 27.2 / 10.4 in)	665 / 690 / 265 mm (26.2 / 27.2 / 10.4 in)	665 / 690 / 265 mm (26.2 / 27.2 / 10.4 in)
59 kg (130,07 lb)	59 kg (130,07 lb)	59 kg (130,07 lb)	59 kg (130,07 lb)
–25 °C … +60 °C (–13 °F … +140 °F)	–25 °C … +60 °C (–13 °F … +140 °F)	–25 °C … +60 °C (–13 °F … +140 °F)	–25 °C … +60 °C (–13 °F … +140 °F)
51 dB(A)	51 dB(A)	51 dB(A)	51 dB(A)
1 W	1 W	1 W	1 W
Transformerless / OptiCool	Transformerless / OptiCool	Transformerless / OptiCool	Transformerless / OptiCool
IP65	IP65	IP65	IP65
4K4H	4K4H	4K4H	4K4H
100 %	100 %	100 %	100 %
SUNCLIX / Spring-type terminal	SUNCLIX / Spring-type terminal	SUNCLIX / Spring-type terminal	SUNCLIX / Spring-type terminal
Graphic	Graphic	Graphic	Graphic
○ / ● / ○ / ○	○ / ● / ○ / ○	○ / ● / ○ / ○	○ / ● / ○ / ○
○ / ○	○ / ○	○ / ○	○ / ○
● / ○ / ○ / ○ / ○	● / ○ / ○ / ○ / ○	● / ○ / ○ / ○ / ○	● / ○ / ○ / ○ / ○
CE, VDE0126-1-1, RD 661/2007, G59/2, PPC, AS4777, SI4777, EN 50438[1], C10/11, PPDS, IEC 61727, UTE C15-712-1, VDE-AR-N 4105, BDEW 2008, RD 1699, CEI 0-21			
STP 10000TL-10	STP 12000TL-10	STP 15000TL-10	STP 17000TL-10

ELTEK

THEIA™ HE-t

The THEIA™ HE-t range defines a new level of efficiency, flexibility and user friendliness for isolated string inverters. Suitable for all PV cell technologies, and ready for use all over the world, the THEIA™ HE-t is the perfect choice for any PV installation.

THEIA™ HE-t

SOLAR INVERTERS: 2.0 kW – 4.6 kW

PERFORMANCE
- Maximum efficiency 97.3 % with galvanic isolation
- Suitable for use with all PV modules of any technology, with the ability to ground the positive or the negative terminal on the DC side
- Compliance with the highest international safety standards
- Early startup and high efficiency at low irradiation gives longer operation time and higher energy yields

EASE OF USE
- Lightweight and easy to install
- With or without DC Disconnect Switch
- Color screen with touch sense buttons
- Intuitive user interface

RELIABILITY
- High quality components, with a robust design
- Bespoke Maximum Power Point Tracking
- Stable operation under extremely dynamic irradiation conditions
- IP65 protection level

MONITORING AND COMMUNICATION
- Complete site overview from one single inverter
- Integrated webserver with easy-to-use monitoring software
- Multilanguage display

Find your local office at: www.eltek.com

Doc No: 357115.DS3 rev8

MODEL	2.0 HE-t	2.9 HE-t	3.8 HE-t	4.4 HE-t	4.6 HE-t
INPUT DATA					
Nominal DC power	2100 W	3000 W	4000 W	4600 W	4800 W
Max. PV power	2625 Wp	3750 Wp	5000 Wp	5750 Wp	6000 Wp
Max. DC voltage	600 Vdc				
Voltage range MPPT	230 to 480 Vdc	230 to 480 Vdc	230 to 480 Vdc	230 to 480 Vdc	230 to 480 Vdc [1]
Max. input current	9.5 A	13.5 A	18.0 A	21.0 A	21.0 A
Number of PV string inputs	3				
Number of MPP trackers	1				
Input features	Reverse polarity protection, Ground fault monitoring, Integral DC switch disconnector (optional), Integral DC fuses for string inputs (optional), Field configurable for positive or negative grounding, or ungrounded				
OUTPUT DATA					
Nominal output power	2000 W	2900 W	3800 W	4450 W	4600 W
Max apparent power	2000 VA	2900 VA	3800 VA	4450 VA	4600 VA
Nominal AC current	9.0 A	13.0 A	17.0 A	19.5 A	20.0 A
Max. AC current	10.5 A	15.2 A	19.7 A	23.0 A	23.0 A
Mains output voltage	230 Vac (+/-20 %) single or split phase				
Mains frequency	50 Hz / 60 Hz (+/-10 %)				
Cos Phi (power factor)	0.8i to 0.8c selectable				
PERFORMANCE DATA					
Maximum efficiency	97.2 %	97.2 %	97.2 %	97.3 %	97.3 %
CEC efficiency	96.8 %	96.8 %	97.0 %	97.0 %	97.0 %
EU efficiency	96.3 %	96.5 %	96.7 %	96.9 %	96.9 %
Power feed starts at	< 7 W				
Night mode power	< 1 W				
MECHANICAL DATA					
Protection degree (EN 60529)	IP 65				
Dimensions	610 H x 353 W x 154 D mm / 24.02 H x 13.90 W x 6.06 D inches				
Weight	< 19 kg / 42 lbs	< 19 kg / 42 lbs	< 21 kg / 46 lbs	< 21 kg / 46 lbs	< 21 kg / 46 lbs
Cable access	Bottom				
Input cable connection	MC3, MC4, Tyco, Screw terminals, Cable clamp, Others on request				
Output cable connection	Screw terminals, Cable clamp				
DESIGN STANDARDS					
EM compatibility	EN 61000-6-2, EN 61000-6-3				
CE marking	Yes				
Other standards	DIN VDE V 0126-1-1, G83/1, EN 50438, AS 4777, CEI 0-21, EN 61000-3-2, EN 61000-3-3, EN 61000-3-11, EN 61000-3-12, IEC 62109-2, IEC 61727, UTE C 15-712-1, C10/11, VDE AR-N 4105, RD1663, G59/2				
ENVIRONMENTAL DATA					
Operating temperature	- 25 °C to + 65 °C / - 13 to + 149 °F (possible power derating above + 45 °C / + 113 °F)				
Storage temperature	- 30 °C to + 80 °C / - 22 to + 176 °F				
Ventilation	Convection cooling				

ADDITIONAL FEATURES	
Topology	High frequency transformer, galvanic isolation
Protection class / Overvoltage category	I / III
Noise Emission	< 37 dB (A)
Communication	Graphical, color display with touch sense buttons, Embedded web-server, Ethernet, CAN and RS485 bus interface, 3x LEDs for visual status indication
Warranty	5 years, 10 years, 15 years, 20 years and 25 years options

1) Output power limitation 230 Vdc to 250 Vdc

EFFICIENCY CURVE THEIA 4.4 HE-t

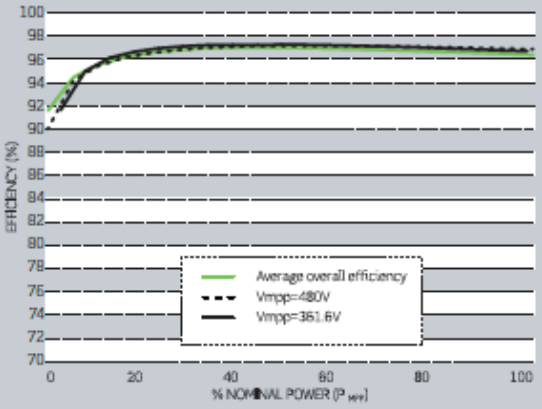

Appendix D: Simulation Results

As PVsyst produces a four-page report from each simulation, and nearly 100 simulations were performed, it would be unfeasible to show all simulation results in the thesis. The most significant results were shown in the results section of the thesis, while this appendix provide additional information about the simulation results.

Table D.1 shows the electrical key characteristics of the best-performing systems from each roof.

System	Modules per string	Strings	Inverters	MPPTs	$U_{mpp, STC}$	$U_{mpp, 70\,C}$	$U_{mpp, 0\,C}$	$U_{OC, -30\,C}$	$I_{mpp, STC}$	$I_{sc, STC}$
1.2	19	8	2	4	518 V	473 V	629 V	830 V	66.2 A	71.3 A
3.2	10	18	9	9	272 V	249 V	331 V	437 V	149 A	159 A
5.2	10	9	9	9	272 V	249 V	331 V	437 V	74.5 A	79.7 A

Table D. 1: Electrical key data for the best-performing systems from each roof.

Table D.2 summarizes the balances and main results from each month for system 1.2. The column to the right shows the system efficiency with respect to available irradiation for each month.

	GlobHor kWh/m²	T Amb °C	GlobInc kWh/m²	GlobEff kWh/m²	EArray MWh	E_Grid MWh	EffArrR %	EffSysR %
January	9.9	-4.10	19.5	5.5	0.184	0.154	3.77	3.16
February	25.8	-4.20	43.3	12.3	0.456	0.409	4.20	3.77
March	64.7	-0.40	89.1	59.6	2.282	2.192	10.21	9.80
April	95.5	4.20	114.4	108.2	3.982	3.842	13.88	13.39
May	146.4	10.30	156.0	147.4	5.279	5.108	13.49	13.05
June	151.8	14.70	155.1	146.4	5.160	4.986	13.27	12.82
July	150.6	15.90	155.4	146.4	5.134	4.960	13.17	12.72
August	115.3	14.90	133.0	125.8	4.444	4.295	13.33	12.88
September	71.5	10.80	93.9	88.8	3.241	3.131	13.76	13.29
October	32.1	6.80	49.1	46.3	1.700	1.623	13.81	13.19
November	11.1	1.20	19.9	18.5	0.699	0.655	13.98	13.09
December	5.8	-2.50	12.1	7.8	0.272	0.240	8.98	7.92
Year	880.4	5.69	1040.8	913.0	32.834	31.594	12.58	12.10

Table D. 2: Balances and main results from the simulations of system 1.2. From PVsyst.

Table D.3 summarizes the balances and main results from each month for system 3.2.

	GlobHor kWh/m²	T Amb °C	GlobInc kWh/m²	GlobEff kWh/m²	EArray kWh	E_Grid kWh	EffArrR %	EffSysR %
January	9.9	-4.10	18.1	4.4	147	128	2.75	2.39
February	25.8	-4.20	41.0	11.2	460	429	3.78	3.52
March	64.7	-0.40	86.6	57.3	2610	2512	10.15	9.77
April	95.5	4.20	112.2	106.0	4670	4496	14.01	13.49
May	146.4	10.30	155.7	147.1	6307	6079	13.63	13.14
June	151.8	14.70	155.8	147.1	6187	5961	13.37	12.88
July	150.6	15.90	156.0	147.1	6168	5944	13.31	12.83
August	115.3	14.90	131.2	124.0	5241	5051	13.45	12.96
September	71.5	10.80	90.8	85.6	3719	3586	13.79	13.30
October	32.1	6.80	46.4	43.3	1859	1784	13.48	12.93
November	11.1	1.20	18.5	15.5	564	532	10.26	9.68
December	5.8	-2.50	11.1	6.2	214	193	6.48	5.84
Year	880.4	5.69	1023.4	894.9	38146	36696	12.55	12.07

Table D. 3: Balances and main results from the simulations of system 3.2. From PVsyst.

Table D.4 summarizes the balances and main results for system 5.2.

	GlobHor kWh/m²	T Amb °C	GlobInc kWh/m²	GlobEff kWh/m²	EArray kWh	E_Grid kWh	EffArrR %	EffSysR %
January	9.9	-4.10	18.1	4.7	85	73	3.15	2.73
February	25.8	-4.20	41.0	11.5	248	227	4.07	3.72
March	64.7	-0.40	86.6	57.3	1305	1242	10.15	9.67
April	95.5	4.20	112.2	106.0	2337	2237	14.02	13.42
May	146.4	10.30	155.7	147.2	3134	3004	13.55	12.99
June	151.8	14.70	155.8	147.2	3074	2945	13.28	12.73
July	150.6	15.90	156.0	147.2	3084	2955	13.31	12.76
August	115.3	14.90	131.2	124.1	2622	2511	13.45	12.89
September	71.5	10.80	90.8	85.7	1863	1782	13.82	13.22
October	32.1	6.80	46.4	43.6	953	906	13.82	13.14
November	11.1	1.20	18.5	16.4	351	328	12.77	11.94
December	5.8	-2.50	11.1	6.5	120	107	7.30	6.52
Year	880.4	5.69	1023.4	897.4	19175	18318	12.62	12.05

Table D. 4: Balances and main results from the simulations of system 5.2. From PVsyst.

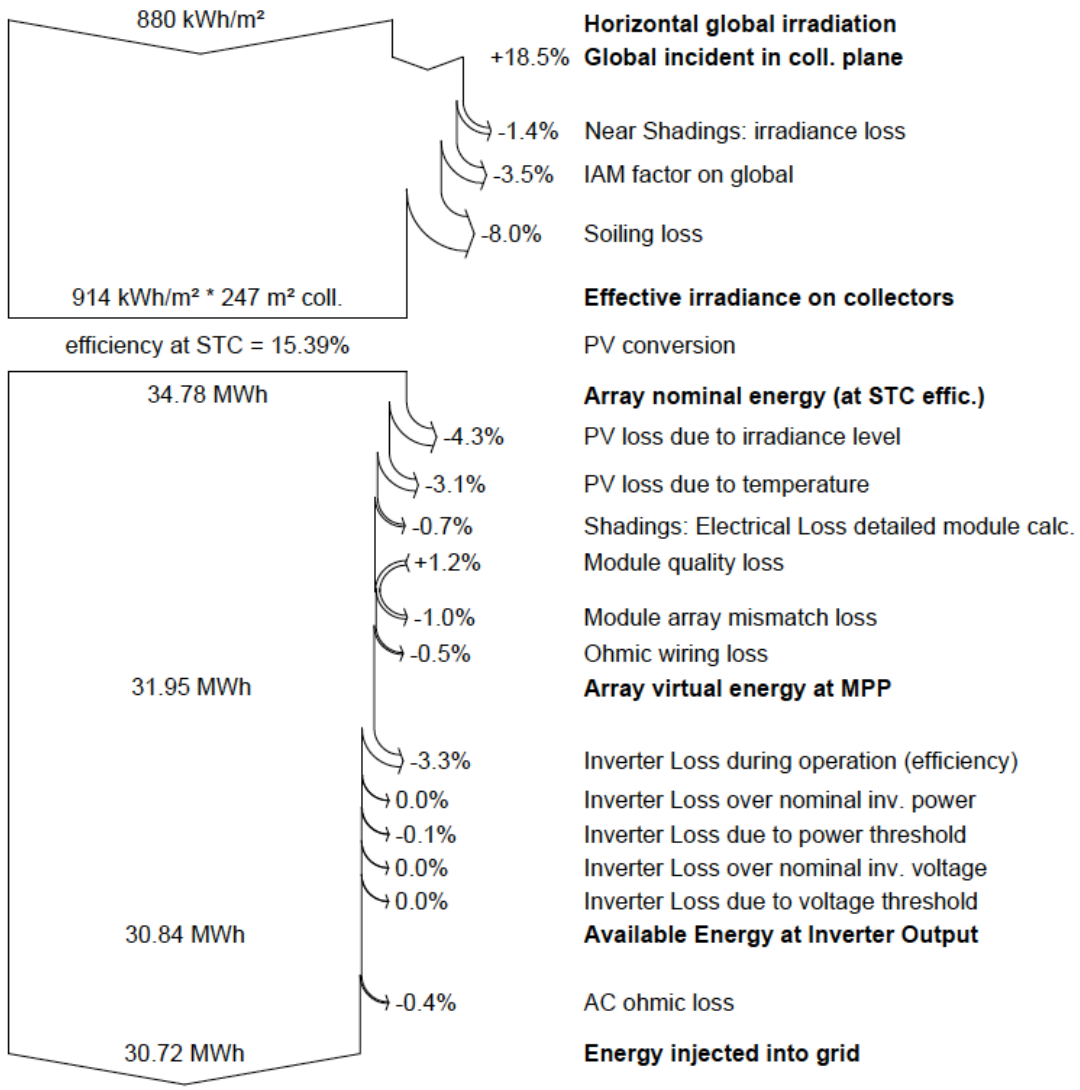

Figure D. 1: Loss diagram from the simulation of system 1.7 from PVsyst.

Figure D.1 shows the average yearly performance of system 1.7, which consisted of a 38 kWp array of Suntech modules and two Sunny Tripower TL17000 inverters.

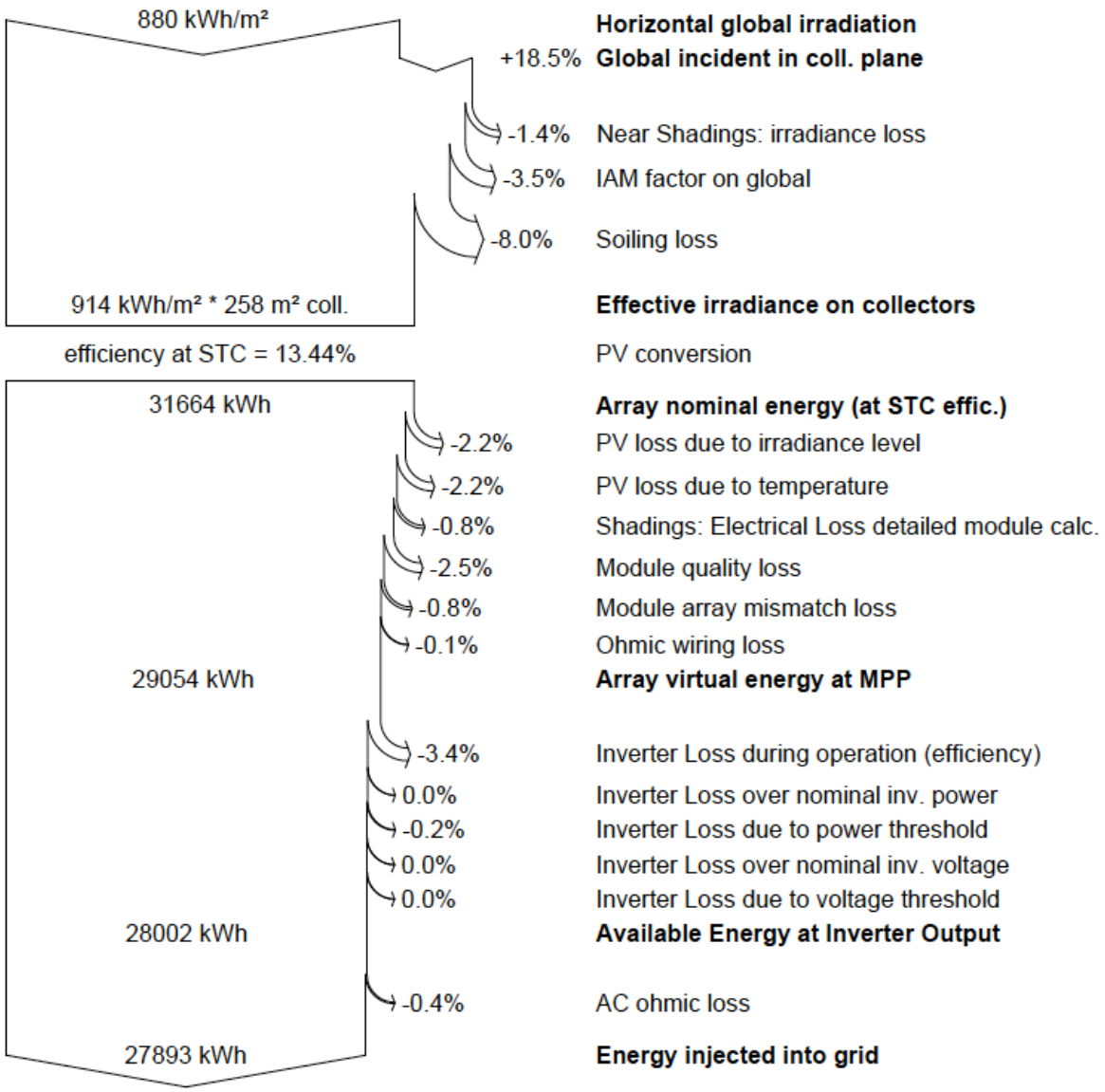

Figure D. 2: Loss diagram from the simulation of system 1.9 from PVsyst.

Figure D.2 shows the yearly performance of system 1.9, which consisted of a 34.6 kWp array of Solar Frontier modules and two Sunny Tripower TL17000 inverters.

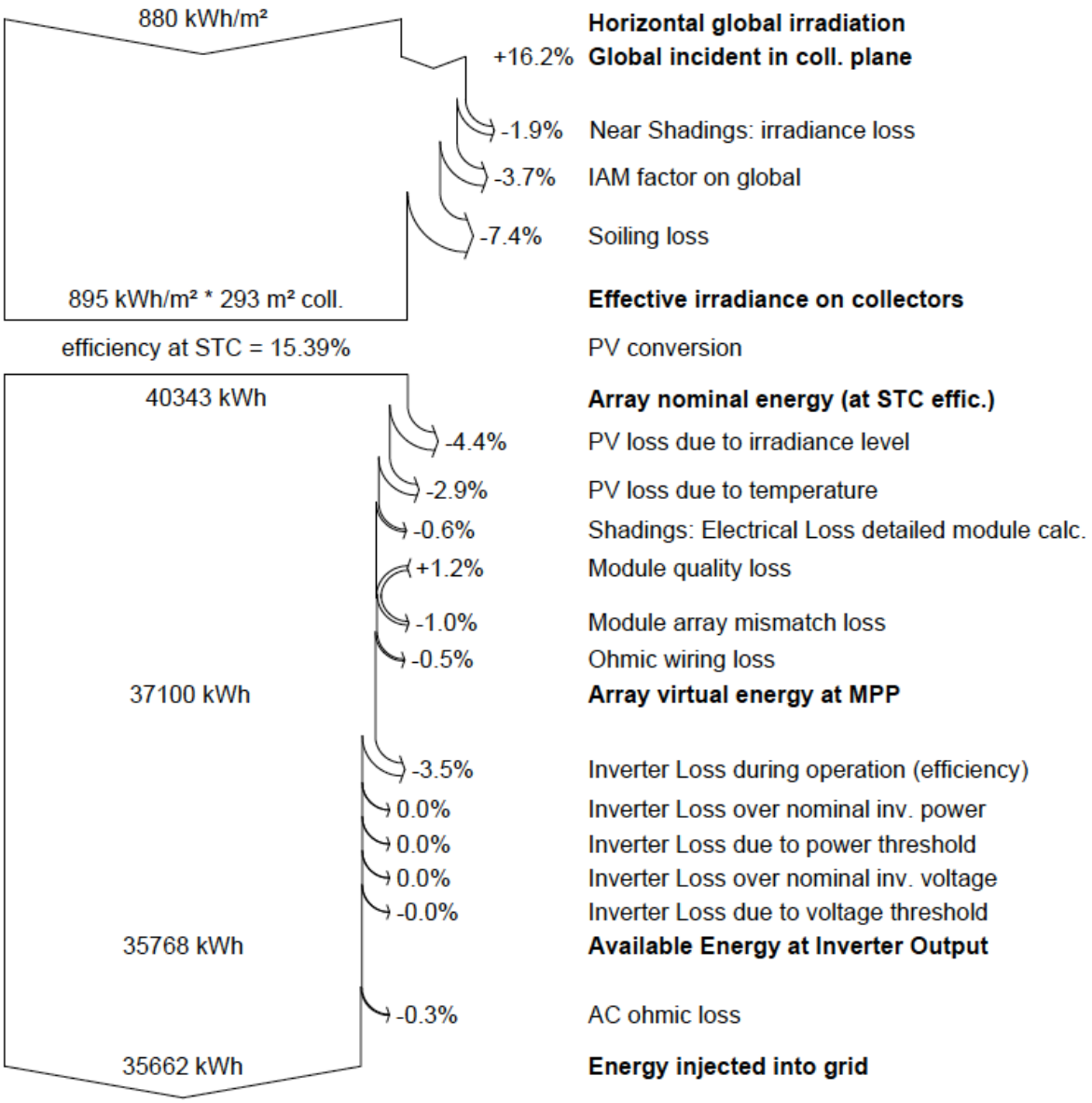

Figure D. 3: Loss diagram from the simulation of system 3.6 from PVsyst.

Figure D.3 shows the yearly performance of system 3.6, which consisted of a 45 kWp array of Suntech modules and nine Eltek Theia He-t inverters.

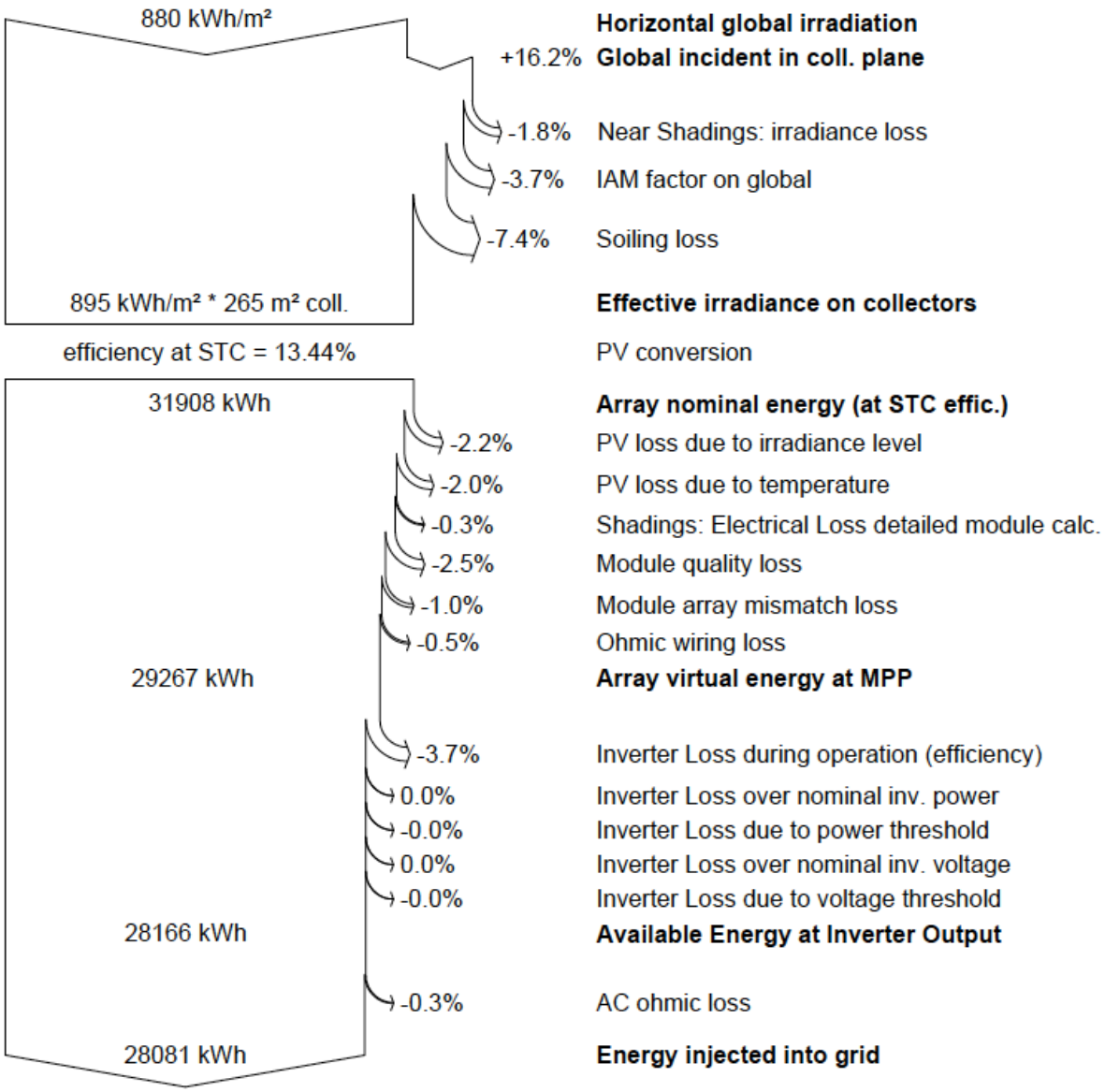

Figure D. 4: Loss diagram from the simulation of system 3.12 from PVsyst.

Figure D.4 shows the yearly performance of system 3.12, which consisted of a 35.6 kWp array of Solar Frontier modules and nine Eltek Theia He-t inverters.

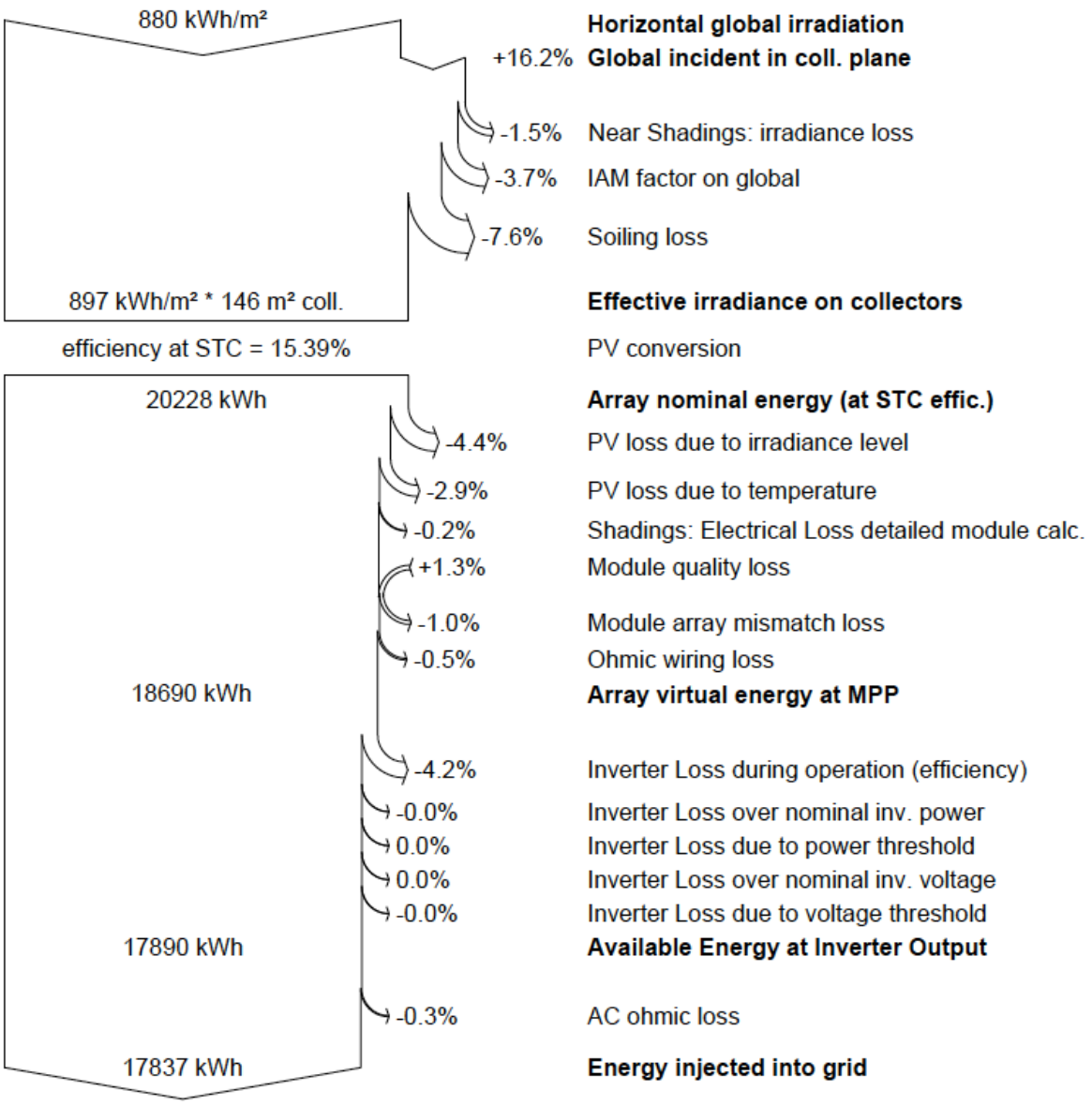

Figure D. 5: Loss diagram from the simulation of system 5.6 from PVsyst.

Figure D.5 shows the yearly performance of system 5.6, which consisted of a 22.5 kWp array of Suntech modules and nine Eltek Theia He-t inverters.

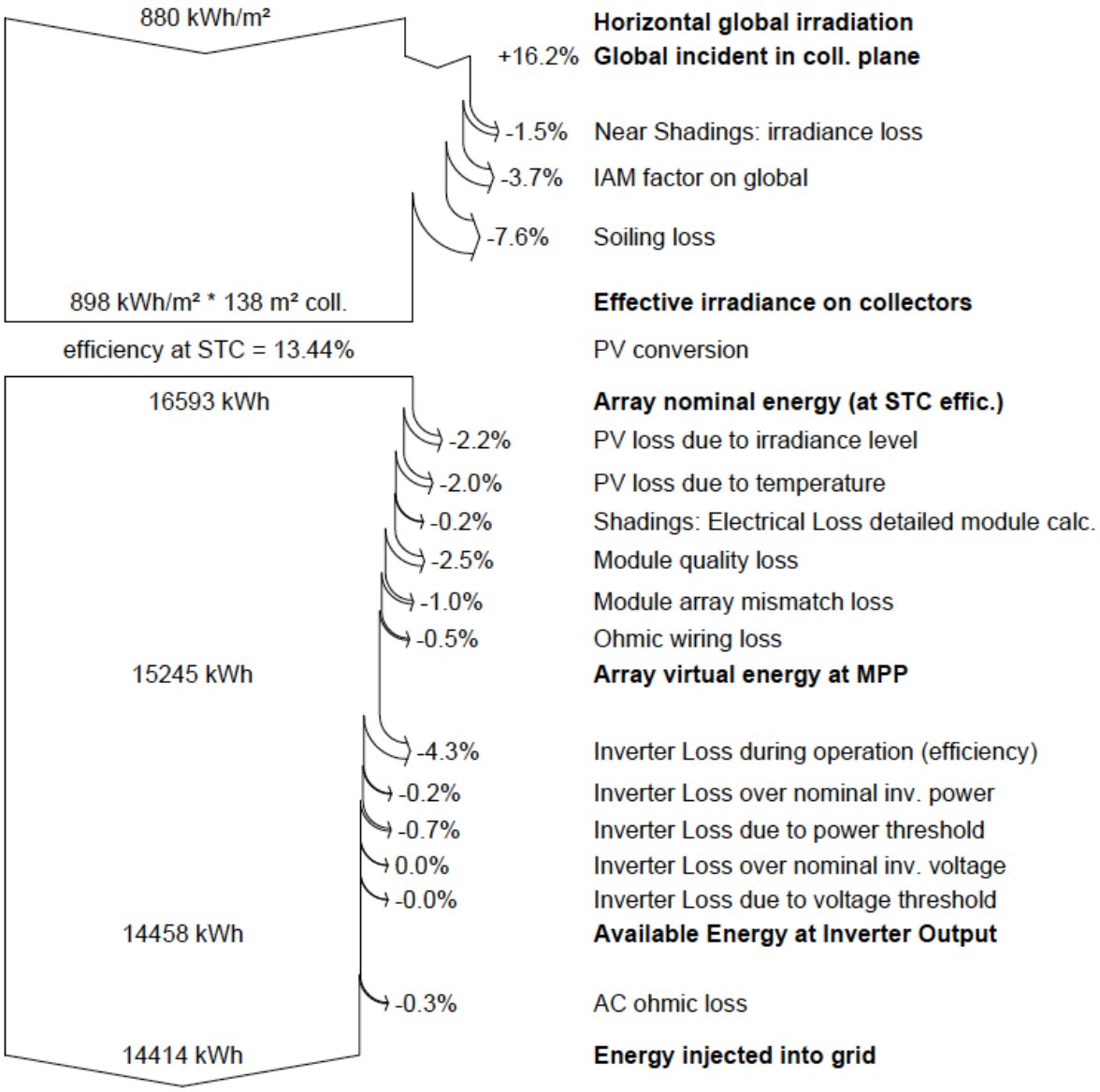

Figure D. 6: Loss diagram from the simulation of system 5.9 from PVsyst.

Figure D.6 shows the yearly performance of system 5.9, which consisted of a 18.5 kWp array of Solar Frontier modules and two SMA Sunny Tripower TL8000 inverters.

Appendix E: Economical Evaluation

Only the main financial assumptions and results of the economical evaluation are shown in the thesis. This appendix is hence created for readers who want a higher level of detail with respect to the calculations.

When using the present value of each year was calculated in Excel and then summarized in order to obtain the NPV for an investment in each system.

Table E.1 shows the net present value analysis for system 1.2, 3.2 and 5.2.

NPV	0	1	2	3	4	5	6	7	8	9	10	11	12	13	14	15	16	17	18	19	20	21	22	23	24	25
Construction cost	(320 000)																									
Electricity value		4 996	4 971	4 946	4 922	4 897	4 873	4 848	4 824	4 800	4 776	4 752	4 728	4 705	4 681	4 658	4 634	4 611	4 588	4 565	4 542	4 520	4 497	4 475	4 452	4 430
Utility value		2 810	2 795	2 781	2 768	2 754	2 740	2 726	2 713	2 699	2 686	2 672	2 659	2 646	2 632	2 619	2 606	2 593	2 580	2 567	2 554	2 542	2 529	2 516	2 504	2 491
Investment support	0																									
Certificate value	(15 000)	3 663	3 645	3 626	3 608	3 590	3 572	3 554	3 537	3 519	3 501	3 484	3 466	3 449	3 432	3 415	3 398	3 381	3 364	3 347	3 330	3 314	3 297	3 281	3 264	3 248
O & M		(733)	(729)	(725)	(722)	(718)	(714)	(711)	(707)	(704)	(700)	(697)	(693)	(690)	(686)	(683)	(680)	(676)	(673)	(669)	(666)	(663)	(659)	(656)	(653)	(650)
Net cash flow	(335 000)	10 736	10 683	10 629	10 576	10 523	10 471	10 418	10 366	10 314	10 263	10 211	10 160	10 059	10 009	9 959	9 909	9 859	9 810	9 761	9 712	9 664	9 615	9 567	9 519	
Discount factor	1.000	0.943	0.890	0.840	0.792	0.747	0.705	0.665	0.627	0.592	0.558	0.527	0.497	0.469	0.442	0.417	0.394	0.371	0.350	0.331	0.312	0.294	0.278	0.262	0.247	0.233
Present value of cash flow	(335 000)	10 129	9 507	8 924	8 377	7 863	7 381	6 929	6 504	6 105	5 731	5 379	(12 842)	4 740	4 449	4 176	3 920	3 680	3 454	3 242	3 044	2 857	2 682	2 517	2 363	2 218
NPV of cash flow	(221 670)																									

NPV	0	1	2	3	4	5	6	7	8	9	10	11	12	13	14	15	16	17	18	19	20	21	22	23	24	25
Construction cost	(605 700)																									
Electricity value		10 005	9 955	9 905	9 856	9 806	9 757	9 709	9 660	9 612	9 564	9 516	9 468	9 421	9 374	9 327	9 280	9 234	9 188	9 142	9 096	9 051	9 005	8 960	8 915	8 871
Utility value		4 933	4 908	4 884	4 859	4 835	4 811	4 787	4 763	4 739	4 715	4 692	4 668	4 645	4 622	4 598	4 576	4 553	4 530	4 507	4 485	4 462	4 440	4 418	4 396	4 374
Investment support	0																									
Certificate value	(15 000)	7 335	7 298	7 262	7 226	7 189	7 153	7 118	7 082	7 047	7 011	6 976	6 942	6 907	6 872	6 838	6 804	6 770	6 736	6 702	6 669	6 635	6 602	6 569	6 536	6 504
O & M		(1 467)	(1 460)	(1 452)	(1 445)	(1 438)	(1 431)	(1 424)	(1 416)	(1 409)	(1 402)	(1 395)	(71 588)	(1 381)	(1 374)	(1 368)	(1 361)	(1 354)	(1 347)	(1 340)	(1 334)	(1 327)	(1 320)	(1 314)	(1 307)	(1 301)
Net cash flow	(620 700)	20 806	20 702	20 598	20 495	20 393	20 291	20 189	20 088	19 988	19 888	19 789	(50 510)	19 591	19 493	19 396	19 299	19 202	19 106	19 011	18 916	18 821	18 727	18 633	18 540	18 447
Discount factor	1.000	0.943	0.890	0.840	0.792	0.747	0.705	0.665	0.627	0.592	0.558	0.527	0.497	0.469	0.442	0.417	0.394	0.371	0.350	0.331	0.312	0.294	0.278	0.262	0.247	0.233
Present value of cash flow	(620 700)	19 628	18 424	17 295	16 234	15 239	14 304	13 427	12 604	11 831	11 105	10 424	(25 102)	9 185	8 622	8 093	7 597	7 131	6 694	6 283	5 898	5 536	5 197	4 878	4 579	4 298
NPV of cash flow	(401 295)																									

NPV	0	1	2	3	4	5	6	7	8	9	10	11	12	13	14	15	16	17	18	19	20	21	22	23	24	25
Construction cost	(531 300)																									
Electricity value		8 614	8 571	8 529	8 486	8 443	8 401	8 359	8 317	8 276	8 234	8 193	8 152	8 112	8 071	8 031	7 991	7 951	7 911	7 871	7 832	7 793	7 754	7 715	7 676	7 638
Utility value		4 446	4 424	4 402	4 380	4 358	4 336	4 314	4 293	4 271	4 250	4 229	4 208	4 187	4 166	4 145	4 124	4 104	4 083	4 063	4 042	4 022	4 002	3 982	3 962	3 942
Investment support	0																									
Certificate value	(15 000)	6 316	6 284	6 253	6 221	6 190	6 159	6 128	6 098	6 067	6 037	6 007	5 977	5 947	5 917	5 888	5 858	5 829	5 800	5 771	5 742	5 713	5 685	5 656	5 628	5 600
O & M		(1 263)	(1 257)	(1 251)	(1 244)	(1 238)	(1 232)	(1 226)	(1 220)	(1 213)	(1 207)	(1 201)	(63 195)	(1 189)	(1 183)	(1 178)	(1 172)	(1 166)	(1 160)	(1 154)	(1 148)	(1 143)	(1 137)	(1 131)	(1 126)	(1 120)
Net cash flow	(546 300)	18 113	18 023	17 932	17 843	17 754	17 665	17 576	17 489	17 401	17 314	17 228	(44 859)	17 056	16 970	16 886	16 801	16 717	16 634	16 550	16 468	16 385	16 303	16 222	16 141	16 060
Discount factor	1.000	0.943	0.890	0.840	0.792	0.747	0.705	0.665	0.627	0.592	0.558	0.527	0.497	0.469	0.442	0.417	0.394	0.371	0.350	0.331	0.312	0.294	0.278	0.262	0.247	0.233
Present value of cash flow	(546 300)	17 088	16 040	15 056	14 133	13 267	12 453	11 689	10 973	10 300	9 668	9 075	(22 293)	7 996	7 506	7 046	6 614	6 208	5 827	5 470	5 135	4 820	4 524	4 247	3 986	3 742
NPV of cash flow	(355 729)																									

Table E. 1: NPV calculations for systems 1.2(left), 3.2 and 5.2.

The LCOE cost is, as mentioned, similar to the NPV method. However, in this case no income from the produced electricity is assumed. Instead, the minimum average value of electricity in order for the investment to break even is calculated.

LCOE																															
Construction cost	0	(320 000)																													
O & M		(320 000)	(733)	(729)	(725)	(722)	(718)	(714)	(711)	(707)	(704)	(700)	(697)	(693)	(690)	(686)	(683)	(680)	(676)	(673)	(669)	(666)	(663)	(659)	(656)	(653)	(650)				
Net cash flow	1.000	(320 000)	0.943	0.890	0.840	0.792	0.747	0.705	0.665	0.627	0.592	0.558	0.527	0.497	0.469	0.442	0.417	0.394	0.371	0.350	0.331	0.312	0.294	0.278	0.262	0.247	0.233				
Discount factor	0	(691)	(649)	(609)	(572)	(537)	(504)	(473)	(444)	(417)	(391)	(367)	(18 235)	(323)	(304)	(285)	(267)	(251)	(236)	(221)	(208)	(195)	(183)	(172)	(161)	(151)					
Present value of cash flow	(320 000)																														
NPV of cash flow	(346 845)																														
	0	1	2	3	4	5	6	7	8	9	10	11	12	13	14	15	16	17	18	19	20	21	22	23	24	25					
Annual production																															
System capacity[kW]	22.5	22.5	22.5	22.5	22.5	22.5	22.5	22.5	22.5	22.5	22.5	22.5	22.5	22.5	22.5	22.5	22.5	22.5	22.5	22.5	22.5	22.5	22.5	22.5	22.5	22.5					
Specific yield[kWh/kWp/year]	0	814	810	806	802	798	794	790	786	782	778	774	770	766	763	759	755	751	748	744	740	736	733	729	725	722					
Annual production	1.000	18315	18223	18132	18042	17951	17862	17772	17684	17595	17507	17420	17332	17246	17160	17074	16988	16903	16819	16735	16651	16568	16485	16403	16321	16239					
Discount factor	1.000	0.943	0.890	0.840	0.792	0.747	0.705	0.665	0.627	0.592	0.558	0.527	0.497	0.469	0.442	0.417	0.394	0.371	0.350	0.331	0.312	0.294	0.278	0.262	0.247	0.233					
Present value of production	0	17278	16219	15224	14291	13414	12592	11820	11095	10415	9776	9176	8614	8086	7590	7124	6687	6277	5892	5531	5192	4874	4575	4294	4031	3784					
Net present value of electricity[kWh]	223850																														
LCOE[NOK/kWh]	1.55																														

LCOE																															
Construction cost	0	(605 700)																													
O & M		(605 700)	(1 467)	(1 460)	(1 452)	(1 445)	(1 438)	(1 431)	(1 424)	(1 416)	(1 409)	(1 402)	(1 395)	(71 588)	(1 381)	(1 374)	(1 368)	(1 361)	(1 354)	(1 347)	(1 340)	(1 334)	(1 327)	(1 320)	(1 314)	(1 307)	(1 301)				
Net cash flow	1.000	(605 700)	0.943	0.890	0.840	0.792	0.747	0.705	0.665	0.627	0.592	0.558	0.527	0.497	0.469	0.442	0.417	0.394	0.371	0.350	0.331	0.312	0.294	0.278	0.262	0.247	0.233				
Discount factor	0	(1 384)	(1 299)	(1 219)	(1 145)	(1 074)	(1 009)	(947)	(889)	(834)	(783)	(735)	(35 577)	(648)	(608)	(571)	(536)	(503)	(472)	(443)	(416)	(390)	(366)	(344)	(323)	(303)					
Present value of cash flow	(658 517)																														
NPV of cash flow																															
	0	1	2	3	4	5	6	7	8	9	10	11	12	13	14	15	16	17	18	19	20	21	22	23	24	25					
Annual production																															
System capacity[kW]	45	45	45	45	45	45	45	45	45	45	45	45	45	45	45	45	45	45	45	45	45	45	45	45	45	45					
Specific yield[kWh/kWp/year]	0	815	811	807	803	799	795	791	787	783	779	775	771	767	764	760	756	752	748	745	741	737	734	730	726	723					
Annual production	1.000	36675	36492	36309	36128	35947	35767	35588	35410	35233	35057	34882	34708	34534	34361	34190	34019	33848	33679	33511	33343	33177	33011	32846	32681	32518					
Discount factor	1.000	0.943	0.890	0.840	0.792	0.747	0.705	0.665	0.627	0.592	0.558	0.527	0.497	0.469	0.442	0.417	0.394	0.371	0.350	0.331	0.312	0.294	0.278	0.262	0.247	0.233					
Present value of production	0	34599	32477	30486	28616	26862	25214	23668	22217	20855	19576	18375	17249	16191	15198	14266	13391	12570	11799	11076	10397	9759	9161	8599	8072	7577					
Net present value of electricity[kWh]	448250																														
LCOE[NOK/kWh]	1.47																														

LCOE																															
Construction cost	0	(531 300)																													
O & M		(531 300)	(1 263)	(1 257)	(1 251)	(1 244)	(1 238)	(1 232)	(1 226)	(1 220)	(1 213)	(1 207)	(1 201)	(63 195)	(1 189)	(1 183)	(1 178)	(1 172)	(1 166)	(1 160)	(1 154)	(1 148)	(1 143)	(1 137)	(1 131)	(1 126)	(1 120)				
Net cash flow	1.000	(531 300)	0.943	0.890	0.840	0.792	0.747	0.705	0.665	0.627	0.592	0.558	0.527	0.497	0.469	0.442	0.417	0.394	0.371	0.350	0.331	0.312	0.294	0.278	0.262	0.247	0.233				
Discount factor	0	(1 192)	(1 119)	(1 050)	(986)	(925)	(868)	(815)	(765)	(718)	(674)	(633)	(31 406)	(558)	(523)	(491)	(461)	(433)	(406)	(381)	(358)	(336)	(316)	(296)	(278)	(261)					
Present value of cash flow	(577 550)																														
NPV of cash flow																															
	0	1	2	3	4	5	6	7	8	9	10	11	12	13	14	15	16	17	18	19	20	21	22	23	24	25					
Annual production																															
System capacity[kW]	38	38	38	38	38	38	38	38	38	38	38	38	38	38	38	38	38	38	38	38	38	38	38	38	38	38					
Specific yield[kWh/kWp/year]	0	831	827	823	819	815	810	806	802	798	794	790	786	782	779	775	771	767	763	759	756	752	748	744	741	737					
Annual production	0	31578	31420	31263	31107	30951	30796	30642	30489	30337	30185	30034	29884	29735	29586	29438	29291	29144	28999	28854	28709	28566	28423	28281	28139	27999					
Discount factor	1.000	0.943	0.890	0.840	0.792	0.747	0.705	0.665	0.627	0.592	0.558	0.527	0.497	0.469	0.442	0.417	0.394	0.371	0.350	0.331	0.312	0.294	0.278	0.262	0.247	0.233					
Present value of production	0	29791	27964	26249	24639	23129	21710	20379	19129	17956	16855	15822	14851	13941	13086	12283	11530	10823	10159	9536	8952	8403	7888	7404	6950	6524					
Net present value of electricity[kWh]	385953																														

Table E. 2: LCOE calculations for systems 1.2 (left), 3.2 and 5.2.

The electricity price was calculated by using the future values for Nordpool spot traded at NASDAQ Commodities. The ticker for the futures used are ENOYR. Table E.3 shows the price for each year and the average value. The data was collected on March 5th 2013.

Conversion rate Euro/Nok = 7.45	
Index	Price[NOK/kWh]
ENOYR-14	0.277
ENOYR-15	0.268
ENOYR-16	0.263
ENOYR-17	0.273
ENOYR-18	0.283
Average	**0.27**

Table E. 3: Future spot prices at NASDAQ Commodities collected on March 5th.